

Design and Development of a prostate phantom model to mechanically mimic human tissue

E. Veldman

Design and Development of a prostate phantom model to mechanically mimic human tissue

To test new instruments developed for brachytherapy

by

E. Veldman

to obtain the degree of Master of Science
at the Delft University of Technology,
to be defended publicly on Tuesday December 16, 2020 at 14:00.

| | | |
|-------------------|--|--|
| Student number: | 4940237 | |
| Project duration: | June, 2020 - December, 2020 | |
| Thesis committee: | Dr. J. J. van den Dobbelen, TU Delft, supervisor | |
| | ir. M. de Vries, TU Delft, supervisor | |
| | Dr.ir. I. Apachitei TU Delft | |

This thesis is confidential and cannot be made public until December 16, 2021.

An electronic version of this thesis is available at <http://repository.tudelft.nl/>.

Preface

Before you lies the thesis “Design and Development of a prostate phantom model to mechanically mimic human tissue”. It has been written to fulfill the graduation requirements of the Biomedical Engineering master program at the Technical University of Delft. I was engaged in researching and writing this thesis from June to December 2020.

Graduating during the COVID-19 pandemic has been a rocky road. Being send home at the start of the lockdown during my first graduation project, not being able to finish the second project and spending the majority of the time working at home was a challenge. However, this has also lead me to the current project which gave me the opportunity to perform practical labwork and dive into the interesting world of phantoms and biomaterials. I have enjoyed working on this project and gained a lot of practical and theoretical experience and knowledge which I am determined to use in my future career. For this I would like to thank my supervisors, John van den Dobbelsteen and Martijn de Vries, for giving me the opportunity and guidance to work on this project and the experience which has been very valuable to me.

While performing the labwork I have received a lot of help from the people at the MISIT lab. This practical and creative environment has been a joy to work in. For this I would like to thank all the people at the MISIT lab, and especially Flip Somerwil for answering all my questions.

A special thanks to my mom, dad, brother and sisters. You have been most patient, supportive and helpful during my graduation projects. Your feedback and advice has been very valuable and helpful in the graduation process. The help, support and encouragement from all of you gave me the strength to take on this journey and successfully complete it.

Last but not least, I would like to thank my friends for their support and advice. The social online get-togethers, support and feedback on each others work made us feel more connected during the lockdown and home-working period of the year 2020. This has meant a lot to me.

*Ellen Veldman
Den Haag, December 2020*

Abstract

Prostate cancer is the most frequently diagnosed type of cancer among males. Brachytherapy has become a common treatment for this disease. In this form of radiotherapy, sealed radiation sources are placed through a implant catheters inside the prostate. This treatment affects the tumor cells locally and reduces damage to healthy tissues. However, accessing all relevant areas is met by difficulties. Innovating brachytherapy instruments can overcome these challenges. These new instruments need to be tested in a lab environment before patient testing is allowed. Phantom models provide a good validation model for testing new medical instruments. The goal of this study is to design and develop a cancerous prostate phantom model which can be used to test newly developed instruments for brachytherapy.

A material study was conducted to find the best mechanically tissue-mimicking materials. The effects of different concentrations, varying volumes, coolant additive and dimethyl-sulfoxide additive on the Young's modulus of poly-vinyl alcohol was tested. Unconfined compression tests were performed after each freeze-thaw cycle for a total of 7 cycles. These results showed that poly-vinyl alcohol can form material which, based on its Young's modulus, can mimic prostate tissue and adipose tissue. An increase in poly-vinyl alcohol concentration, volume, coolant additive, dimethyl-sulfoxide additive and the number of freeze-thaw cycles were each found to increase the Young's modulus of the material.

Three cancerous prostate phantom models were made of poly-vinyl material with each a different stiffness value achieved by varying the poly-vinyl alcohol concentrations. A low Young's modulus for model 1, medium for model 2 and high for model 3. The poly-vinyl alcohol was solved in a mixture of distilled water:DMSO (10:90 ratio) to produce a transparent material. Each model included a prostate, urethra and surrounding adipose tissue. The models were surrounded by a transparent casing which included an opening and template for needle insertion at the front. A pubic bone was added to model 2 and 3 to simulate prostate blockage by this tissue. Model 1 and 2 did not achieve the transparency that was required. The transparency was found to be sufficient in model 3.

A needle insertion experiment was conducted to validate the prostate phantom models. An 18Gauge brachytherapy needle was inserted 13, 10 and 20 times in model 1, 2 and 3 respectively with a velocity of 5 mm/s. Mean peak forces, describing the force upon puncture of the prostate material, for model 1 (0.57 N) and 2 (3.54 N) were lower than multiple peak forces found in literature. The median peak force of model 3 (6.17 N) came close to the peak force found during in patients with prostate cancer (6.28 N) in the study of Podder et al. (2006). Higher Young's moduli values produced higher peak forces. The insertion force in the adipose tissue of the models was lower than the results found in literature.

This study has shown that poly-vinyl alcohol can function as an easily controlled tissue mimicking material. The material study created an overview of the effects of concentration, volume, coolant, DMSO and freeze-thaw cycles on the Young's modulus of poly-vinyl alcohol. An easy to manufacture cancerous prostate phantom model was made of poly-vinyl alcohol and DMSO. Model 3 developed in this project can function as a test model for newly developed instruments meant for brachytherapy.

Contents

| | |
|--|-------------|
| List of Figures | ix |
| List of Tables | xiii |
| 1 Introduction | 1 |
| 1.1 Background information | 1 |
| 1.2 Motivation & Research Goal | 2 |
| 1.3 Study Outline | 2 |
| 1.4 Requirements | 2 |
| 1.4.1 Anatomical and geometrical correctness | 2 |
| 1.4.2 Mechanical correctness | 3 |
| 1.4.3 Demonstrative qualities | 4 |
| 1.4.4 Practical qualities | 4 |
| 1.4.5 List of Requirements | 4 |
| 1.5 Theory | 5 |
| 1.5.1 Polyvinyl alcohol | 5 |
| 1.5.2 Solvent | 7 |
| 1.5.3 Volume | 7 |
| 1.5.4 Swelling | 7 |
| 1.5.5 Transparency | 8 |
| 2 Part I: Material Study | 9 |
| 2.1 Methods | 9 |
| 2.1.1 Specimen preparation | 9 |
| 2.1.2 Mechanical Testing | 10 |
| 2.1.3 Data Analysis | 12 |
| 2.1.4 Extra study: Storing PVA in Water | 14 |
| 2.2 Results | 15 |
| 2.2.1 Mechanical characteristics | 15 |
| 2.2.2 Noise identification | 20 |
| 2.2.3 Comparison with literature | 20 |
| 2.2.4 Visual characteristics | 21 |
| 2.2.5 Mass fluctuations | 23 |
| 2.2.6 Extra study: Storing PVA in water | 23 |
| 2.3 Discussion | 25 |
| 2.3.1 Recommendation for Part II | 27 |
| 3 Part II: Phantom Design | 29 |
| 3.1 Previous work | 29 |
| 3.2 Design | 30 |
| 3.3 Methods | 31 |
| 3.3.1 Casing | 31 |
| 3.3.2 Rectum | 32 |
| 3.3.3 Prostate and Urethra | 32 |
| 3.3.4 Pubic arch | 34 |
| 3.3.5 Adipose tissue | 35 |
| 3.3.6 Template | 36 |
| 3.4 Results | 37 |
| 3.4.1 Model 1 | 37 |
| 3.4.2 Model 2 | 37 |
| 3.4.3 Model 3 | 38 |

| | | |
|----------|-------------------------------------|-----------|
| 3.5 | Discussion | 39 |
| 4 | Part III: Phantom Validation | 41 |
| 4.1 | Methods | 41 |
| 4.1.1 | Materials | 41 |
| 4.1.2 | Protocol | 41 |
| 4.1.3 | Experimental Set-up | 41 |
| 4.1.4 | Data Analysis | 42 |
| 4.2 | Results | 44 |
| 4.2.1 | Mean Peak Force | 44 |
| 4.2.2 | Validation | 45 |
| 4.3 | Discussion | 48 |
| 5 | Final Discussion | 51 |
| 5.1 | Conclusion | 51 |
| 5.2 | Future Research | 51 |
| | Bibliography | 53 |
| A | Appendices | 57 |
| A.1 | Needle Insertion Figures Model 1 | 59 |
| A.2 | Needle Insertion Figures Model 2 | 62 |
| A.3 | Needle Insertion Figures Model 3 | 65 |
| A.4 | Needle Insertion Peak Forces | 68 |

List of Figures

| | | |
|------|---|----|
| 1.1 | Prostate brachytherapy treatment. A transrectal ultrasound probe (TRUS) is inserted inside the rectum to visualize the prostate during treatment. Implant catheters are inserted through a template, inside the prostate. Seeds are placed inside the prostate through the implant catheters. Figure derived from the Prostate Cancer Foundation of Australia [1] | 1 |
| 1.2 | Formula of polyvinyl alcohol $[CH_2CH(OH)]_n$. The molecule includes one OH-group which can form 3 hydrogen bonds in total. | 5 |
| 1.3 | The formation of hydrogen bonds between a negatively charged oxygen element (O) and a slightly positively charged hydrogen element (H), both present in a OH-group. | 6 |
| 1.4 | The process of freeze-thawing induces the formation of crosslinks based on the formed hydrogen bonds between PVA and water. Figure is derived from the study of Kim et al. (2015) [2] | 6 |
| 1.5 | Formula of ethylene glycol $(CH_2OH)_2$. The molecule includes two OH-groups which can form 6 hydrogen bonds in total. | 8 |
| 1.6 | Formula of dimethyl-sulfoxide (C_2H_6SO) . The molecule includes one O-group which can form two hydrogen bonds. | 8 |
| 2.1 | Specimen preparation set-up including a glass beaker containing PVA powder solved in distilled water and coolant covered with aluminum foil placed on a stirring plate. The place is set to heat the sample until 90°C and stirring 300 rounds per minute. A sensor is placed in the mixture to measure the temperature. | 10 |
| 2.2 | A typical stress-strain curve of a soft tissue starting with a non-linear toe-region followed by the linear elastic region. After the yield point, the plastic region occurs which is finished by a failure point. Figure derived from Korhonen Saarakkala (2011) [3] | 11 |
| 2.3 | Experimental set up of the unconfined compression test. The sample is placed on tissue located on an elevator plate. A square metal plate functions as a compression plate. | 12 |
| 2.4 | Gravitational force (Fz) in Newton vs. the mean voltage output in Volt. The resulting converting formula calculated by Excel is presented right next to the trend-line. | 13 |
| 2.5 | Mean stress values vs. strain values. The grey line represents the mean values of unfiltered data including noise. The red line shows the mean-average taken over 200 sampling points. | 13 |
| 2.6 | Stress-strain curves of all groups focusing on different PVA concentrations until a maximal strain of 0.3. The stress values varied from 0 to 23.8 kPa. | 15 |
| 2.7 | Stress-strain curves of all groups focusing on the effect of different volumes until a maximal strain of 0.3. The stress values varied from 0 to 24.8 kPa. | 16 |
| 2.8 | Stress-strain curves of all groups focusing on the effect of different coolant concentrations until a maximal strain of 0.3. The stress values varied from 0 to 24.8 kPa. | 17 |
| 2.9 | Stress-strain curves of all groups focusing on different DMSO concentrations until a maximal strain of 0.3. The 'Base' line presents the graph of group B, 10% PVA without additives. | 18 |
| 2.10 | Stress-strain curves of all groups focusing on different PVA concentrations until a maximal strain of 0.3. The stress values varied from 0 to 23.8 kPa. | 20 |
| 2.11 | A decrease of translucency was observed after the number of cycles increased. (a) shows a low amount of coolant sample after one freeze-thaw cycle, (b) shows the same sample after 7 freeze-thaw cycles. | 21 |
| 2.12 | A bump protruding from the bottom of sample E1. The bump developed after the second freeze-thaw cycle in the large volume group. The bump was removed after this cycle. | 22 |
| 2.13 | Pictures of the different specimens in the coolant group. (a) shows group F, (b) shows group G and (c) shows group H. Different levels in brightness of the colour pink were found between the groups. | 22 |

| | | |
|------|---|----|
| 2.14 | Pictures of the different specimens in the DMSO group. (a) shows group I, (b) shows group J and (c) shows group K. Different levels of translucency were found between the groups. | 23 |
| 2.15 | Decrease in mass occurred for every group after each cycle. The mass decrease was the most evident in group A and the least evident in group K. | 23 |
| 2.16 | Overview of the mass fluctuations per sample. Group X describes the samples which were not emerged into water in the period between the freeze-thaw cycles and group Y describes the samples which were emerged into water in the period between the freeze-thaw cycles. The Y-axis denotes the freeze-thaw cycles (C1 - C5) and the periods between the freeze-thaw cycles (P1 - P3). Mass fluctuations occurred for all samples with the most fluctuations happening in the periods between the freeze-thaw cycles for group Y. | 24 |
| 3.1 | Multiple prostate phantom models found in previous work. Different designs are used as well as varying materials. Each models uses a casing to surround the inlaying materials and present the model. | 30 |
| 3.2 | Example design of the prostate phantom model. The model includes the prostate and the relevant tissues around the prostate which interact with the instruments during brachytherapy treatment. | 31 |
| 3.3 | Casing of the prostate phantom model. The model is made of transparent PMMA material with 4 mm thickness. The outer dimensions of the casing conclude 120 x 120 x 208 mm. An opening is present at the front which enables needle insertion. A round opening is made for a rectal insert. | 32 |
| 3.4 | Casing of the prostate phantom model including the rectum insert. The grooves between the rectum and casing are covered with tacky tape to make the casing water tight. The opening for needle insertion is covered with a PMMA plate and the grooves are also covered in tacky tape to make it water tight. | 32 |
| 3.5 | The two halves of the prostate mould (a) and the two halves of the mould placed on top of each other, sealed with M4 bolts, including an urethra model and closed of with tacky tape (b). | 33 |
| 3.6 | A finished prostate model including an urethra inside the mould (a). An implant inserted in the top of the prostate model meant as a target for steerable needles (b). | 34 |
| 3.7 | Two models of the pubic arch (a). Above: the smaller model of the pubic arch designed for phantom model 2. Below: the larger model of the pubic arch designed for phantom model 3. An assembly of all the objects shows the final model before adding the adipose tissue material (b). | 35 |
| 3.8 | A 3D model of the template meant to guide the needles during brachytherapy (a) and the holder to keep the template in place (b) | 36 |
| 3.9 | Model 1 (a) the side-view (b) and the upper-view (c). The model includes a prostate, urethra and adipose tissue. In front, the template for guiding the needles and the front of the rectal insert can be seen. | 37 |
| 3.10 | Model 2 (a) the side-view (b) and the upper-view (c). The model includes a prostate, urethra, a small pubic bone and adipose tissue. In front, the template for guiding the needles and the front of the rectal insert can be seen. | 38 |
| 3.11 | Model 3 (a) the side-view (b) and the upper-view (c). The model includes a prostate, urethra, large pubic bone and adipose tissue. In front, the template for guiding the needles and the front of the rectal insert can be seen. | 38 |
| 4.1 | Experimental set-up of the needle insertion test consisting of a linear stage, a sensor, a needle and a model. The model is placed on its back with its opening to the top. | 42 |

- 4.2 An example of the measured force over time over a full needle insertion into a prostate phantom model. First the needle inserts into the adipose tissue material (A). Secondly, the needle is inserted into the prostate phantom which results in the peak force in this graph (B). After the needle has punctured the prostate phantom the force measured is due to the friction between the needle and the prostate phantom material (C). Thereupon, the needle is retracted in the prostate which results in a negative measured force (D). After this, the period is shown when the needle is retracted from the adipose tissue (E). The last part visualized a non moving retracted needle (F). 42
- 4.3 A boxplot showing the peak force in Newton per model. The red line represents the median and the bottom and top edges of the box indicate the 25th and 75th percentiles, respectively. The horizontal black lower and upper lines represent the minimal and maximal value, respectively. 44
- 4.4 Graph derived from Podder et al. (2006) which shows the peak force measured on the insertion of one 18Gauge needle during brachytherapy [4]. A maximal peak force of 8.46 N on the needle is applied when puncturing the perineum. After this insertion the needle drives through the tissue laying between the perineum and the prostate where an insertion force of 5-5.5 N is measured. Finally, an insertion force of 5.82 N is seen when puncturing the prostate. 46
- 4.5 Graph derived from Hungr et al. (2012) which shows the peak force measured on the insertion of one 18Gauge needle into the phantom model [5]. The graph shows the insertion of the needle into the perineum (A), the interlaying tissue (B) and the prostate (C). The last part visualized the relaxation of the material (D). 47

List of Tables

| | | |
|-----|--|----|
| 1.1 | Overview of the Young's moduli of a prostate found in the conducted literature study. Different prostate tissue types were used which originated from the peripheral zone (PZ), central zone (CG) and the transitional zone (TZ). | 3 |
| 1.2 | Overview of the Young's moduli of adipose tissue found in the conducted literature study. Different adipose tissue types were used which originated from breast tissue, abdominal tissue, pericardial tissue, omental tissue and tissue from the thymus. | 4 |
| 2.1 | The overview of the experimental design of this study. The code used for each combination, description of the specimen, the amount of each component (PVA, distilled water (DW), coolant and DMSO) used in the mixture, the total weight per sample that was used of this mixture and the total samples. | 10 |
| 2.2 | The overview of the calibration values used to convert the voltage output to force. The mass of the weights, the mean of the 3 voltage outputs and the corresponding gravitational force (Fz) values are given. | 12 |
| 2.3 | Mean Young's modulus values (E) in kPa per PVA concentration group: 5% (A), 10% (B) and 15% (C). The values were measured after each freeze-thaw cycle for a total of 7 cycles. The standard deviation (SD) is denoted. Also, the part of the elastic region (ER), given in strain values, over which the Young's modulus was calculated is given. | 19 |
| 2.4 | Mean Young's modulus values (E) in kPa per volume group: small (B), medium (D) and large (E). The values were measured after each freeze-thaw cycle for a total of 7 cycles. The standard deviation (SD) is denoted. Also, the part of the elastic region (ER), given in strain values, over which the Young's modulus was calculated is given. | 19 |
| 2.5 | Mean Young's modulus values (E) in kPa per coolant group: low (F), medium (G) and high (H) concentration of coolant. The values were measured after each freeze-thaw cycle for a total of 7 cycles. The standard deviation (SD) is denoted. Also, the part of the elastic region (ER), given in strain values, over which the Young's modulus was calculated is given. | 19 |
| 2.6 | Mean Young's modulus values (E) in kPa per DMSO group: low (I), medium (J) and high (K) concentration DMSO. The values were measured after each freeze-thaw cycle for a total of 7 cycles. The standard deviation (SD) is denoted. Also, the part of the elastic region (ER), given in strain values, over which the Young's modulus was calculated is given. | 19 |
| 3.1 | Overview of the Young's moduli for the materials with and without DMSO as additive after two freeze-thaw cycles. Estimated values are given in cursive. | 34 |
| 3.2 | Overview of the Young's moduli for the materials with and without DMSO as additive after two freeze-thaw cycles. Estimated values are given in cursive. | 36 |
| 4.1 | Overview of the mean peak force per model and its median and standard deviation (SD). The sample size (N) per model consists of 13, 10 and 20 for model 1, model 2 and model 3 respectively. | 45 |
| 4.2 | Overview of the peak insertion forces into prostate tissue/phantom material found in the conducted literature study. Different prostate tissue types and phantom materials were used. The total range of peak forces found consisted of 5.2 - 9 N. The '≈' sign describes results read out of graphs presented in the corresponding study | 46 |

Introduction

1.1. Background information

According to the World Health Organization, cancer is the second leading cause of death worldwide, causing 1 in 6 deaths globally and a total of 9.6 million deaths in 2018 [6]. The most frequent diagnosed cancer among males is prostate cancer [6]. According to the American Cancer Association, 1 in 9 man will be diagnosed with prostate cancer during his life [7]. Prostate cancer defines the growth of tumor cells in the prostate. The prostate is a small, male and walnut-shaped organ found below the bladder with an urethra passing through it. The function of the prostate is to produce and contain fluid as a part of the semen. Prostate brachytherapy has become a very common treatment used for localized prostate cancer [8]. In this form of radiotherapy, sealed radiation sources are placed in the prostate. This treatment involves different steps. First, a transrectal ultrasound probe (TRUS) is inserted inside the rectum which is used to visualize the prostate during the treatment [9]. A template is used in front of the perineum to correctly place the brachytherapy needles [1]. The brachytherapy needles, or implant catheters, are inserted through the template, the perineum, the adipose tissue and ending into the prostate [10]. The radiation seeds are then injected into the prostate via the implant catheters [9]. A visualization of the prostate brachytherapy treatment can be found in figure 1.1.

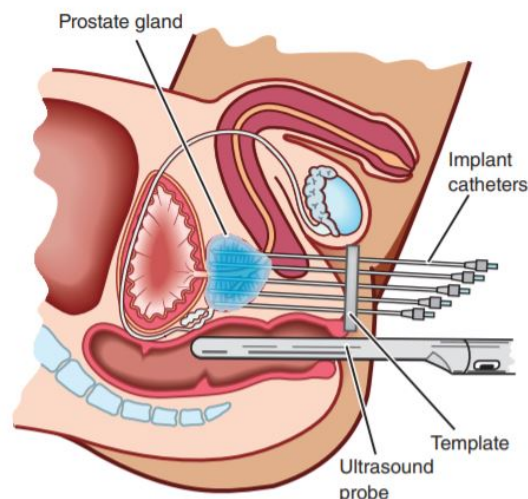


Figure 1.1: Prostate brachytherapy treatment. A transrectal ultrasound probe (TRUS) is inserted inside the rectum to visualize the prostate during treatment. Implant catheters are inserted through a template, inside the prostate. Seeds are placed inside the prostate through the implant catheters. Figure derived from the Prostate Cancer Foundation of Australia [1]

1.2. Motivation & Research Goal

Radiation, as a result of brachytherapy, only affects a very local area around the sealed sources, which is a major advantage. Damage caused due to radiation on healthy tissues is therefore reduced [9]. However, the local effects also requires this treatment to be precise. During the treatment it is important that all the cancerous areas in the prostate are targeted. Multiple variables present during the treatment cause difficulties for a brachytherapy needle to access all the cancerous areas in the prostate [11–13]. Possible factors include the varying sizes of the prostate among patients [14], prostate movement [15, 16], deflection of the brachytherapy needle [17] and the blockage of the prostate by a part of the pubic bone; the pubic arch [10]. The use of steerable needles and other innovative instruments during this treatment could form a possible solution to this problem. Research is being conducted in developing improved instruments for brachytherapy [18–20]. These new instruments need to be tested in a lab environment before they can be tested on patients. Phantom models of organs can provide a good validation model when testing new medical instruments in this phase [21–23]. Phantom models are often made of tissue mimicking biomaterials and used as a replacement of using rare human and animal tissue. Multiple prostate phantom models have been made before [5, 24, 25]. However, finding the right biomaterials with optimal tissue mimicking characteristics is a challenge. An overview of the exact material characteristics of biomaterials is lacking. Also, the specific influence of varying concentrations, additives and differences in protocols is not known. A validated prostate phantom model which gives a good representation of a real prostate is still to be designed. The goal of this project is therefore to design, develop and validate a prostate phantom model which simulates a cancerous prostate and its surrounding tissues. The purpose of this model is to function as a testing model for a newly developed instruments for brachytherapy. To achieve this, a materials study will be performed in which exact material characteristics will be determined.

1.3. Study Outline

The project will be carried out in three parts. This is elaborated below:

1. Part I: Conduct a material study. First a literature study will be performed to collect information on needed biomaterials and additives based on the requirements of this study. A list of biomaterials and additives will be made which will be developed and mechanically tested in a lab to determine their specific mechanical characteristics.
2. Part II: Design and manufacture a cancerous prostate phantom model. A design will be made to develop a phantom prostate model based on the requirements. Based on the results of the material study from part I, the best tissue-mimicking biomaterials will be selected for the design of the phantom prostate model.
3. Part III: Validate the cancerous prostate phantom model. A test will be set-up to validate the model. The results of the test will be compared with the results of similar tests performed on a prostate resulting from literature. Based on this comparison, a conclusion can be made on the tissue-mimicking characteristics of the cancerous prostate phantom model.

1.4. Requirements

1.4.1. Anatomical and geometrical correctness

In order to test new instruments needed for brachytherapy, the phantom should represent a cancerous prostate and its surrounding tissues as much as possible. The phantom should mimic the different tissues and organs which interact with a needle or ultrasound probe during brachytherapy. Figure 1.1 shows the instruments used during brachytherapy and the tissues they interact with. Based on this, a prostate, rectum, urethra and the tissue located between the perineum and prostate should be present in the phantom. A cancerous prostate has the minimal height of 3 cm, a width of 4 cm and a volume of 40 ml [26]. These dimensions should form the minimal dimensions of the prostate model. The distance between perineum and prostate was found to be 40-72 mm [27]. Therefore, the distance between the front, simulating the perineum, of the phantom model and prostate phantom should also be 40-72 mm long. Literature shows that the distance between rectum and prostate differs from no distance, or direct contact to a distance of 37 mm. This range is also required for the distance between these

parts in the model. An urethra has a diameter of 6 mm which will also be used in the phantom model [28]. A rectal probe, which will be inserted inside the rectum, has a minimal diameter of 19 mm [29]. This should also be the minimal diameter of the rectal opening in the model. The interlaying tissue consists of multiple tissues as muscles, arteries, veins and adipose tissue. Since the majority of this tissue is formed by adipose tissue, this part in the phantom will mimic adipose tissue. The front of the phantom should have an opening and a place for a template for the brachytherapy needles to enter. Since the target of the instruments in the prostate, the opening should have a minimal size equal to the size of the prostate. This means that the opening should have the minimal dimensions of 3x4 cm.

1.4.2. Mechanical correctness

To test the interaction between the needle and the relevant organs and tissues, the phantom must represent a prostate and its surrounding tissues in terms of mechanical characteristics. The focus will be on the stiffness also known as the Young's modulus of the material. Table 1.1 presents an overview of multiple studies and their results which have performed tests to find the Young's modulus of a prostate. The total range of the Young's moduli that were found consisted of 2.2 - 221 kPa for a prostate. For healthy prostate material the range varied from 2.2 - 70 kPa. For prostate tissue with benign hyperplasia the values varied from 24 - 40 kPa and for cancerous prostate tissue the total range found was 62.9 - 221 kPa. The goal of this project is to simulate cancerous prostate tissue. This means that a stiffness of the prostate phantom material should fall into the range of 62.9 - 221 kPa.

Table 1.1: Overview of the Young's moduli of a prostate found in the conducted literature study. Different prostate tissue types were used which originated from the peripheral zone (PZ), central zone (CG) and the transitional zone (TZ).

| Study | Tissue type | Young's Modulus (kPa) |
|-----------------------------|---------------------------------|-----------------------|
| Kemper et al. (2004) [30] | CG healthy | 2.2±0.3 |
| | PZ healthy | 3.3±0.5 |
| Krouskop et al. (1998) [31] | CG healthy | 63±18 |
| | PZ healthy | 70±14 |
| | PZ cancerous | 221±32 |
| | PZ benign prostatic hyperplasia | 36±11 |
| Phipps et al. (2005) [32] | TG cancerous (treated) | 118±50 |
| | TG cancerous (untreated) | 110±2 |
| Yang et al. (2006) [33] | PZ benign prostatic hyperplasia | 200 |
| Zhang et al. (2008) [34] | PZ healthy | 15.9±5.9 |
| | PZ cancerous | 40.4±15.7 |
| | PZ healthy | 19.2 |
| | PZ cancerous | 62.9 |
| Zhang et al. (2014) [35] | PZ benign prostatic hyperplasia | 24.1±4.9 |
| | TZ benign prostatic hyperplasia | 32.2±5.9 |

The tissue laying between the prostate and skin is mainly consisting of adipose tissue. This phantom tissue should consist of a heterogeneous material having a Young's modulus value which lies in the range of adipose tissue. Research has found different values of the Young's modulus of adipose tissue resulting in a total range of 0.12 - 50 kPa, as can be seen in an overview of these results in table 1.2.

Table 1.2: Overview of the Young's moduli of adipose tissue found in the conducted literature study. Different adipose tissue types were used which originated from breast tissue, abdominal tissue, pericardial tissue, omental tissue and tissue from the thymus.

| Study | Adipose Tissue type | Young's Modulus (kPa) |
|--------------------------------|---------------------|-----------------------|
| Geerligs (2006) [36] | Multiple tissues | 0.12-50 |
| Nightingale et al. (2003) [37] | Breast | 3.8±1.4 |
| | Abdomen | 5.6 ± 3.1 |
| Omidi et al. (2014) [38] | Breast | 3.46±1.210 |
| | Abdomen | 3.365±0.685 |
| | Pericardium | 2.504±1.152 |
| | Omentum | 2.37±0.399 |
| | Thymus | 2.109±0.685 |
| Samani et al. (2007) [39] | Breast | 3.25 ± 0.91 |

1.4.3. Demonstrative qualities

As mentioned before, the goal of this phantom is to demonstrate new instruments used for brachytherapy. Because of this, the phantom must have good demonstrative qualities. The testing of the instruments in the phantom must be visible. This can either be achieved by using an ultrasound, which is also done during the brachytherapy treatment itself, or by making the interlaying tissue and the surrounding case of the phantom transparent so all inner parts can be seen. When using an ultrasound probe, a rectum must be present which offers contact with the interlaying tissue. A rectal probe has a minimal diameter of 19 mm [29]. This should also be the minimal diameter of the rectal opening in the model. Since the phantom will first be tested in the MISIT lab, where no medical ultrasound is available, it is a wish to create a transparent phantom. Ideally, a rectum will be present and transparency will be present, so both wishes can be met.

1.4.4. Practical qualities

The phantom will be made in the Minimally Invasive Surgery and Interventional Techniques (MISIT) lab at the Mechanical, Maritime and Materials Engineering (3mE) faculty of the Technical University of Delft. One of the purposes of the phantom is to demonstrate new instruments developed for brachytherapy. The phantom must be transportable so it can be used for demonstrations in scientific events at different locations. Maximal dimensions of 30x30x30 cm for carrying the model are acceptable. For practical reasons, it also needs to be durable so appointments for demonstrations can be made beforehand. Therefore, the phantom must remain usable for at least one week. At last, it is required that the phantom is reproducible. After a demonstration, multiple instruments or needles can have punctured the phantom after which it cannot be used to present again. Hence, it must be possible to reproduce a new phantom with exactly the same features with the equipment and materials present at the 3mE faculty. Since it is assumed that the models will be reproduced and that they will be reproduced in more numbers, it is required that the phantom should be easy to manufacture. This should be done by creating a relatively easy and short-lasting manufacturing process. To achieve this, a clear list of used equipment, materials and its preparation is needed and the method protocol must be clear. The phantom should be made with equipment and materials present at the 3mE faculty. A maximal manufacturing time of one week is required.

1.4.5. List of Requirements

Based on the section above, the following list of requirements was made. This list will be used when making an prostate phantom model during the following project.

- **Geometrical**

- The phantom should include a prostate, urethra, adipose tissue and a rectum.
- The phantom should include an opening for needle insertion with minimal dimensions of 3x4 cm and a needle insertion template.
- Preferably, a part of a pubic bone to block needle insertion should be present.

- Similar shape and size of the tissues compared to a human.
 - ◊ The prostate should have a minimal height of 3 cm, width of 4 cm and volume of 40 ml. The distance between the front of the casing and prostate should be 40-72 mm. The distance between rectum and prostate should be 0-37 mm.
 - ◊ The urethra should have a diameter of 6 mm.
 - ◊ The rectum should have a minimal diameter of 19 mm.
- **Mechanical**
 - Prostate material with a Young's modulus falling into the 62.9 - 221 kPa range.
 - Adipose tissue material with a Young's modulus falling into the 0.12 - 50 kPa range.
- **Demonstrative qualities**
 - The prostate material should be transparent. Inserting instruments should be visible.
 - The adipose tissue material should be transparent. Different parts/tissues in this material should be visible.
 - A rectum should be present for inserting an ultrasound probe which opening should have a minimal diameter of 19 mm.
 - The casing holding the phantom should be transparent. All the parts present in the casing should be visible.
- **Practical**
 - The model should be transportable. Maximal dimensions of 30x30x30 cm are required.
 - The phantom material should be durable for at least one week.
 - The manufacturing process should be reproducible with the equipment and materials present at the 3mE faculty.
 - The model should be easy to manufacture with equipment and materials present at the 3mE faculty and a maximal manufacturing time of one week.

1.5. Theory

1.5.1. Polyvinyl alcohol

Because of excellent biocompatibility, heterogeneous characteristics and its similar mechanical characteristics to human tissues, Polyvinyl Alcohol (PVA) is one of the most frequently used material for biomedical applications [2, 40–42]. Polyvinyl alcohol (PVA) is a water-soluble synthetic polymer or hydrogel prepared by the hydrolysis of polyvinyl acetate. It has an idealized formula known as $[CH_2CH(OH)]_n$, also shown in figure 1.2. This formula shows the presence of one hydrogen group, the OH-group, per molecule. This group is able to form hydrogen bonds.

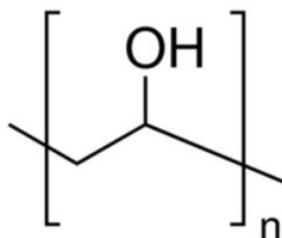


Figure 1.2: Formula of polyvinyl alcohol $[CH_2CH(OH)]_n$. The molecule includes one OH-group which can form 3 hydrogen bonds in total.

Hydrogen bonds are formed by the presence of an electronegative element. For example, the electronegative element oxygen (O) can cause the formation of hydrogen bonds. An electronegative element is characterized by the fact that their nucleus is positively charged due to the presence of

a higher amount of protons. This positive charge will hold the surrounding electrons tightly to the nucleus. It therefore also attracts nearby electrons to the element. If an electronegative element is bonded to a less electronegative, for example hydrogen, or even electropositive element, the electrons in this hydrogen element will re-locate themselves towards the electronegative element, resulting in an slightly more negative electronegative element (δ^-) and a slightly more positive hydrogen element (δ^+). This phenomenon describes a polar bond in which a separation of charge between one end and the other end is present. A typical polar bond is formed between oxygen (O) and hydrogen (H), forming the so-called OH-group. Due to the separation of charges, the OH-groups are able to form hydrogen bonds. This bond describes a non-covalent bond between a slightly electronegative part and a slightly electropositively part in which an electron pair is shared between the two parts. A so-called hydrogen bond between two OH-groups can be seen in figure 1.3. Every oxygen element is able to form 2 hydrogen bonds to a hydrogen bonding group and every hydrogen element is able to form one hydrogen bond to an hydrogen bonding group. Figure 1.2 shows one present OH-group for PVA. This suggests that PVA can form hydrogen bonds.

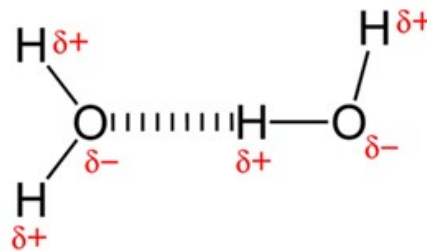


Figure 1.3: The formation of hydrogen bonds between a negatively charged oxygen element (O) and a slightly positively charged hydrogen element (H), both present in a OH-group.

Research has shown that applying a period of freezing followed by a period of thawing, a so called freeze-thaw cycle, to PVA solved in water results in an increase in stiffness of the material [43, 44]. PVA has the tendency to grow crosslinks, based on hydrogen bonds between multiple organic structures. When solving PVA, hydrogen bonds can be formed between PVA molecules. A freeze-thaw cycle induces the formation of these crosslinks, which cause heterogeneity. This process can be viewed in figure 1.4. As more freeze-thaw cycles are applied, additional crosslinks reinforces the original gel network [2]. Reinforcement mainly involves the formation of new crosslinks, but the primary crosslinks created in the first cycle can also grow [2]. Applying freeze-thaw cycles can offer the ability to control the mechanical characteristics of the PVA material. No prove was found of the effect of freezing time on the elastic modulus. Wan, Campbell, Zhang, Hui, Boughner (2002) compared holding times of 1 and 6 hours at -20°C on PVA [45]. No significant difference was found in the elastic modulus of the materials. The study did find that a fast thawing rate resulted in a lower elastic modulus. In this study, freeze-thaw cycles of 24h each will be applied. The reason for this is the limited opening hours of the MISIT laboratory. A freeze cycle of 24 hours at -14°C will be executed followed by a thawing round on 24 hours at room temperature. This is based on the available equipment at the laboratory.

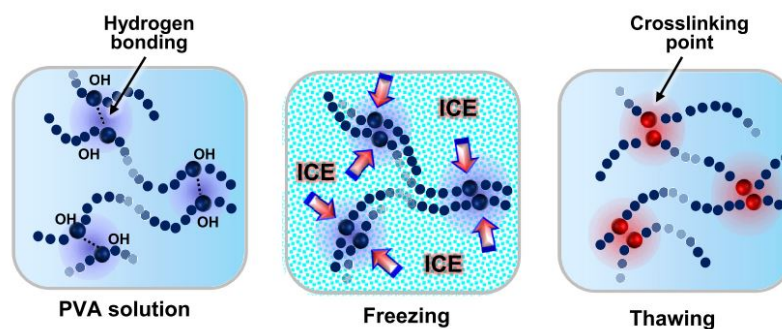


Figure 1.4: The process of freeze-thawing induces the formation of crosslinks based on the formed hydrogen bonds between PVA and water. Figure is derived from the study of Kim et al. (2015) [2]

There are three important commercially available grades of PVA. These are distinguished by the mole percent residual acetate groups in the polymer chain [46]:

1. Fully hydrolyzed: 1 – 2 mol% acetate groups
2. Intermediate hydrolyzed: 3 – 7 mol% acetate group
3. Partially hydrolyzed: 10 – 15 mol% acetate groups

In theory, more hydrolysis allows for more hydrogen bonds to occur during the freeze-thaw process which can result in a higher Young's modulus. In this study, a fully hydrolyzed PVA powder will be used. The PVA powder with a molecular weight of 89,000 – 98,000 g mol⁻¹ (>99% hydrolyzed) will be used.

PVA is one of the most frequently used biomaterial in the MISIT lab. However, an overview of its specific mechanical characteristics is not yet available. Therefore this research will focus on the biomaterial PVA and its mechanical characteristics.

1.5.2. Solvent

A hydrogen bonding liquid can be used to solve PVA powder. Water is usually added as a solvent to the PVA powder to induce the formation of hydrogen bonds and create a gel. The electrolyte concentration in water being added to a polymer greatly affects the amount of water which can be absorbed per gram of polymer [47]. When a polymer is immersed in water an osmotic pressure is created which diffuses the water into the polymer. A lower electrolyte concentration in the water, for example distilled water, creates a higher osmotic gradient which diffuses more water into the polymer. A higher electrolyte concentration in the water, for example tap water, would result in a lower osmotic gradient and therefore less diffusion of water into the polymer. According to this, a super absorbent polymer can absorb about 800 times its own weight in distilled water, 300 times its weight in tap water and 60 times its weight in 0.9% sodium chloride solution [47]. The electrolyte concentration can therefore influence the water absorption and with that mechanical characteristics of the created PVA. In this study distilled water will be used to create an optimal diffusion of water into the polymer.

1.5.3. Volume

Research has shown that product thickness and product shape have an influence on the freezing time of a volume [48]. This study suggests that a higher thickness results in a longer freezing time in which volumes less than 50 mm thick a 2 times longer freezing time is needed for a doubling in thickness. Besides this, the study concludes that in volumes with a thickness of 100 mm or more, a doubling of thickness may result in an increase of freezing time in fourfold. It should also be considered that the shape of a volume has an influence on the freezing time which is dependent on the ratio of surface area to volume, as does the volume itself. As mentioned before, it is not yet prove that the freezing time has an influence on the creating of crosslinks and therefore an influence on the resulting Young's modulus after the freeze-thaw cycles. This study will investigate the effect of volume on the Young's modulus.

1.5.4. Swelling

The freeze-thawing process is often accompanied by swelling [43]. Pre-tests in the MISIT lab have shown that coolant can be added to PVA to prevent swelling. Swelling is sometimes wished to be avoided due to the usage of moulds which can break by swelling of the inner material. A coolant is a mixture of ethylene glycol ((CH₂OH)₂) and water and is known for its lowering effect on the freezing-point of a material. The structure formula of ethylene glycol, seen in figure 1.5, shows the presence of two OH-groups which are both able to form hydrogen bonds. Because of this, coolant can be used as a solvent for PVA. However, due to the lowering effect on the freezing point of the coolant, it might prevent the PVA and its solvent from freezing or decrease the freezing time or rate. Freezing the material is necessary for the formation of crosslinks. Using coolant as a solvent or additive might therefore have a lowering effect on the formation of crosslinks and can therefore decrease the resulting stiffness value of the material. However, this is yet to be tested. This study will focus on the effect on the Young's modulus of coolant as additive to PVA.

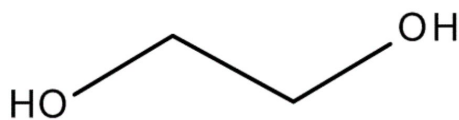


Figure 1.5: Formula of ethylene glycol ($(CH_2OH)_2$). The molecule includes two OH-groups which can form 6 hydrogen bonds in total.

1.5.5. Transparency

The prostate phantom will be made with the goal to test a newly developed instruments used during brachytherapy. To see the behaviour of these instruments in the phantom, a transparent material, mimicking prostate and adipose tissue, is necessary. Transparency in PVA can be achieved by adding dimethyl-sulfoxide (DMSO) [49]. Denoted by formula C_2H_6SO in figure 1.6, this liquid includes one oxygen group which is able to form two hydrogen bonds. Therefore, this material can function as a solvent for PVA. DMSO is known to be used as a medicine and as a solvent for making materials transparent. When maintaining a weight ratio of the PVA solution and DMSO of 20/80, it can result in a PVA hydrogel with transparency greater than 90% [49]. Hoshino, Okada, Urakawa, Kajiwara (1996) found that the growth of crystal in PVA is interlinked with the material becoming turbid [50]. Adding DMSO might have an influence on crystal growth and the Young's modulus of the material. This is however still to be tested.

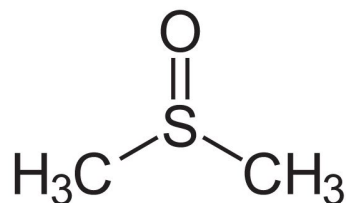


Figure 1.6: Formula of dimethyl-sulfoxide (C_2H_6SO). The molecule includes one O-group which can form two hydrogen bonds.

2

Part I: Material Study

2.1. Methods

2.1.1. Specimen preparation

In this section, the methods used to prepare different combinations of PVA biomaterial which could possibly function as a prostate phantom are presented.

Materials

The PVA specimens were made with 99+% hydrolyzed, 89,000-98,000 molecular weight PVA powder (Sigma-Aldrich, Lot# MKCJ5322). Distilled water was used as a solvent for the PVA powder. Different, common used, additives were used in this study to research their influence on the mechanical characteristics of the specimen. These additives included 99.7% DMSO (Laboriumdiscounter, CAS 67-68-5, Iden.# 80.IL084) and $>-30^{\circ}\text{C}$ coolant (Gamma, Iden.# 613079). Two different magnetic stirring plates including temperature control and sensors (IKA C-Mag HS 7, Iden.# 0020002694 and DLAB MS-H-PRO+, Iden.# 8030101110) were used for the preparation of the specimens. The materials were stored using TU Delft coffee cups and aluminum foil.

Protocol

For all the specimens in this study, the needed materials were selected and weighted first. A glass beaker containing the distilled water was placed on the magnetic stirring plate and selected to stir 300 rounds per minute. For the PVA specimens, PVA powder was slowly added to the stirring distilled water. In case of the coolant and DMSO specimens, coolant or DMSO was first added to the stirring distilled water and after one minute of stirring, the PVA powder was slowly added to the stirring mixture. After the powder was added, the glass beaker was covered in aluminum foil to preserve the heat, the temperature sensor was placed through the aluminum foil into the mixture and the whole was heated until 90°C . This set-up can be seen in figure 2.1. Once this temperature was reached, the stirring continued for 30 minutes at 90°C after which the mixture was placed off the stirring plate and left to cool for 20 minutes. Finally, the predetermined amount of the cooled fluid was put into the coffee cups which were covered with aluminum foil. The cups were frozen at -14°C for 24 hours after which they were thawed at room temperature for 24 hours. These 48 hours of freeze-thawing included one cycle. After each freeze-thaw cycle, the samples were removed from the cups and dried with a paper tissue. The mass of each sample was measured after every cycle to take into account the possible mass fluctuations due to the freeze-thaw cycles. Also, a picture was taken after each freeze-thaw cycle to study the visible changes in color and translucency of the samples. During the weekends, when the lab is closed, the specimens were stored at 4°C . This occurred 3 times in total. After every freeze-thaw cycle, the specimens were mechanically tested.



Figure 2.1: Specimen preparation set-up including a glass beaker containing PVA powder solved in distilled water and coolant covered with aluminum foil placed on a stirring plate. The place is set to heat the sample until 90°C and stirring 300 rounds per minute. A sensor is placed in the mixture to measure the temperature.

Experimental Design

In total, 11 different combination of PVA specimens were included in this study. The specimens can be divided into 4 groups. The first group studied the varying concentrations of PVA, the second group focused on the effect of volume of PVA, the third group studied the effect of a coolant additive and the last group focused on the effect of a DMSO additive. Each group included 3 different mixtures, except the volume group, which included 2 different mixtures. Of each mixture 3 different specimens were created which resulted in 33 specimens in total. An overview of these specimens can be seen in table 2.1.

Table 2.1: The overview of the experimental design of this study. The code used for each combination, description of the specimen, the amount of each component (PVA, distilled water (DW), coolant and DMSO) used in the mixture, the total weight per sample that was used of this mixture and the total samples.

| N=33 | | PVA (g) | DW (g) | Coolant (g) | DMSO (g) | Mass/sample (g) | N |
|------|------------------------|---------|--------|-------------|----------|-----------------|---|
| A | 5% PVA | 2.25 | 45 | | | 45 | 3 |
| B | 10% PVA | 4.5 | 45 | | | 45 | 3 |
| C | 15% PVA | 6.75 | 45 | | | 45 | 3 |
| D | 90 g | 9 | 90 | | | 90 | 3 |
| E | 135 g | 13.5 | 135 | | | 135 | 3 |
| F | PVA:DW:C=10:(90:10) | 4.5 | 40.5 | 4.5 | | 45 | 3 |
| G | PVA:DW:C=10:(50:50) | 4.5 | 22.5 | 22.5 | | 45 | 3 |
| H | PVA:DW:C=10:(10:90) | 4.5 | 4.5 | 40.5 | | 45 | 3 |
| I | PVA:DW:DMSO=10:(90:10) | 4.5 | 40.5 | | 4.5 | 45 | 3 |
| J | PVA:DW:DMSO=10:(50:50) | 4.5 | 22.5 | | 22.5 | 45 | 3 |
| K | PVA:DW:DMSO=10:(10:90) | 4.5 | 4.5 | | 40.5 | 45 | 3 |

2.1.2. Mechanical Testing

In this section, the methods used to determine the mechanical characteristics of the specimens are presented.

Unconfined Compression Tests

In order to determine the mechanical characteristics of the samples, an unconfined compression test was used. In this test, a sample is compressed for a predetermined part (ΔL) of the total length (L_0) of the sample, which result in the so-called strain (ϵ). The resisting force for of the sample is collected. This force (F) and the total cross sectional area of contact between the specimen and the compression plate (A), determine the stress (σ) throughout the sample. Considering the resulting stress and strain

in the elastic region of the stress-strain curve, the Young's Modulus of the material can be calculated using equation 2.1.

$$E = \frac{\sigma}{\varepsilon} = \frac{F/A}{\Delta L/L_0} \quad (2.1)$$

These mechanical properties were calculated while assuming incompressibility which states that the volume of the samples remains constant while deforming. The unconfined compression test was set to compress the samples at a strain rate of 1 mm/min. A strain of 30% was applied on the specimens and the data was collected with a sample rate of 2000 Hz. An unconfined compression test was applied 3 times on each sample after every freeze-thaw cycle. This resulted in a total of 99 unconfined compression tests for each test session.

The goal of the data analysis was to construct a stress-strain curve of which visualize the mechanical behaviour of the material being compressed. A typical stress strain curve for a human soft tissue, which PVA mimics, can be seen in figure 2.2. The stress-strain curves shows that the material presents both non-linear as linear mechanical behaviour. First, the stress-strain curves starts with a non-linear region, also called the 'toe-region'. This region represents the first period of the compression tests in which the individual links or fibers, which can be folded, are not interconnected and lie loose, in the material are flattened or rearranged. After the toe-region, the linear or elastic region of the stress-strain curve starts. When the the links in the material are rearranged, extension of the links will occur resulting in a linear relationship between the stress and the strain. Based on the stress and strain results in this region, the Young's modulus can be determined by using formula 2.1. Consequently, a plastic region starts after the yield point in which small fractures occur in the links. Total fracture happen in the final region of the stress strain curve after the so-called failure point.

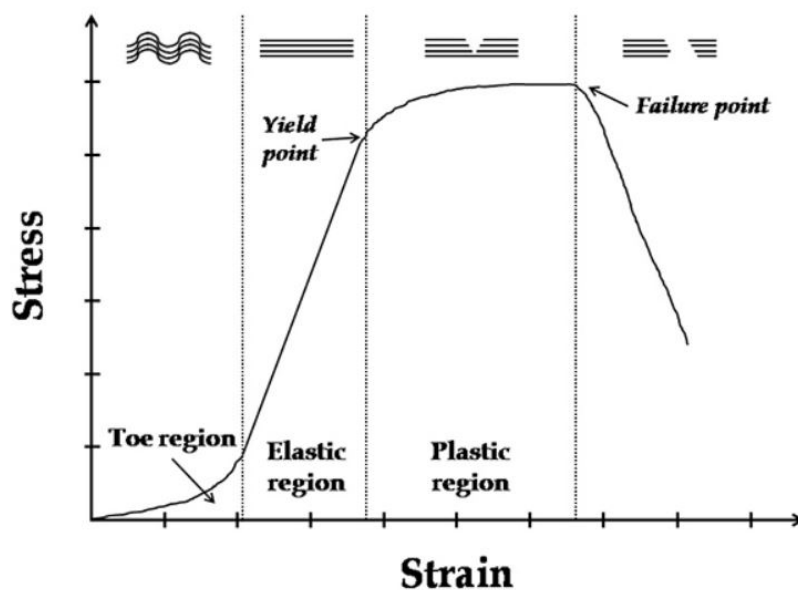


Figure 2.2: A typical stress-strain curve of a soft tissue starting with a non-linear toe-region followed by the linear elastic region. After the yield point, the plastic region occurs which is finished by a failure point. Figure derived from Korhonen Saarakkala (2011) [3]

Experimental Set-Up

The unconfined compression test set-up consisted of a linear stage (Aerotech ACT115, model MTC300) which was used to exert the force for compressing the specimens. A square metal plate with a cross sectional area of 1681 mm² was mounted on the linear stage to use as a compression plate. The samples were located on an elevator plate underneath the linear stage. A paper tissue was used between the elevator plate and the specimen to avoid the specimen from slipping away. A 22 N force sensor (Futek, iden. LSB200) was used to measure the resisting force of the samples.

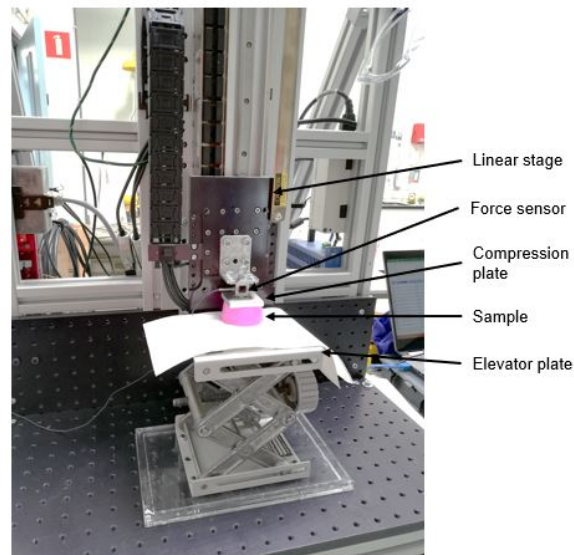


Figure 2.3: Experimental set up of the unconfined compression test. The sample is placed on tissue located on an elevator plate. A square metal plate functions as a compression plate.

2.1.3. Data Analysis

The raw data resulting from the unconfined compression tests consisted of the voltage output measured over time. To convert these voltage values to force output, the linear stage was calibrated. This was done by applying different weights onto the linear stage, varying from 0-300 g, and measuring the output voltage of these weights 3 times per weight. The corresponding gravitational force of the weights was calculated and the mean of the 3 measurements was determined. The mean force was used to generate a formula to convert the voltage to force. An overview example of the voltage output values resulting from the calibration of one test session are given in table 2.2. The corresponding determination of the converting formula is presented in figure 2.4. Before every test session, the linear stage was calibrated.

Table 2.2: The overview of the calibration values used to convert the voltage output to force. The mass of the weights, the mean of the 3 voltage outputs and the corresponding gravitational force (F_z) values are given.

| Mass (kg) | Mean Voltage (V) | F_z (N) |
|-----------|------------------|-----------|
| 0 | 0.0517 | 0 |
| 0.05 | 0.019467 | 0.4905 |
| 0.1 | -0.012233 | 0.981 |
| 0.15 | -0.0446 | 1.4715 |
| 0.2 | -0.07633 | 1.962 |
| 0.25 | -0.109433 | 2.4525 |
| 0.3 | -0.143467 | 2.943 |

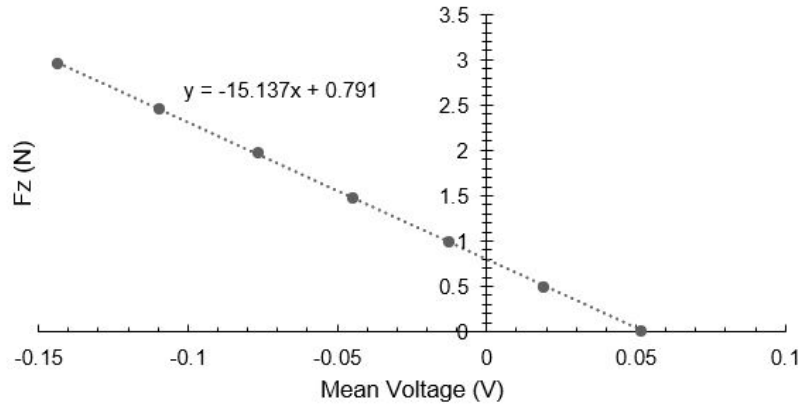


Figure 2.4: Gravitational force (F_z) in Newton vs. the mean voltage output in Volt. The resulting converting formula calculated by Excel is presented right next to the trend-line.

At the time of this study, the linear stage was unfortunately not able to measure the position of the moving compression plate. The current position (Δx) was therefore determined by hand by multiplying the passed time (Δt) by the strain rate (v) following equation 2.2.

$$\Delta x = v * \Delta t \quad (2.2)$$

The current position and the total length of the sample determined the strain. Besides this, the applied force calculated by converting the voltage output and the total cross sectional area of contact between the sample and the compression plate were used to calculate the stress. Subsequently, a stress-strain curve could be derived for each compression test. For each subgroup, 3 samples and 3 tests per sample resulted in 9 stress-strain curves per subgroup per test session. One mean stress-strain curve was derived of these 9 stress-strain curves. A moving-average fit was used to smooth this mean curve and eliminate the noise present in the data. The moving-average fit was applied based on a number of sampling points in which a low number of sampling points is more susceptible to noise but a high number of sampling points tends to eliminate important data. The moving-average was applied by using a low number of sampling points and increasing it after each run. After multiple runs, the optimal moving-average fit was found at a number of sampling points of 200. Therefore, the mean stress-strain curve of each subgroup was averaged over 200 sampling points with a moving-average fit. An example of a mean stress-strain curve including noise and the corresponding moving-average are shown in figure 2.5. All the following calculations were carried out on this filtered data.

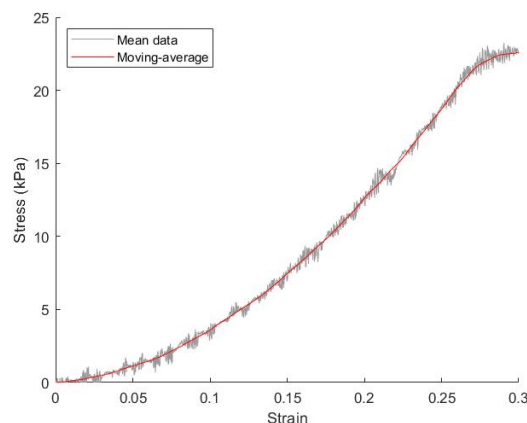


Figure 2.5: Mean stress values vs. strain values. The grey line represents the mean values of unfiltered data including noise. The red line shows the mean-average taken over 200 sampling points.

The Young's moduli of the samples were calculated according to equation 2.1. For each subgroup,

the Young's modulus was calculated by determining the strain value and its corresponding stress value in the elastic region, also known as the linear region, of the curve. The 9 stress-strain curves per subgroup produces 9 Young's moduli values. A mean value of these represents the Young's modulus of the specific subgroup after each cycle. The standard deviation was determined considering all 9 values.

2.1.4. Extra study: Storing PVA in Water

An extra test was incorporated into this part of the project. In the MISIT lab it is common to store PVA materials emerged into water between the freeze-thaw cycles. The reason for this is that it is thought that this would prevent dehydration of the materials. To test if this has any effect on the materials, an experiment was performed. In total, four samples were made of 10% PVA concentration without additives. These samples were divided into two groups: one group which was emerged into water between the freeze-thaw cycles and one group which was not emerged into water between the freeze-thaw cycles. The samples were stored in tap-water. After every freeze-thaw cycle and after every period between the freeze-thaw cycles, the samples weighted and the mass of the samples was determined. The protocol mentioned earlier in this part of the project was used for preparing the materials.

2.2. Results

2.2.1. Mechanical characteristics

In this section the results of the unconfined compression tests performed on the created PVA specimens are presented. Four different groups of PVA samples were made which each focused on the following: The first group studied the varying concentrations of PVA, the second group focused on the effect of volume of PVA, the third group studied the effect of a coolant additive and the last group focused on the effect of a DMSO additive. Unconfined compression tests were carried out after each freeze-thaw cycle for 7 cycles in total.

PVA Concentration

Three different PVA concentration were used in this project: 5%, 10% and 15%. Figure 2.6 and table 2.3 present the stress-strain curves and the Young's moduli of these different groups. An graph of the varying Young's moduli of these groups can be seen in figure 2.10a. Each stress-strain curve covers the mean average of 9 unconfined compression tests on 3 different samples. A maximal strain of 0.3 was applied. The Young's moduli were calculated using the results from a part of the elastic range of the stress-strain curve. This part was shown to be 0.2-0.25 or 0.15-0.2 in strain values. The stress values varied from 0 to 23.8 kPa. A variation in mechanical behaviour was observed in the stress-strain curves and the Young's moduli within the groups and between the groups. The stress-strain curves show a non-linear part at the beginning of the curves for all the graphs. This non-linear part shortens when the number of cycles increases. Besides this, a yield point is observed in all graphs, except the first three graphs of the 5% PVA concentration. The stress-strain curves show that the yield point occurs at a lower strain rate when the number of cycles increases. The elastic region in the curves also seem to steepen at higher cycles. Table 2.3 and figure 2.10a show more insight in the changes in Young's moduli of the samples. It is observed in the PVA concentration of 5% that higher cycles complied with higher and Young's moduli until the 6th cycle, with an exception of the 4th cycle. The other two groups also showed these results until the 4th cycle for both the 10% and the 15% concentration groups. An increase in Young's modulus is also observed for higher PVA concentrations.

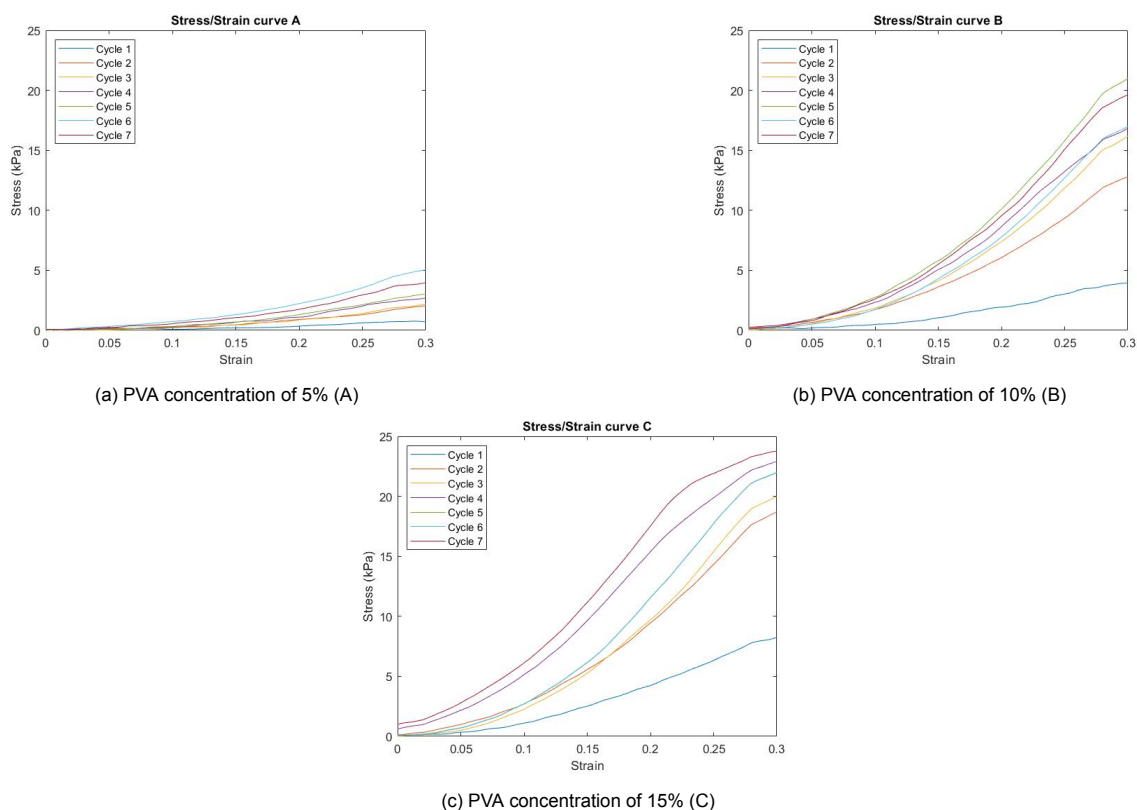


Figure 2.6: Stress-strain curves of all groups focusing on different PVA concentrations until a maximal strain of 0.3. The stress values varied from 0 to 23.8 kPa.

Volume

Three different volumes were used in this project based on the total weight: small, medium and large size, aka, 45 g, 90 g and 135 g. Each group had a PVA concentration of 10%. Figure 2.7 and 2.10b and table 2.4 present the stress-strain curves and the Young's moduli of these different groups. Each stress-strain curve covers the mean average of 9 unconfined compression tests on 3 different samples. A maximal strain of up to 0.3 was applied. Lower strains were applied for samples which were too stiff for the sensor to collect data. A minimum strain of 0.25 was applied on each sample. The Young's moduli were calculated using the results from a part of the elastic range of the stress-strain curve. This part was shown to be 0.2-0.25 or 0.15-0.2 in strain values. The stress values varied from 0 to 24.8 kPa. A variation in mechanical behaviour was observed in the stress-strain curves and the Young's moduli within the groups and between the groups. The stress-strain curves show a non-linear part at the beginning of the curves for all the graphs. This non-linear part shortens when the number of cycles increases. Besides this, a yield point is observed in all graphs, except the graphs after one cycle for each group. The stress-strain curves show that the yield point occurs at a lower strain rate when the number of cycles increases. The elastic region in the curves also seem to steepen at higher cycles. The variation in Young's moduli in these groups is seen in table 2.4 and figure 2.10b. A higher cycle value resulted in a higher Young's moduli until the 5th cycle for the small and medium group and until the 4th cycle for the large group. Between the groups, a mechanical difference was also observed, larger volumes tend to result in higher Young's modulus values.

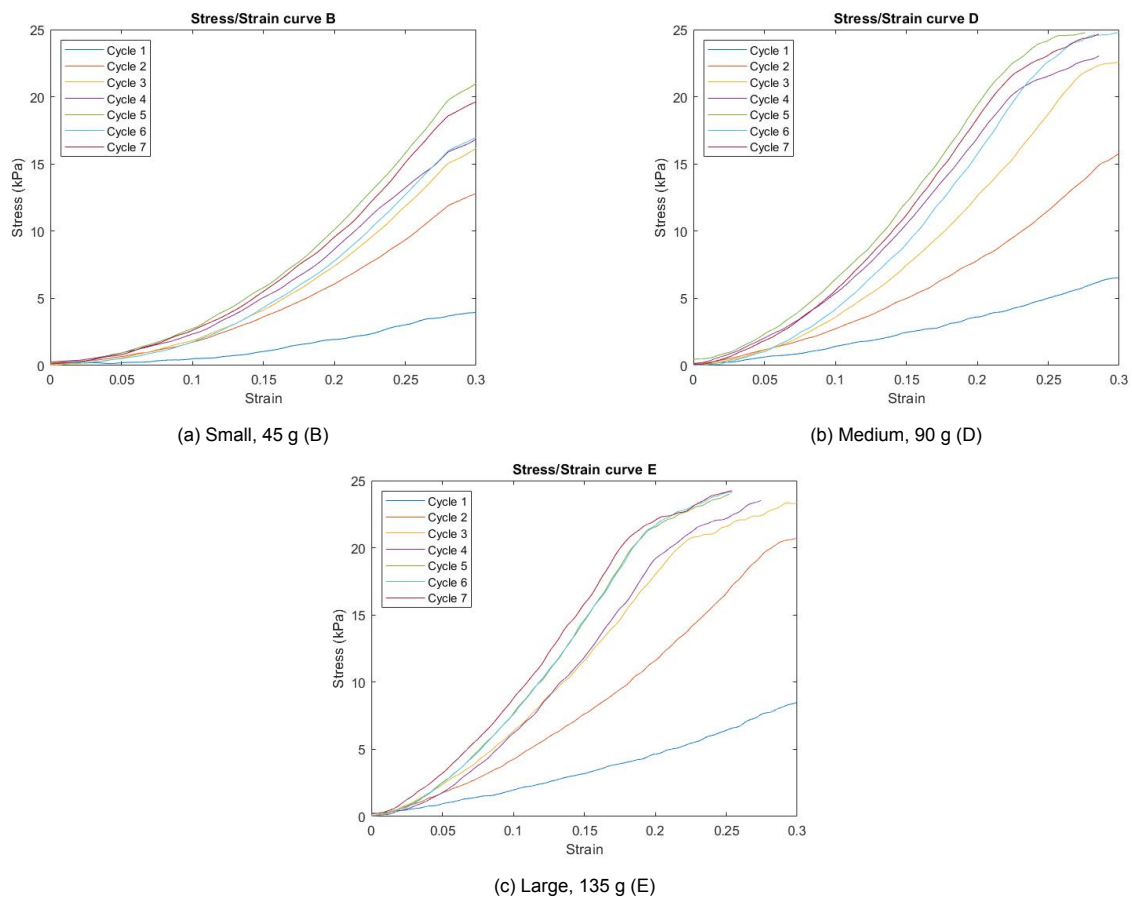


Figure 2.7: Stress-strain curves of all groups focusing on the effect of different volumes until a maximal strain of 0.3. The stress values varied from 0 to 24.8 kPa.

Coolant

Three different specimens were created in the coolant group. The first group had a low concentration of coolant (PVA:distilled water:coolant=10:(90:10)), the second a medium concentration of coolant (PVA:distilled water:coolant=10:(50:50)) and the third a high concentration of coolant (PVA:distilled wa-

ter:coolant=10:(10:90)). Each sample had a PVA concentration of 10%. Figure 2.8 and 2.10c and table 2.5 present the stress-strain curves and the Young's moduli of these different groups. Each stress-strain curve covers the mean average of 9 unconfined compression tests on 3 different samples. A maximal strain of 0.3 was applied on each sample. The Young's moduli were calculated using the results from a part of the elastic range of the stress-strain curve. This part was shown to be 0.2-0.25 or 0.15-0.2 in strain values. The stress values varied from 0 to 24.8 kPa. A variation in mechanical behaviour was observed in the stress-strain curves and the Young's moduli within the groups and between the groups. The stress-strain curves show a non-linear part at the beginning of the curves for all the graphs. This non-linear part shortens when the number of cycles increases. Besides this, a yield point is observed in all graphs. The stress-strain curves show that the yield point occurs at a lower strain rate when the number of cycles increases. The elastic region in the curves also seem to steepen at higher cycles. Table 2.5 and figure 2.10c give more insight in the variations of the Young's moduli. A variation in mechanical behaviour was observed within the groups. A higher cycle value resulted in a higher Young's modulus until the 6th cycle for both the low and medium group. This increase was observed until the 7th cycle for the high amount of coolant group. A mechanical difference can also be observed between the groups. The results show that a higher concentration of coolant is associated with higher Young's moduli. When comparing the coolant group with the 10% PVA concentration, denoted as 'Base' in figure 2.10c, it can be seen that the coolant group reaches higher Young's moduli than the PVA without coolant.

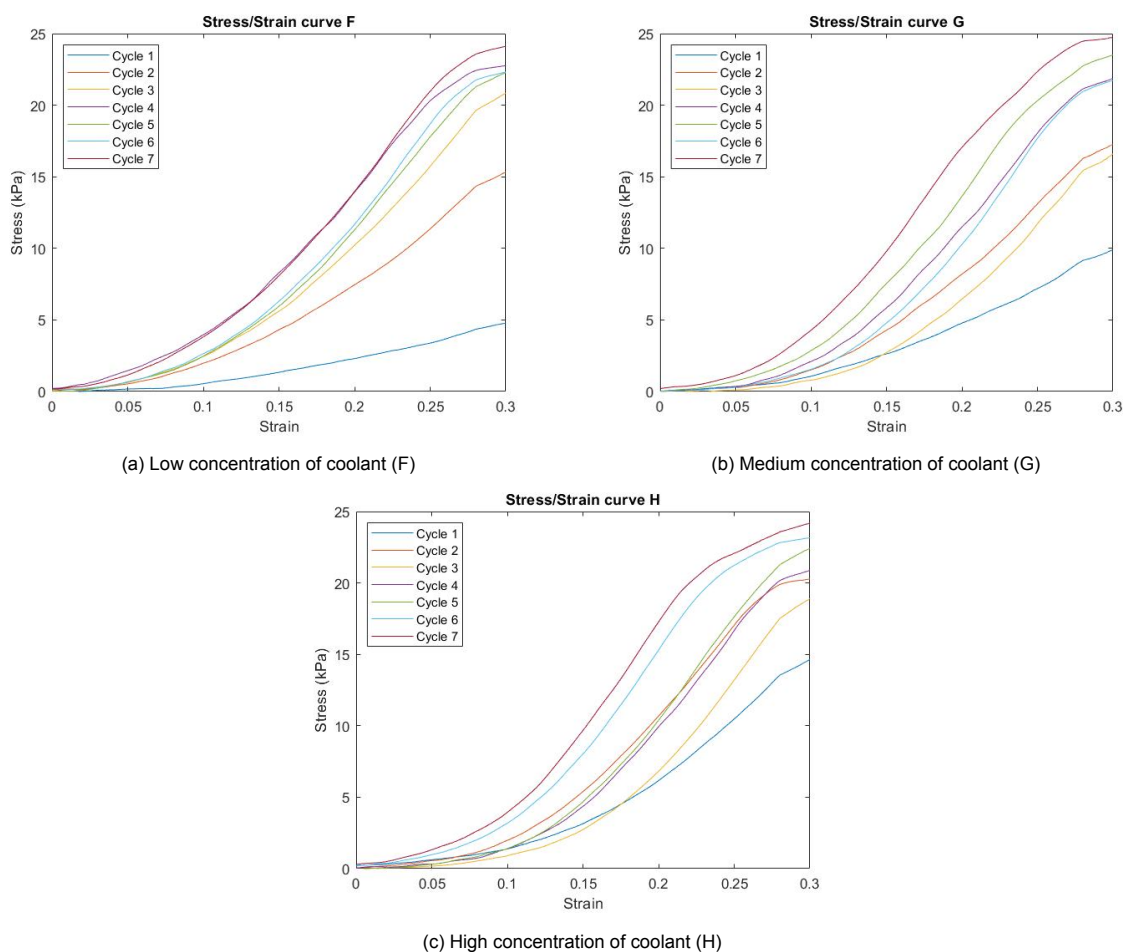


Figure 2.8: Stress-strain curves of all groups focusing on the effect of different coolant concentrations until a maximal strain of 0.3. The stress values varied from 0 to 24.8 kPa.

DMSO

Three different specimens were created in the DMSO group. The first group had a low concentration of DMSO (PVA:distilled water:DMSO=10:(90:10)), the second a medium concentration of DMSO

(PVA:distilled water:DMSO=10:(50:50)) and the third a high concentration of DMSO (PVA:distilled water:DMSO=10:(10:90)). Each sample had a PVA concentration of 10%. Figure 2.9 and table 2.6 present the stress-strain curves and the Young's moduli of these different groups. Each stress-strain curve covers the mean average of 9 unconfined compression tests on 3 different samples. A maximal strain of up to 0.3 was applied. Lower strains were applied for samples which were too stiff for the sensor to collect data. A minimum strain of 0.25 was applied on each sample. The Young's moduli were calculated using the results from a part of the elastic range of the stress-strain curve. This part was shown to be 0.2-0.25 or 0.15-0.2 in strain values. The stress values varied from 0 to 23.3 kPa. The stress-strain curves show a non-linear part at the beginning of the curves for all the graphs. This non-linear part shortens when the number of cycles increases. Besides this, a yield point is observed in all graphs. The stress-strain curves show that the yield point occurs at a lower strain rate when the number of cycles increases for group I and K. The occurrence of the yield point in group J varies among the number of cycles. The elastic region in the curves seem to steepen at higher cycles. A variation in mechanical behaviour was observed within the groups. A higher cycle value resulted in a higher Young's modulus until the 6th and 7th cycle for the low and high concentration of DMSO groups respectively. The group with the medium amount of DMSO showed many variations in the Young's modulus and high standard deviation levels. When comparing the DMSO groups with the 10% PVA concentration in figure 2.10d, it can be seen that the low amount of DMSO groups show similar Young's modulus levels to the 10% PVA group. The stiffness values of the medium and high amount of DMSO groups seem a lot higher and slightly higher, respectively.

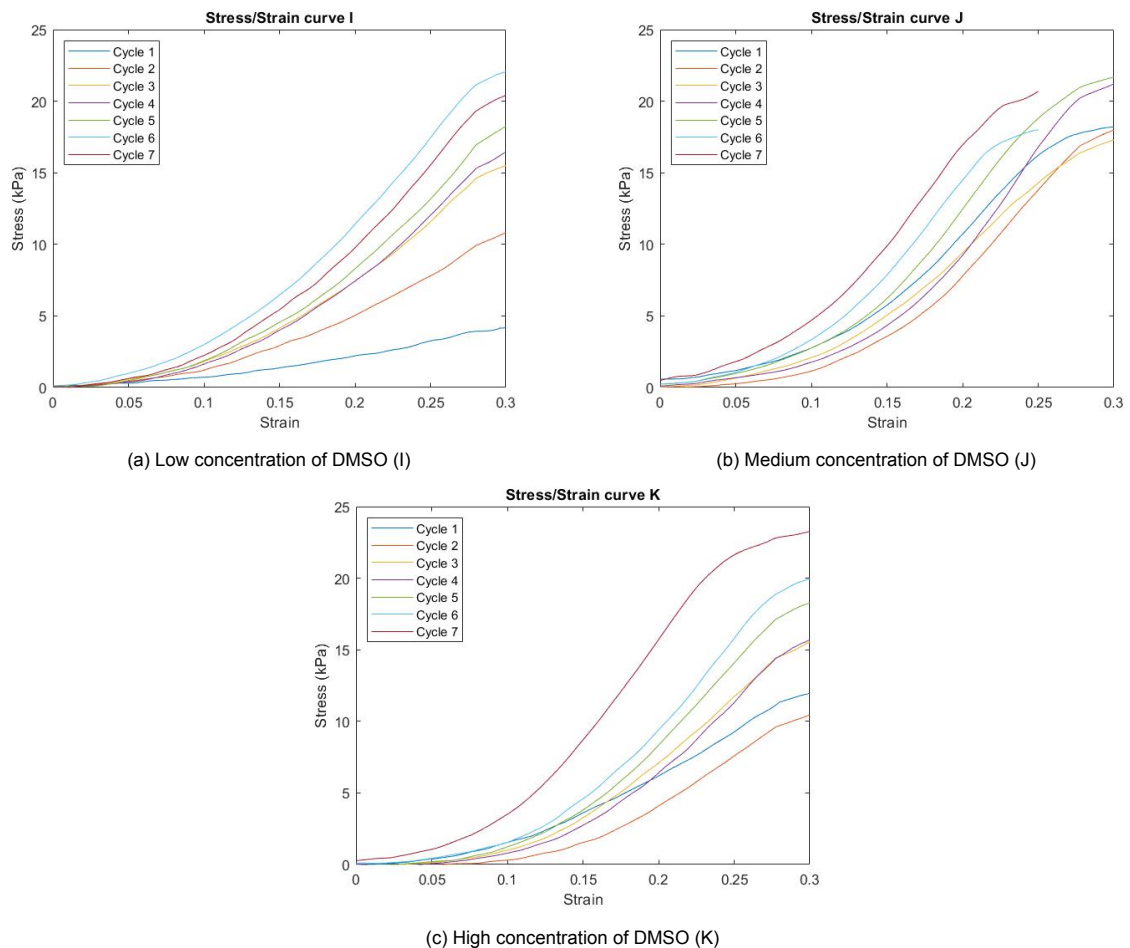


Figure 2.9: Stress-strain curves of all groups focusing on different DMSO concentrations until a maximal strain of 0.3. The 'Base' line presents the graph of group B, 10% PVA without additives.

Table 2.3: Mean Young's modulus values (E) in kPa per PVA concentration group: 5% (A), 10% (B) and 15% (C). The values were measured after each freeze-thaw cycle for a total of 7 cycles. The standard deviation (SD) is denoted. Also, the part of the elastic region (ER), given in strain values, over which the Young's modulus was calculated is given.

| | A | | | B | | | C | | |
|---------|-------|------|----------|--------|-------|----------|--------|-------|----------|
| | E | SD | ER | E | SD | ER | E | SD | ER |
| Cycle 1 | 5.57 | 1.56 | 0.2-0.25 | 21.81 | 4.19 | 0.2-0.25 | 41.78 | 6.81 | 0.2-0.25 |
| Cycle 2 | 7.18 | 1.85 | 0.2-0.25 | 65.91 | 5.29 | 0.2-0.25 | 97.68 | 15.01 | 0.2-0.25 |
| Cycle 3 | 10.79 | 5.83 | 0.2-0.25 | 89.49 | 10.69 | 0.2-0.25 | 114.08 | 19.91 | 0.2-0.25 |
| Cycle 4 | 18.43 | 7.16 | 0.2-0.25 | 91.74 | 27.50 | 0.2-0.25 | 114.85 | 24.90 | 0.15-0.2 |
| Cycle 5 | 16.21 | 5.91 | 0.2-0.25 | 113.65 | 12.79 | 0.2-0.25 | 123.55 | 15.45 | 0.2-0.25 |
| Cycle 6 | 26.45 | 3.28 | 0.2-0.25 | 98.65 | 18.58 | 0.2-0.25 | 123.57 | 15.45 | 0.2-0.25 |
| Cycle 7 | 24.12 | 5.10 | 0.2-0.25 | 110.66 | 18.07 | 0.2-0.25 | 127.42 | 8.47 | 0.15-0.2 |

Table 2.4: Mean Young's modulus values (E) in kPa per volume group: small (B), medium (D) and large (E). The values were measured after each freeze-thaw cycle for a total of 7 cycles. The standard deviation (SD) is denoted. Also, the part of the elastic region (ER), given in strain values, over which the Young's modulus was calculated is given.

| | B | | | D | | | E | | |
|---------|--------|-------|----------|--------|------|----------|--------|-------|----------|
| | E | SD | ER | E | SD | ER | E | SD | ER |
| Cycle 1 | 21.81 | 4.19 | 0.2-0.25 | 28.26 | 2.95 | 0.2-0.25 | 35.45 | 6.46 | 0.2-0.25 |
| Cycle 2 | 65.91 | 5.29 | 0.2-0.25 | 74.06 | 4.37 | 0.2-0.25 | 100.13 | 6.26 | 0.2-0.25 |
| Cycle 3 | 89.49 | 10.69 | 0.2-0.25 | 121.71 | 3.29 | 0.2-0.25 | 128.48 | 9.86 | 0.15-0.2 |
| Cycle 4 | 91.74 | 27.50 | 0.2-0.25 | 128.34 | 5.66 | 0.15-0.2 | 146.60 | 12.72 | 0.15-0.2 |
| Cycle 5 | 113.65 | 12.79 | 0.2-0.25 | 145.16 | 6.10 | 0.15-0.2 | 140.19 | 17.10 | 0.15-0.2 |
| Cycle 6 | 98.65 | 18.58 | 0.2-0.25 | 134.55 | 8.59 | 0.15-0.2 | 140.51 | 24.19 | 0.15-0.2 |
| Cycle 7 | 110.66 | 18.07 | 0.2-0.25 | 143.83 | 8.61 | 0.15-0.2 | 124.41 | 13.97 | 0.15-0.2 |

Table 2.5: Mean Young's modulus values (E) in kPa per coolant group: low (F), medium (G) and high (H) concentration of coolant. The values were measured after each freeze-thaw cycle for a total of 7 cycles. The standard deviation (SD) is denoted. Also, the part of the elastic region (ER), given in strain values, over which the Young's modulus was calculated is given.

| | F | | | G | | | H | | |
|---------|--------|-------|----------|--------|-------|----------|--------|-------|----------|
| | E | SD | ER | E | SD | ER | E | SD | ER |
| Cycle 1 | 21.66 | 3.74 | 0.2-0.25 | 48.37 | 6.29 | 0.2-0.25 | 86.39 | 8.94 | 0.2-0.25 |
| Cycle 2 | 78.17 | 6.43 | 0.2-0.25 | 98.14 | 6.76 | 0.2-0.25 | 127.08 | 10.70 | 0.2-0.25 |
| Cycle 3 | 110.30 | 10.06 | 0.2-0.25 | 105.15 | 11.80 | 0.2-0.25 | 127.73 | 15.09 | 0.2-0.25 |
| Cycle 4 | 112.46 | 11.68 | 0.15-0.2 | 131.09 | 9.92 | 0.2-0.25 | 134.67 | 21.57 | 0.2-0.25 |
| Cycle 5 | 129.95 | 9.98 | 0.2-0.25 | 133.62 | 16.26 | 0.2-0.25 | 144.90 | 18.86 | 0.2-0.25 |
| Cycle 6 | 140.37 | 33.49 | 0.2-0.25 | 148.17 | 12.31 | 0.2-0.25 | 145.40 | 18.30 | 0.15-0.2 |
| Cycle 7 | 117.52 | 13.55 | 0.15-0.2 | 145.25 | 19.58 | 0.15-0.2 | 151.91 | 13.64 | 0.15-0.2 |

Table 2.6: Mean Young's modulus values (E) in kPa per DMSO group: low (I), medium (J) and high (K) concentration DMSO. The values were measured after each freeze-thaw cycle for a total of 7 cycles. The standard deviation (SD) is denoted. Also, the part of the elastic region (ER), given in strain values, over which the Young's modulus was calculated is given.

| | I | | | J | | | K | | |
|---------|--------|-------|----------|--------|-------|----------|--------|-------|----------|
| | E | SD | ER | E | SD | ER | E | SD | ER |
| Cycle 1 | 20.85 | 2.16 | 0.2-0.25 | 110.03 | 43.26 | 0.2-0.25 | 61.50 | 7.07 | 0.2-0.25 |
| Cycle 2 | 55.32 | 3.57 | 0.2-0.25 | 120.36 | 34.12 | 0.2-0.25 | 69.69 | 6.26 | 0.2-0.25 |
| Cycle 3 | 82.94 | 5.77 | 0.2-0.25 | 97.68 | 25.74 | 0.2-0.25 | 92.65 | 8.51 | 0.2-0.25 |
| Cycle 4 | 92.01 | 9.76 | 0.2-0.25 | 151.15 | 29.30 | 0.2-0.25 | 98.23 | 5.19 | 0.2-0.25 |
| Cycle 5 | 97.47 | 13.80 | 0.2-0.25 | 126.79 | 43.39 | 0.2-0.25 | 114.94 | 10.13 | 0.2-0.25 |
| Cycle 6 | 120.92 | 8.26 | 0.2-0.25 | 132.57 | 46.69 | 0.15-0.2 | 127.75 | 20.29 | 0.2-0.25 |
| Cycle 7 | 115.51 | 9.39 | 0.2-0.25 | 141.31 | 28.73 | 0.15-0.2 | 140.10 | 7.71 | 0.15-0.2 |

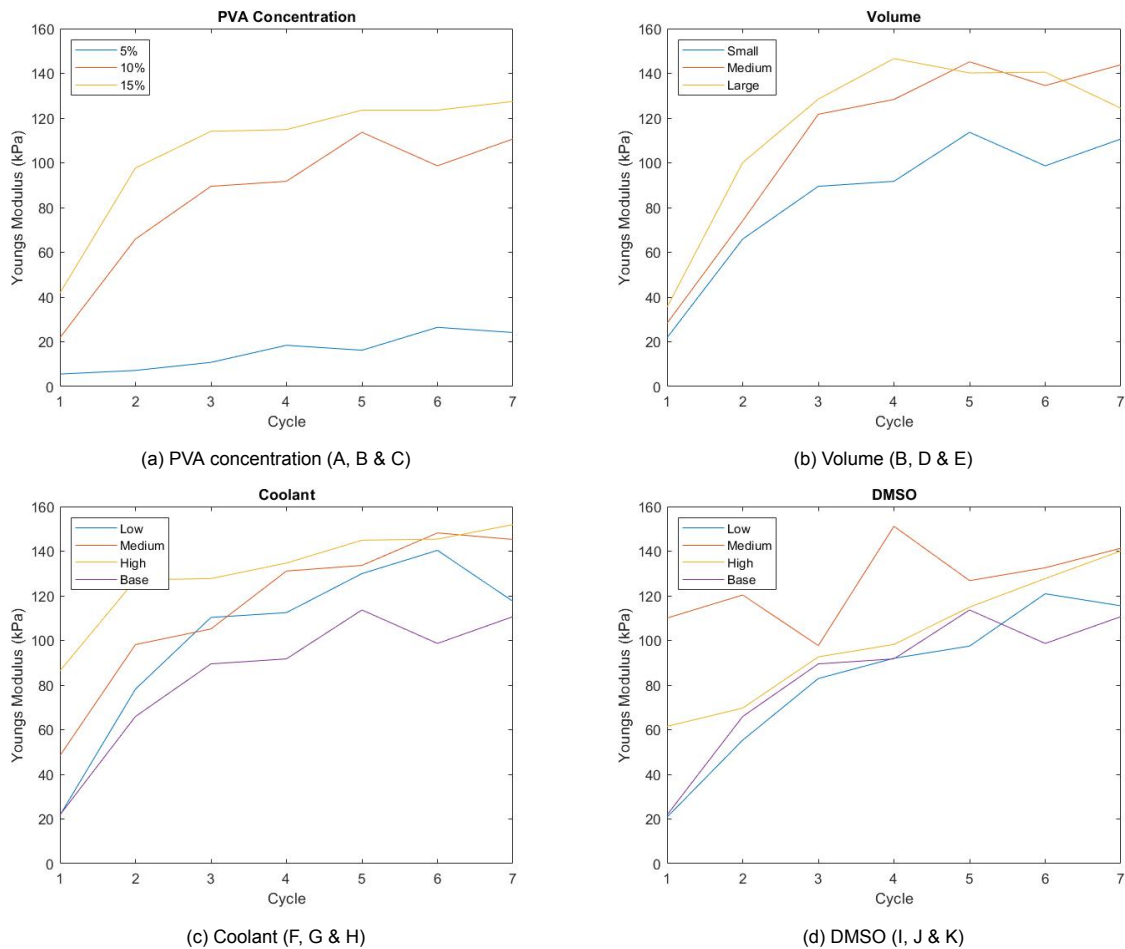


Figure 2.10: Stress-strain curves of all groups focusing on different PVA concentrations until a maximal strain of 0.3. The stress values varied from 0 to 23.8 kPa.

2.2.2. Noise identification

Within sample analysis

Each sample underwent 3 compression tests per cycle. For each sample, the 3 different tests performed per cycle were compared with each other to identify possible noise. For sample I3 after the 4th cycle, one test of the 3 missed, resulting in two tests performed on this sample at this point in the experiment. This was also the case for sample F3 after the 6th cycle. After the 4th cycle, the third test performed on sample B3 showed a higher stress-strain curve than the first and second test. This also counted for the second test performed on sample C2 after the first cycle. Overall, the tests per sample showed that the first test performed seems slightly higher than test two and three.

Between samples analysis

Every subgroup consisted of three samples in total. The stress-strain curves between samples within one subgroup were compared to identify possible noise. It was observed that sample B2 and C1 had a higher and lower stress-strain curve respectively compared to the other samples in the subgroup after the 4th cycle. It was also observed that the samples in group J showed varying stress-strain curves between the sample groups after the first, 4th, 5th and 6th cycle. This included higher or lower stress-strain curves but also differences in shape between the stress-strain curves.

2.2.3. Comparison with literature

A literature study into the mechanical characteristics of prostate tissue and adipose tissue was conducted to compare these results with the results from this study. An overview of these values and corresponding studies can be found in table 1.1 and 1.2. For prostate tissue, these results show a

Young's modulus range of 2.2 - 70 kPa for healthy prostate tissue, 24 - 40 kPa for prostate tissue with benign hyperplasia and 62.9 - 221 kPa for cancerous prostate tissue. The goal of this project is to create a cancerous prostate phantom model. Therefore, a material with a Young's modulus of 62.9 - 221 kPa is wished. Based on table 2.3, 2.4, 2.5 and 2.6, the materials from group B (cycle 2-7), C (cycle 2-7), D (cycle 2-7), E (cycle 2-7), F (cycle 2-7), G (cycle 2-7), H (cycle 1-7), I (cycle 3-7), J (cycle 1-7) and K (cycle 2-7) would fall into this range. Depending on the wishes for colour, transparency and the wish to stop swelling for the usage of moulds, one can pick a specific material. For adipose tissue, the results from literature suggest a Young's modulus range of 0.12 - 50 kPa. The results show in the tables 2.3, 2.4, 2.5 and 2.6, that group A (cycle 1-7), group B (cycle 1), C (cycle 1), D (cycle 1), E (cycle 1), F (cycle 1), G (cycle 1) and I (cycle 1) have Young's modulus values that would fall into this range.

2.2.4. Visual characteristics

After every freeze-thaw cycle a photo was taken of each specimen. By doing this, visual changes could be observed between the cycles for the specimens.

PVA concentration

The PVA samples without additives were found to be white. For group A and B, also known as, 5% PVA and 10% PVA, the initial samples were slightly translucent. The samples became less translucent after each cycle. This also happened for group F (low concentration of coolant). An example is shown in figure 2.11. A few deformities were found in the PVA samples. The group with the low concentration of PVA, group A, was found to be very soft after the first cycle which caused it to collapse to an extent and resulted in an decreased height of the samples. The sample of the second sample of the 10% PVA group (sample B2) was found to be askew. This was likely the cause of misplacement of the samples in the freezer during the first cycle. The PVA samples developed small bumps at the bottom of the sample (at the opening of the holder) which increased in size slightly after each cycle. The development of a protrusion could be a result of swelling. These bumps were small in size and did not need to be removed. At the first cycle, the PVA samples contained very smooth edges. After each cycle, these edges became less smooth.

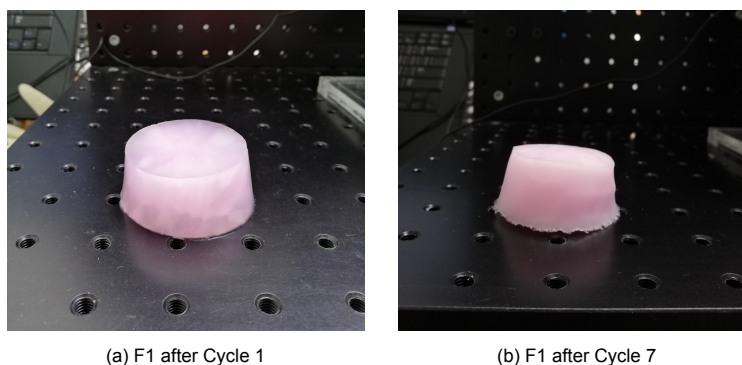


Figure 2.11: A decrease of translucency was observed after the number of cycles increased. (a) shows a low amount of coolant sample after one freeze-thaw cycle, (b) shows the same sample after 7 freeze-thaw cycles.

Volume

As mentioned above, the PVA samples were found to be white. Also, group D and E also started off with smooth edges which became less smooth with increasing cycle. After the second cycle, a bump developed in two samples of the large volume group (group E) as can be seen in figure 2.12. This bump was located on the bottom of the sample (at the side of the opening of the holder). It was protruding in such a way that the sample could not stand without falling on its side. Because of this reason, the bumps were cut off these specimens. This bump also developed in the medium volume group (group D) and the third sample of the high volume group (group E) after the third cycle and was then cut off. At the first cycle, the PVA samples contained very smooth edges. After each cycle, these edges became less smooth.

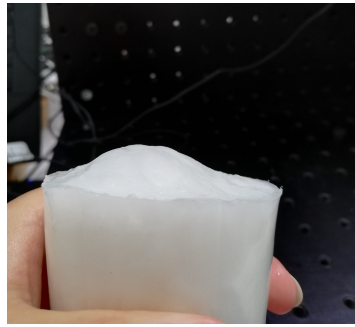
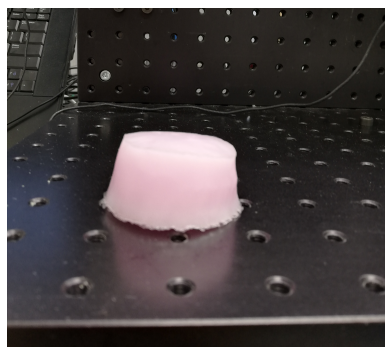


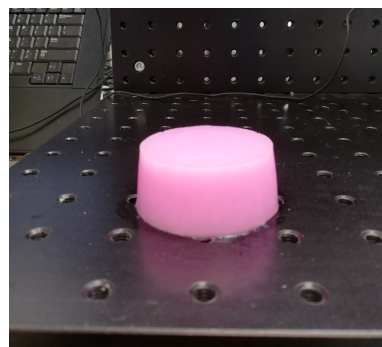
Figure 2.12: A bump protruding from the bottom of sample E1. The bump developed after the second freeze-thaw cycle in the large volume group. The bump was removed after this cycle.

Coolant

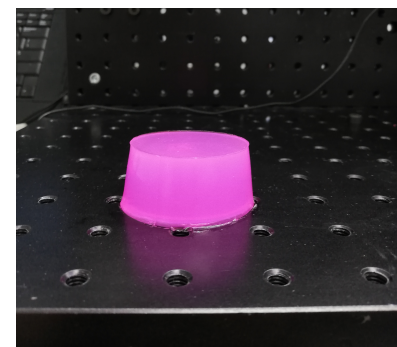
The coolant which was added to the coolant groups had a bright pink colour. This caused the samples in the coolant group to have a pink colour as well. The samples with a low concentration of coolant (group F) had a light pink colour. An increase in coolant concentration showed a brighter pink colour in the samples as can be seen in figure 2.13. Group H was also found to show signs of translucency. As mentioned above, the low concentration of coolant group (group F) started off with slight signs of translucency, which disappeared after the second cycle as shown in figure 2.11. A few deformities were found in the coolant samples. One sample of the medium concentration of coolant group (G3) and two samples of the high concentration of coolant group (H2 and H3) were found to be askew. Group F also developed a small bump at the bottom of the sample which remained small in size and was not removed. Group G and H did not develop a bump or showed any signs of swelling. All samples contained smooth edges after the first cycle. The edges of group F became less smooth with increasing cycle, however, the edges of group G and H remained smooth.



(a) Low concentration of Coolant



(b) Medium concentration of Coolant



(c) High concentration of Coolant

Figure 2.13: Pictures of the different specimens in the coolant group. (a) shows group F, (b) shows group G and (c) shows group H. Different levels in brightness of the colour pink were found between the groups.

DMSO

DMSO was used as additive to observe its effect on the translucency of the samples. Pictures of the differences between the DMSO groups can be seen in figure 2.14. The samples with a low concentration of DMSO (group I) showed no visible signs of translucency and were found to be white coloured. The material of this group was found to be brittle and therefore fragile. The group with a medium concentration of DMSO (group J) was found to be slightly more translucent than the low concentration of DMSO group. These samples were found to be turbid but not fully translucent. The last group with the high concentration of DMSO (group K) were found to be more translucent than the other DMSO groups. The samples were slightly turbid but still sufficiently translucent. The medium concentration of DMSO group was hard to remove from the cups after the first cycle. The removal induced deformities for the first and second samples of this group. The first sample (J1) contained a small scratch on the head (located at the bottom of the holder) while the second sample (J2) had a severe damaged head. The third sample (J3) was not damaged during the removal but was found to be askew. All the DMSO

samples did not develop any bumps nor did they show signs of swelling. The samples also remained smooth during the entire experiment.

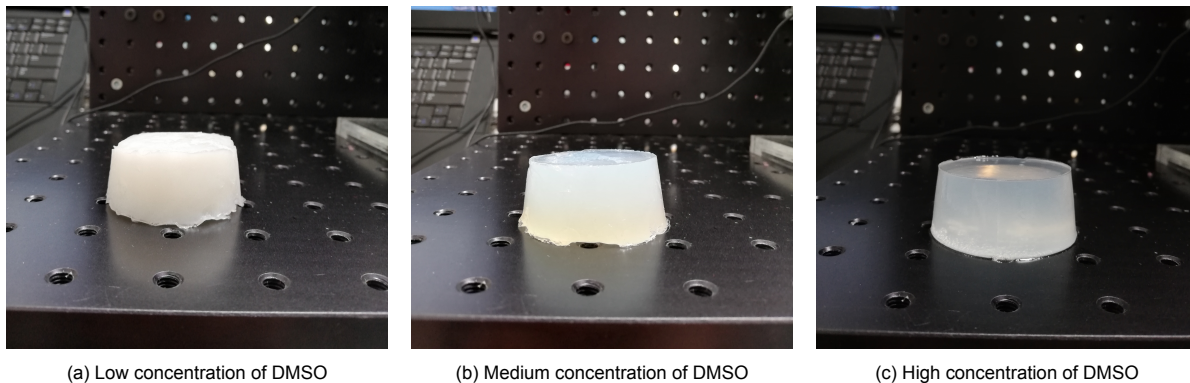


Figure 2.14: Pictures of the different specimens in the DMSO group. (a) shows group I, (b) shows group J and (c) shows group K. Different levels of translucency were found between the groups.

2.2.5. Mass fluctuations

After every freeze-thaw cycle, the mass of each specimen was noted. With this information, the mass increase/decrease was observed. An overview of the mass fluctuations can be found in figure 2.15. Each column represents the mean mass of the given group after the specified cycle. Only in the high concentration DMSO samples (group K) a mass increase was found after the first two freeze-thaw cycles. The highest mass decrease was found in the 5% PVA samples (group A) after the second cycle.

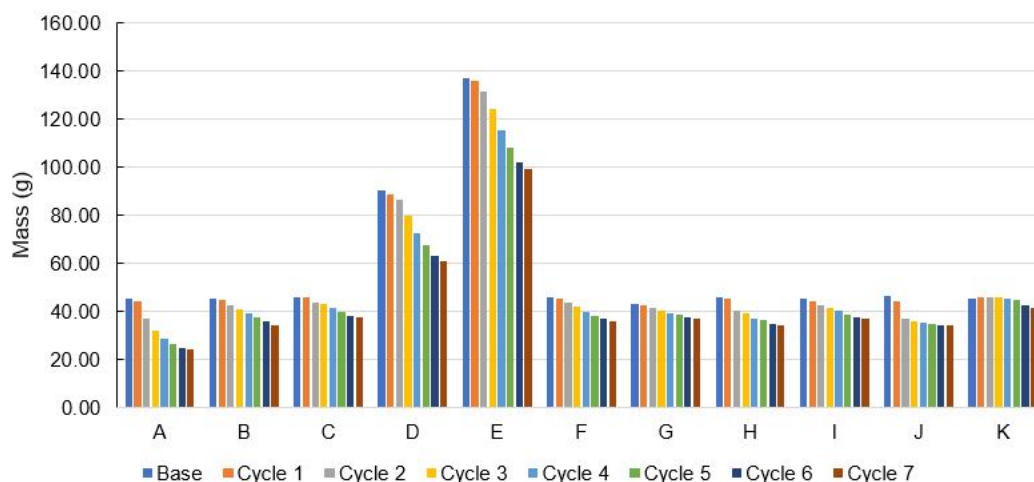


Figure 2.15: Decrease in mass occurred for every group after each cycle. The mass decrease was the most evident in group A and the least evident in group K.

2.2.6. Extra study: Storing PVA in water

Four extra samples of 10% PVA were made for an extra experiment. These samples were divided into two groups: one group which was emerged into water in the period between the freeze-thaw cycles (group Y) and one group which was not emerged into water in the period between the freeze-thaw cycles (group X). The results were determined by measuring their weight after each cycle and after each period between cycles. An overview of the determined weight of each samples after these periods can be seen in figure 2.16. The results show mass fluctuations for all samples over time. The greatest mass fluctuations occur during the period between freeze-thaw cycles for the group that was emerged into water (group Y). Group X shows a slight decrease in mass over time.

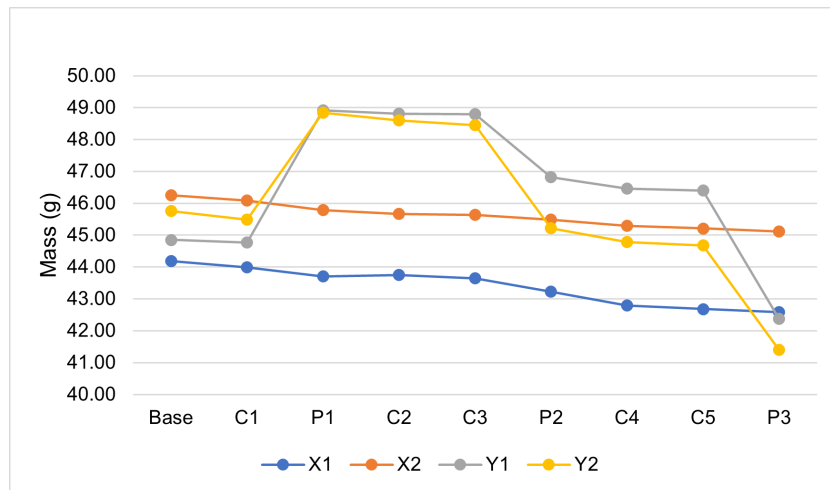


Figure 2.16: Overview of the mass fluctuations per sample. Group X describes the samples which were not emerged into water in the period between the freeze-thaw cycles and group Y describes the samples which were emerged into water in the period between the freeze-thaw cycles. The Y-axis denotes the freeze-thaw cycles (C1 - C5) and the periods between the freeze-thaw cycles (P1 - P3). Mass fluctuations occurred for all samples with the most fluctuations happening in the periods between the freeze-thaw cycles for group Y.

2.3. Discussion

The goal of this project is to develop a mechanically tissue-mimicking phantom cancerous prostate model of PVA material. To find the optimal mechanical characteristics of PVA, a material study was conducted. The goal of this part of the study was to determine the mechanical characteristics of varying PVA specimens. This was achieved by mechanically testing multiple PVA samples, varying in composition, with or without additives, by performing unconfined compression tests. Four different groups in total were tested, one group varying in PVA concentration, one group varying in volume, one group differing in amount of coolant additive and one group varying in amount of DMSO additive. This section discusses the results of the material study in this project.

The stress-strain curves of the materials consisted of a non-linear part, an linear or elastic part and a yield point. Comparing these graphs to figure 2.2, indicates that these materials show similar mechanical behaviour to a human tissue when undergoing deformation. This is also supported by the study of Noguchi et al. (1991) which demonstrated the biocompatible qualities of PVA and its similar mechanical characteristics to human tissue [42]. These findings show that PVA, in terms of mechanical behaviour, is able to mimic human tissue.

The results show that the Young's moduli increase after each freeze-thaw cycle until minimally the 4th cycle. This could be due to the increased crosslinks, contributing to the strength and stiffness of the material, that are formed under low temperatures during each freeze-thaw cycle. These findings prove that freeze-thaw cycles can be used to adapt the Young's modulus of PVA material in a controlled matter. This finding is confirmed by multiple studies which investigated the effect of freeze-thaw cycles on the mechanical characteristics of PVA [43, 44, 51]. The results also show that the Young's moduli increase for higher concentrations of PVA. Higher stiffness of the material can be contributed to more crosslinks that have formed due to the increase of particles per volume unit. The study by Wahab et al. (2019) found higher Young's moduli for higher concentrations of PVA and thereby confirms this finding [52]. Larger volumes were also found to give higher Young's moduli values. These results for larger volumes can also be attributed to the development of more crosslinks in the larger material. Larger volumes therefore cause higher stiffness values.

The results also show higher stiffness values for PVA material with coolant additive compared to PVA without coolant additive. This is in contrast with the original hypothesis. It was hypothesized that adding coolant would decrease the stiffness values. Lowering the freezing point, which can be an effect of adding coolant, would cause a decrease in the formation of crosslinks and therefore a lower stiffness value of the material. However, during the experiment it was observed that the samples including the coolant were all frozen during the freezing periods. The coolant did therefore not prevent the total freezing of the materials. An explanation for the higher Young's moduli can lie in the structure formula of ethylene glycol, present in the coolant. This material consists of two OH-groups which are each able to form 3 hydrogen bonds, which makes a total of 6 hydrogen bonds possible. This is equal to the amount of hydrogen bonds that water can form. However, ethylene glycol also consists of two CH_2 -groups which makes it an organic structure. As mentioned in the introduction of this project, freeze-thaw cycles induce the formation of crosslinks based on hydrogen bonds between organic structures. PVA solved in water creates the crosslinks between the PVA molecules. However, when coolant is added, more organic structures with a hydrogen bonding group are present and therefore, more crosslinks can be formed. In this case, besides the PVA-PVA crosslinking, formation of crosslinks between PVA and ethylene glycol can also occur. This would increase the number of crosslinks in the material and can therefore cause a higher stiffness value. It can be concluded that using coolant as solvent for PVA, compared to distilled water, increases the Young's modulus of the material.

DMSO was found to have a slightly increasing effect on the Young's modulus values when comparing these materials to PVA without additive. Since DMSO is also an organic structure, as is ethylene glycol, one would expect that the Young's moduli for the DMSO material would have increased more. The results show however that adding coolant results in a higher increase in Young's modulus than DMSO does. This can be explained by the structure formula of DMSO. As mentioned before, both water and ethylene glycol have two OH-groups which can in total form 6 hydrogen bonds. The hydrogen bonding part in DMSO consists of an oxygen group (O) which is able to form two hydrogen bonds. This

causes the formation of less hydrogen bonds compared to the coolant materials. Since the formation of crosslinks is based on hydrogen bonds, this also results in less formation of crosslinks and therefore lower increase in Young's modulus. It can be concluded that using DMSO as a solvent for PVA, compared to distilled water, slightly increases the stiffness values, but not as much as adding coolant does.

It should be noted that the samples group J were damaged or had a skewed head. The DMSO samples were stuck tightly to their surrounding cups and therefore difficult to remove undamaged. The stress-strain curves of these samples also showed frequent present noise in the sense that they did not all match in height and shape. The varying Young's moduli and high standard deviation levels confirm the fact that the results from these tests are not reliable. This makes it hard to draw any conclusion on this group.

It was observed that the stress-strain curve of the first test of the 3 tests performed on each sample was higher than the following two tests. This results was however minimal and can be explained by the presence of more water in the material during the first test. During the first test water was pressed out. Less water in the material can cause lower stiffness levels and lower stress-strain curves. This result was however minimal. It was also observed that the noise frequency in each individual test, as seen in figure 2.5, was reasonably high. A moving average was used to filter this noise. The noise in the raw data can be decreased by using other improved experimental materials. However, for this study, the results are reliable due to the minimal noise present per sample and the used filter. Therefore the used materials and results are judged to be sufficient reliable.

The visual characteristics clearly show differences between the material groups. PVA shows to have a white color while the added coolant causes a pink color for the material which increase in intensity with more added coolant. Also, the results show that DMSO induce transparency in the material. A high concentration of DMSO is necessary to achieve sufficient transparency (demiwater:DMSO ratio of 10:90). The pictures also show that swelling and less smooth edges emerged in the PVA material without additives and PVA material with little added coolant. These swellings and unsmooth edges occurred more often as the freeze-thaw cycles increased. As mentioned before, PVA is known to be a heterogeneous material. This heterogeneity might cause the swelling and the unsmooth edges. This would also explain the increase in occurrence of the swelling and unsmooth edges with increasing freeze-thaw cycles as more crosslinks occur which are known to increase the heterogeneity. Coolant and DMSO, when added in sufficient amounts, might have a smoothening influence over the material. Further research is needed to examine any effects on the heterogeneity of the material.

The mass fluctuations of the materials all show a decrease in total mass over time. The 5% PVA material shows the most mass decrease of all samples. The mass decrease can be explained by drying of the material over time. This also explains the highest mass decrease of the 5% material which contains the most water of all the samples and is therefore more prone to drying. Keeping the material in an air-tight casing during the storing periods in the experiment can prevent dehydration. This keeps the mass of the material as constant as possible.

An extra study in the effect of adding tap water to PVA during the storing periods was performed on four PVA samples with equal concentrations. During the storage periods in the weekends, two of these samples were submerged into tap water while the other two were stored without tap water. The mass of these samples was determined after each cycle and after each weekend. Unfortunately, due to technical difficulties, it was not possible to determine the Young's modulus of these materials during these experiments. The extra study on the mass fluctuations of PVA material shows that more mass decrease takes place when submerged into water. The decrease in mass could have two possible causes. First, it is possible that the material dissolves in the surrounding water. secondly the material may discharge its water outward. Both causes can have an influence on the stiffness of the material. To keep the materials as constant as possible, it is advised to not add water to the material during the experiment.

Based on this material study, the following can be concluded:

- PVA can form a material which, based on its Young's modulus, can mimic prostate tissue and adipose tissue.
- The number of freeze-thaw cycles applied to PVA influences its mechanical characteristics. An increase in number of freeze-thaw cycles tends to increase the Young's modulus of the material.
- The concentration of PVA used in the material also has an influence on its mechanical characteristics. Increasing the concentration leads to a higher Young's modulus.
- The volume of the material influences the Young's modulus of the material. Larger volumes give higher Young's moduli values
- Using coolant in the solvent used for PVA also has an influence on the mechanical characteristics of the material. Using this additive in the solvent, when lowering the amount of demineralized water, tends to increase the Young's modulus.
- Adding DMSO to the solvent for PVA has an influence on the mechanical characteristics of the material. Using this additive in the solvent, when lowering the amount of demineralized water, tends to increase the Young's modulus slightly.
- Adding tap water to PVA materials during storage has an influence on the mass of the material and can cause mass fluctuations.

It is recommended to perform even more research in PVA materials, its additives and its mechanical characteristics. Using larger sample sizes, more variations in PVA concentrations, volumes and method of adding other materials will give an even better insight in the behavior of this material.

2.3.1. Recommendation for Part II

The prostate phantom which will be made in part II of this study has a list of requirements. The Young's modulus of the material used for the prostate and adipose tissue should mimic the Young's modulus of the equivalent human tissue. The results suggest multiple materials combinations which would fall into this range of prostate tissue and adipose tissue. When considering another requirement, the transparency that is needed for both the cancerous prostate tissue and the adipose tissue, one possible material is left. The results show that group K (high concentration of DMSO) contains the best transparency and the only sufficient transparency characteristics. Therefore, this material will be used for both the prostate and the adipose tissue. Finally, considering the requirement to make the phantom easy to build, it is considered to use as less as freeze-thaw cycles as possible. To increase the Young's modulus, an increase in PVA concentration will be used rather than an increase in freeze-thaw cycles. This is especially necessary for the adipose tissue since this study has not shown Young's moduli of this transparent material which fall into the adipose tissue range. To achieve a stiffness value into this range, the PVA concentration should be lowered.

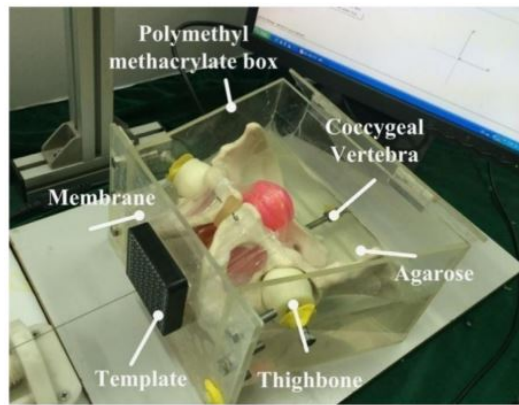
3

Part II: Phantom Design

This section describes the design process and the manufacturing process of the prostate phantom. Because of the broad range found in literature for both prostate tissue as adipose tissue, a goal was set to create three different prostate phantoms. Each model would have a different Young's modulus for both the prostate as the adipose tissue with the following goal: Model 1 with a low Young's modulus, model 2 containing a medium Young's modulus and model three having a high Young's modulus. Each Young's modulus was set to fall into the range of the found cancerous prostate tissue (62.9 - 221 kPa) and adipose tissue (0.12 - 50 kPa).

3.1. Previous work

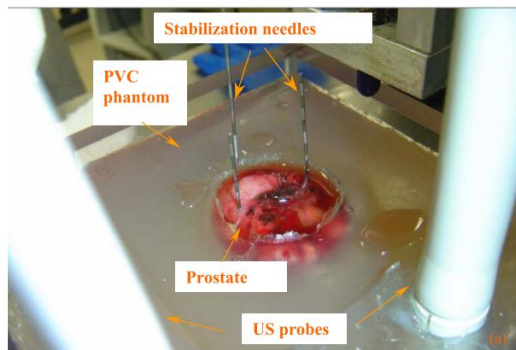
Literature reports multiple studies focusing on prostate phantom models which can be used for testing instruments [5, 24, 25, 53, 54]. Yan et al. (2009) [53] collected prostate samples from patients who underwent radical prostatectomy. These prostate samples were placed in a polyvinylchloride phantom, creating a phantom model including real prostate tissue and surrounding phantom material which can be seen in figure 3.1c. A major advantage is the presence of real prostate tissue in this model which forms the best material for testing new instruments. However, the usage of this tissue also makes it harder to reproduce since real prostate tissue is rarely available. For reproduction purposes and ease of manufacturing, which is required in this project, it would be best to use biomaterials and not real tissue samples. Li et al. (2015) [54] used many parts to create a complete prostate phantom model including an entire pubic bone and a template for needle insertion. This would create a high level of geometrical correctness. However, due to the entire pubic bone that was used, the phantom model is large and not easy to transport or reproduce which is required for this project, as can be seen in figure 3.1a. Hungr et al. (2012) [5] and Cao et al. (2013) [24] created a simplistic phantom model including a prostate, rectum and surrounding tissue. These models are shown in figures 3.1d and 3.1b This provides a good base model to test new instruments on. What is lacking is an opening for needle insertion and more surrounding tissues are needed to mimic a human prostate area and satisfy the requirements of this project. Also, for demonstrative purposes, transparent tissues are needed. Chiu et al. (2020) [25] developed the most recent prostate phantom model which is shown in figure 3.1e. The geometrical design provides multiple parts surrounding the prostate phantom, as an urethra and rectum. The rectum is made by using an inlet which is placed in the surrounding tissue. After manufacturing this inlet can be removed which creates a hole for an ultrasound probe where probe to material contact, also known as probe to rectum contact, is possible. This is necessary to use an ultrasound probe. Also, the model is compact and easy to transport but the model does not provide heterogeneous surrounding tissue around the prostate and not transparent casing. For this project, it is required to create a model which has good demonstrative qualities, geometrical correctness and mechanical correctness. Each of these studies used a casing to surround all the parts in the phantom model. A translucent casing would be ideal since this would make the phantom model eligible for demonstrations.



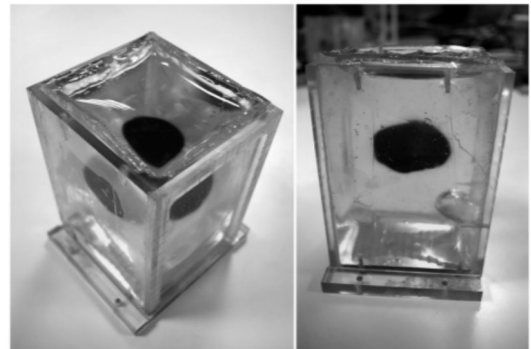
(a) Phantom by Li et al. (2015) [54]



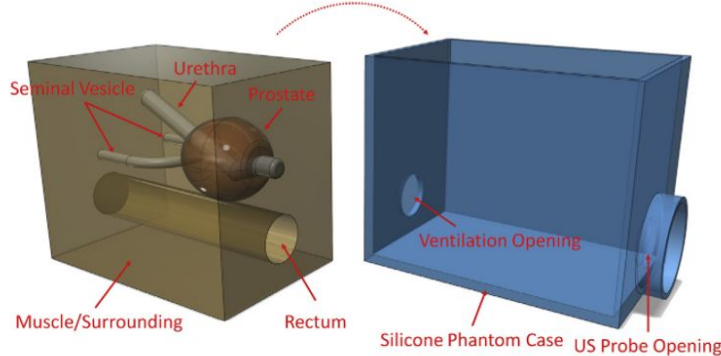
(b) Phantom by Cao et al. (2013) [24]



(c) Phantom by Yan et al. (2009) [53]



(d) Phantom by Hungr et al. (2012) [5]



(e) Phantom design by Chiu et al. (2020) [25]

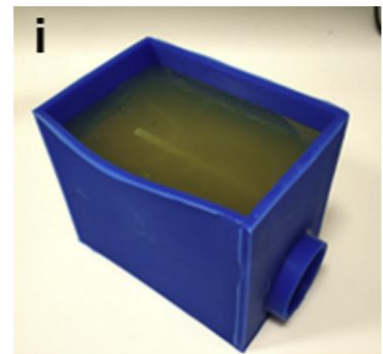


Figure 3.1: Multiple prostate phantom models found in previous work. Different designs are used as well as varying materials. Each models uses a casing to surround the inlaying materials and present the model.

Overall, these phantom models are valuable resources and form a good inspiration for the phantom design of this project. However, neither of these studies focused on achieving mechanical and geometrical correctness and create a demonstrative phantom model. To satisfy the goal of creating a phantom model which can be used to test new instruments, better matching materials and a more precise design is both necessary.

3.2. Design

The introduction of this project describes the list of requirements for the prostate phantom model. This includes geometrical correctness: the phantom should include an prostate, urethra, adipose tissue, a rectum, an opening for needle insertion and a needle insertion template. The tissues should have similar shape and sizes to that of a human. Additionally, a pubic bone can be added to simulate blockage of the prostate when entering a needle. The mechanical characteristics of the prostate and

adipose tissue parts of the phantom should be similar to that of real tissue. This means that the Young's modulus of the prostate should fall into the X-X kPa range and the adipose tissue should fall into the X-X kPa range. The model will be used for demonstrative purposes which requires the prostate, adipose tissue and the casing to be transparent. Also, a rectum is necessary to insert an ultrasound probe which can be used to perform ultrasound imaging on the prostate which is usually done during brachytherapy. Finally, the phantom should be practical which includes that the model has to be transportable, durable, reproducible and easy to manufacture. Based on these requirements and on the previous work found in literature, a design was made of the phantom prostate including all the relevant tissues/organs which can be found in figure 3.2. The needle insertion side is located behind the template. Additionally, a pubic bone can be added to this design. The results from the material study performed in part I of this project will be used to select the materials which will fall into the required Young's modulus range for the prostate and the adipose tissue.

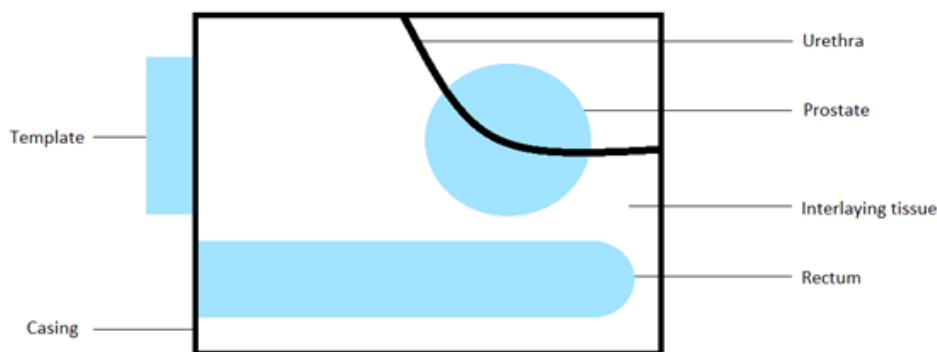


Figure 3.2: Example design of the prostate phantom model. The model includes the prostate and the relevant tissues around the prostate which interact with the instruments during brachytherapy treatment.

3.3. Methods

The following section described the designing and manufacturing process of the prostate phantom models.

3.3.1. Casing

A casing was made to surround the phantom. The material chosen for the casing was 4 mm thick Poly-methyl methacrylate. This material is known for its excellent transparent properties which is necessary to make the insight of the phantom visible. The material is also known to be a very strong material and easy to make watertight which is also necessary in the creation of this phantom. A SolidWorks template made by M. de Vries was used as the base for this model. It consisted of a rectangle shaped box which had the right dimension to include a prostate, urethra, rectal opening and a pubic bone (120 x 120 x 208 mm). The model was adapted for this phantom and the final design can be seen in figure 3.3. A rectangle opening was made in the front of the casing of 50x50 mm. Through this opening, needle puncture will be made possible. Another round opening with a 26 mm diameter was made at the front of the casing through which a rectal insert can be placed. The final design was made in the program SolidWorks 2020. The casing was made by lasercutting the drawing of a 4mm thick Poly-methyl methacrylate plate. The sides, front, back and bottom of the casing were glued together with Acrifix 192. After 24h drying time, the inner and outer grooves which were still open were covered in a layer of Acrifix 192. This made the casing water tight. The top of the casing was left off during the manufacturing phase. During the manufacturing period of the phantom, the front openings were closed off with a polymethyl methacrylate plate and a rectum insert. These were made water tight by closing the objects off to the casing with sealant tape (polyestershoppen.nl, SK2ST200-1). In total, 3 casings were made which each had the same features.



Figure 3.3: Casing of the prostate phantom model. The model is made of transparent PMMA material with 4 mm thickness. The outer dimensions of the casing conclude 120 x 120 x 208 mm. An opening is present at the front which enables needle insertion. A round opening is made for a rectal insert.

3.3.2. Rectum

An insert was created to simulate a rectum inside the casing. The purpose of the insert is to create a rectal opening. This is necessary for the use of a rectal probe when applying ultrasound during the brachytherapy procedure. When using a rectal probe during ultrasound, probe-to-rectum contact is necessary. Therefore an insert was made which can be covered in PVA mimicking adipose tissue. When the PVA is finished, the rectal insert can be removed after which a rectal opening is created. The insert design was made in the program SolidWorks 2020. The design was 3D printed with an Ultimaker 3 printer using polylactic acid (PLA) as print material. The insert, with a diameter of 26 mm, was placed through the opening in the casing and left there during the entire manufacturing process as can be seen in figure 3.4. Sealant tape was applied between the casing and the outer part of the insert to close off possible grooves and make the casing watertight. In total, 3 rectal inserts were made, one for each model and each having the same features.

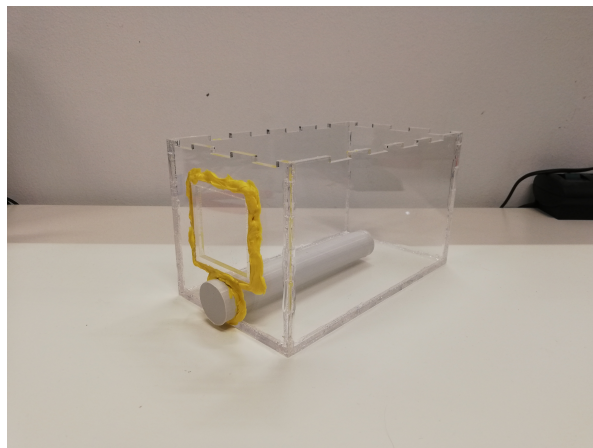


Figure 3.4: Casing of the prostate phantom model including the rectum insert. The grooves between the rectum and casing are covered with tacky tape to make the casing water tight. The opening for needle insertion is covered with a PMMA plate and the grooves are also covered in tacky tape to make it water tight.

3.3.3. Prostate and Urethra

A prostate phantom was made by using a pre-designed mould made by C. Stockley, L. Bennett and L. Wymenga (2020) [55]. This mould was made based on DICOM files of medical MRI and ultrasound scans of multiple prostates, simulating the shape and size of a real prostate as best as possible. The simulated prostate made by the mould had a volume of 45 ml. The mould consisted of two parts and

had two 6 mm diameter outer openings at the sides through which a tube can be inserted, simulating an urethra passing through the prostate. The two halves of the mould can be seen in figure 3.5a. Another opening is present at the top through which the prostate material can be poured. The mould was 3D printed with an Ultimaker 3 printer using tough PLA as the selected material.

A 6 mm diameter wide polymethyl methacrylate tube (Bowden Tube 1266) was used to simulate an urethra. The material polymethyl methacrylate was selected because it is known for its good chemical resistance. Since the tube will be covered in DMSO, which can chemically damage other materials, it was necessary to select a material which can withstand chemical stress.

The two halves of the mould were put together and the tube was inserted inside the mould. Four M4 bolts and screws were used to keep the two halves of the mould together. Sealant tape was applied on the outer groove of the mould and on the outer groove between the tube and the mould to make it water tight. The result of this step is shown in figure 3.5b.

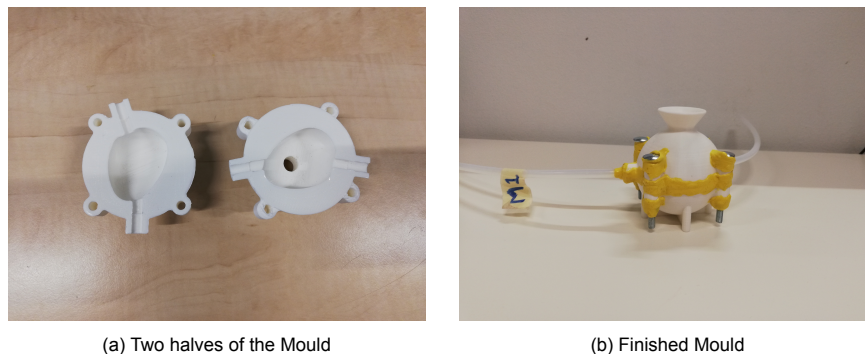


Figure 3.5: The two halves of the prostate mould (a) and the two halves of the mould placed on top of each other, sealed with M4 bolts, including an urethra model and closed of with tacky tape (b).

For the 3 models that were made, 3 different prostates were created. The material used for the prostate consisted of PVA powder, demiwater and DMSO. This combination was chosen to make the prostate transparent. A high level of DMSO was used (demiwater:DMSO=10:90) as a solvent since the material study in this project showed that this combination produced the best transparent properties. PVA material needs at least one freeze-thaw cycle. After making the prostate material, this material is poured over with PVA adipose tissue material, which also needs at least one freeze-thaw cycle. This means that the prostate material undergoes at least two freeze-thaw cycles. To reserve the time needed to create a model and thereby see to an easier manufacturing process, it was decided to apply two freeze-thaw cycles in total. The PVA concentrations needed for the material was adapted keeping the demiwater:DMSO ratio (10:90), the two freeze-thaw cycles and the Young's moduli values for a cancerous prostate in mind.

The material study in the first part of this project estimated the Young's modulus of 10% PVA in the specific demiwater:DMSO ratio to be around 69.69 kPa after two freeze-thaw cycles. These results can be used to estimate higher PVA concentrations and the effect of adding DMSO to higher concentrations. Increasing 10% (65.91 kPa) to 15% (97.68 kPa) PVA resulted in a rise in Young's modulus of 1.48 times after two freeze-thaw cycles. Assuming this multiplication factor also holds for increasing 15% to 20%, the Young's modulus for 20% PVA after two freeze-thaw cycles is estimated to be 144.57 kPa. Observing the difference between 10% PVA without additive (65.91 kPa) and 10% PVA with a demiwater:DMSO ratio of 10:90 (69.69 kPa) it can be assumed that replacing the demiwater with DMSO causes an increase of 1.06 times of the Young's modulus after two freeze-thaw cycles. Assuming this increase number also counts for the other PVA concentrations after two freeze-thaw cycles, the influence of adding DMSO to 15% PVA can be calculated. Increasing the Young's modulus of 15% PVA without additive (97.68 kPa) with 1.06 times would result in a Young's modulus of 103.54 kPa for a material of 15% PVA with a demiwater:DMSO ratio of 10:90. Multiplying the estimated Young's modulus of 20% PVA concentration (144.57 kPa) gives a stiffness value of 153.24 kPa for 20% PVA concentration with a demiwater:DMSO ratio of 10:90. An overview of all these mentioned Young's moduli values can be seen in table 3.1. This gives the following Young's moduli for the prostate tissue material for the three models: model 1: 69.69 kPa, model 2: 103.54 kPa and model 3: 144.57 kPa. These values fall into the cancerous prostate range found in literature.

Table 3.1: Overview of the Young's moduli for the materials with and without DMSO as additive after two freeze-thaw cycles. Estimated values are given in cursive.

| PVA | No additives (kPa) | Adding DMSO (kPa) |
|-----|--------------------|-------------------|
| 10% | 65.91 | 69.69 |
| 15% | 97.68 | <i>103.54</i> |
| 20% | <i>144.57</i> | <i>153.24</i> |

Following this estimation, a PVA concentration of 10%, 15% and 20% with DMSO additive would each result in a higher Young's modulus after two freeze-thaw cycles, while these values still fall into the range of a cancerous prostate. A maximum of 20% PVA was selected since pre-testing showed that a higher PVA concentration could not guarantee transparency in the material. Choosing the concentrations 10%, 15% and 20% would provide three different models, which are transparent, with increasing Young's moduli which would each lie in the cancerous prostate Young's moduli range. Therefore the following PVA concentrations were chosen for the prostate material: 10% PVA for model 1, 15% PVA for model 2 and 20% PVA for model 3. The prostates were each made following the PVA preparation protocol used in Part I of this project. Each prostate was given one freeze-thaw cycle of in total 48 hours. An examples of one of the prostate models can be seen in figure 3.6a. After this freeze-thaw cycle, a cubic black plastic target of 2x2x2 mm was placed inside the prostate at the top. This target can be used in future research investigating the displacement of the target after needle insertion and with that the displacement of the prostate. Next to that, it also functions as a target to reach for newly developed steerable needles. The target was place in the top of the prostate since here it is best viewed for displacement studies as can be seen in figure 3.6b. Besides this, it is also a place hard to reach with non-steerable needles since it can be blocked by a part of the pubic bone. In this way, by reaching the target with the steerable needle, the needle can show its potential. A suspension system was made to add the prostate to the casing. Two aluminum beams were taped with duct tape and tacky tape to the front and the back of the casing. The beams were placed in the middle of the casing. The prostate was hanged at these beams by taping the urethra to the beams with duct tape. The height between the bottom of the casing and the top of the prostate concluded 7.6 cm. The prostate was positioned 1 cm above the rectum. The distance between the opening of the casing and the prostate was 7 cm. The suspension system can be viewed in figure 3.7b. After placement in the casing, it was covered in adipose tissue material and given another freeze-thaw cycle of 48 hours in total.

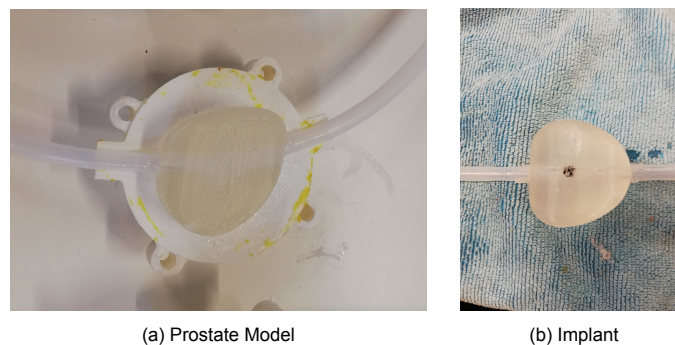


Figure 3.6: A finished prostate model including an urethra inside the mould (a). An implant inserted in the top of the prostate model meant as a target for steerable needles (b).

3.3.4. Pubic arch

A pubic bone was added to the phantom design to simulate a part of the pubic arch which can block needles during brachytherapy from reaching the prostate. Since this 'blocking' is not always present and when it is, it varies a lot among patients, it was decided to create three different 'blockage situations'. Model 1 received no pubic arch and therefore no blockage was applied, in model 2 the prostate was covered by a small part of the pubic arch and model 3 received a large part of the pubic arch which resulted in a large blockage of the prostate. A free-accessible stl file of the entire pubic bone made by the Database Center for Life Science was used to create the two models of the pubic arch [56]. A part of the pubic arch small in height and a part longer in height was cut out of the 3D model. The

first one represents the small blockage pubic arch and the second one consists of the large blockage pubic arch. The models were 3D printed with an Ultimaker 3 printer using white tough PLA as print material which can be viewed in figure 3.7a. An aluminum beam was used as a suspension system for the bones. The bones were attached at the top with sealant tape to the aluminum beam which was placed on the top of the casing 3 cm away from the front. The beam was also attached to the casing with sealant tape to prevent it from moving. The suspension system of the pubic arch can be seen in figure 3.7b.

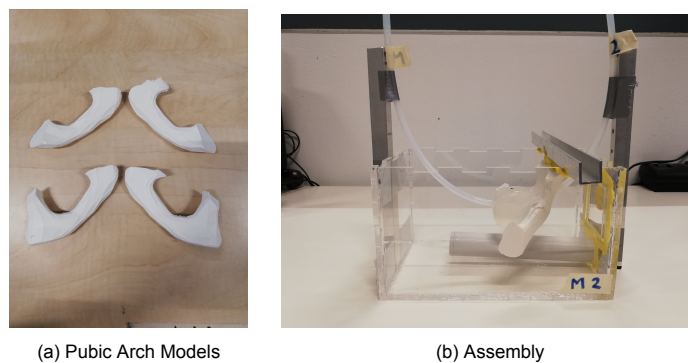


Figure 3.7: Two models of the pubic arch (a). Above: the smaller model of the pubic arch designed for phantom model 2. Below: the larger model of the pubic arch designed for phantom model 3. An assembly of all the objects shows the final model before adding the adipose tissue material (b).

3.3.5. Adipose tissue

The adipose tissue consisted of 2.4 litres of PVA material. The goal for this material was to be transparent and to have a Young's modulus value falling in the range of adipose tissue found in literature. Furthermore, each model should have a different Young's modulus value. To make the material transparent, the solvent DMSO was used again. The ratio between demiwater and DMSO of 10:90 was used which was also used for the prostates. As mentioned in the previous section, to not extend the manufacturing time, the material used for adipose tissue was set on receiving one freeze-thaw cycle. Since the stiffness values of adipose tissue found in literature were so low, a low level of PVA concentration was needed for this material. The value for the 10:90 ratio between demiwater and DMSO added to 10% PVA after one freeze-thaw cycle (61.50 kPa) exceeds the maximal value of the stiffness ratio of adipose tissue. Therefore, the PVA concentration used for these models must be lower than the 10%. The lowest value of PVA concentration was set on 3% since pre-testing showed that lower concentrations resulted in a material which was found to be too fluid. For the other models, the concentration was slightly increased to maintain the low Young's modulus value. This resulted in the following PVA concentrations: 3% PVA for model 1, 5% PVA for model 2 and 7% PVA for model 3. The results of the materials study in part I gave a Young's modulus value of 5.57 kPa and 21.81 kPa for 5% and 10% PVA without additive, respectively, after one freeze-thaw cycle. These results can be used to estimate higher PVA concentrations and the effect of adding DMSO to lower concentrations. A multiplication factor of 3.916 between the 5% and 10% PVA without additives after one freeze-thaw cycle can be observed. When calculating the stiffness values for 3% and 7%, a decrease and increase of 2% (40% of the 5% range) compared to the 5% is needed. It is assumed that the multiplication factor of 3.916 also holds for this range, and covers a 5% range. A multiplication factor of 1.566 (40% of 3.916) can be used to determine increases and decreases of 2% in this range. Multiplying 5.57 kPa with 1.566 gives a Young's modulus value of 8.72 kPa for a 7% PVA concentration. Dividing 5.57 kPa by 1.566 gives a Young's modulus of 3.56 kPa for a 3% PVA concentration. The material study also showed that the Young's modulus of 10% PVA (21.81 kPa) is increased with a multiplication factor of 2.820 when adding a solvent of demiwater:DMSO (10:90) (61.50 kPa) after one freeze-thaw cycle. It is assumed that this multiplication factor also holds for the calculation of lower concentration ranges. Multiplying the Young's moduli, and estimated Young's moduli, of 3%, 5% and 7% PVA with a multiplication factor of 2.820 gives the following results: 10.04, 15.71 and 24.59 kPa for 3%, 5% and 7%, respectively, with demiwater:DMSO additive (10:90) after one freeze thaw cycle. An overview of all these mentioned Young's moduli values can be seen in table 3.2. This gives the following Young's moduli for the adipose tissue material for the three models: model 1: 10.04 kPa, model 2: 15.71 kPa and model 3: 24.59 kPa.

Table 3.2: Overview of the Young's moduli for the materials with and without DMSO as additive after two freeze-thaw cycles. Estimated values are given in cursive.

| PVA | No additives (kPa) | Adding DMSO (kPa) |
|-----|--------------------|-------------------|
| 3% | <i>3.56</i> | <i>10.04</i> |
| 5% | <i>7.18</i> | <i>15.71</i> |
| 7% | <i>8.72</i> | <i>24.59</i> |

The adipose tissue materials were each made following the PVA preparation protocol used in Part I of this project except the cooling time was increased from 20 minutes to 60 minutes since the large volumes needed a longer time to cool down. The material was added to the assembly and frozen for 24 hours after it was thawed at room temperature for 24 hours.

3.3.6. Template

A template was made to guide the brachytherapy needles during the treatment. Using the program SolidWorks, a 3D model of the template was made which would cover the opening in the casing. Also a cover was made which would keep the template in place. The template consisted of 81 insertion spots for the needles which each had a diameter of 1.8 mm. The total dimensions of the template were 59.5 x 59.5 x 9.5 mm. The holder was build around these dimensions. The template and its holder were printed with an Ultimaker 3 printer using the material PLA. The 3D model of template and its holder can be seen in figure 3.8. The holder was mounted onto the models after they were finished with Acrifix 192. The template moved into its place inside the holder.

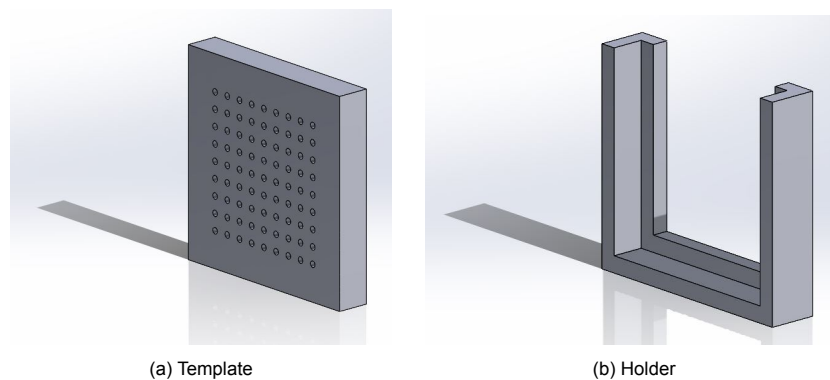


Figure 3.8: A 3D model of the template meant to guide the needles during brachytherapy (a) and the holder to keep the template in place (b)

3.4. Results

In this section the results of the manufacturing process of the prostate phantom models are presented. In total, three different models were made. Model 1 contains low Young's moduli for the prostate and adipose tissue and has no pubic bone. Model 2 contains medium Young's moduli for the prostate and adipose tissue and a small pubic bone which blocks the prostate. Finally, model 3 contains high Young's moduli for the prostate and adipose tissue and a large pubic bone which blocks the prostate.

3.4.1. Model 1

Model 1 consist of a transparent casing including a prostate phantom, an urethra phantom and and adipose phantom. The prostate was made of 10% PVA which was solved in a mixture of demiwater and DMSO (10:90) in which a black tracker was inserted at the top of the prostate. Two freeze-thaw cycles were applied on this material. The adipose tissue material consisted of 3% PVA which was solved in a mixture of demiwater and DMSO (10:90). In total, this adipose material underwent one freeze-thaw cycle and consisted of about 2.5 L. The material did not satisfy the expectations of transparency. The material is slightly transparent but it is too cloudy and not transparent enough to sufficiently observe a needle. Because of this, the prostate material and urethra are also hard to see. The rectum insert can be seen through the cloudy material. Figure 3.9 shows model 1 and its transparency. Note that the transparency is not well captured on pictures, in real life the transparency seems improved. The material that was used for the adipose tissue turned out very soft and almost liquid. Because of this the material does not seem strong and collapses under its own weight. This caused the height of the material to fall lower. The rectal insert can be removed but because of the softness of the material, the hole that is left is filled with adipose material which collapses under its own weight. However, a ultrasound probe can still be inserted since the material also easily slide away when the insert in reinserted again. This also results in a good contact between the probe and the material.

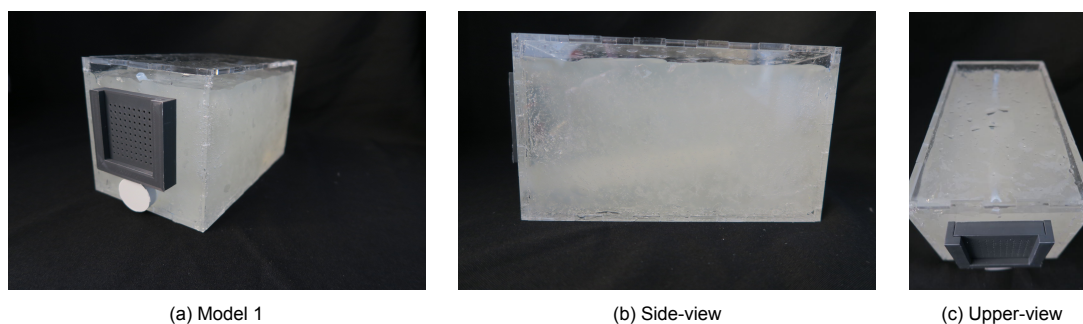


Figure 3.9: Model 1 (a) the side-view (b) and the upper-view (c). The model includes a prostate, urethra and adipose tissue. In front, the template for guiding the needles and the front of the rectal insert can be seen.

3.4.2. Model 2

Model 2 consist of a transparent casing including a prostate phantom, an urethra phantom, a small pubic bone and and adipose phantom. The prostate was made of 15% PVA which was solved in a mixture of demiwater and DMSO (10:90) in which a black tracker was inserted at the top of the prostate. Two freeze-thaw cycles were applied on this material. The adipose tissue material consisted of 5% PVA which was solved in a mixture of demiwater and DMSO (10:90). In total, this adipose material underwent one freeze-thaw cycle and consisted of about 2.5 L. The material was more transparent than the material used in model 1. However, there is still a bit cloudiness present. The pubic bone, rectum insert and urethra can be seen through the material. The contours of the prostate are still hard to view. Figure 3.10 shows model 2 and its transparency. Note that the transparency is not well captured on pictures, in real life the transparency seems improved. The material that was used for the adipose tissue turned out soft but more stiff than the material used in model 1. The pubic bones are situated in front of the prostate and can be viewed well.

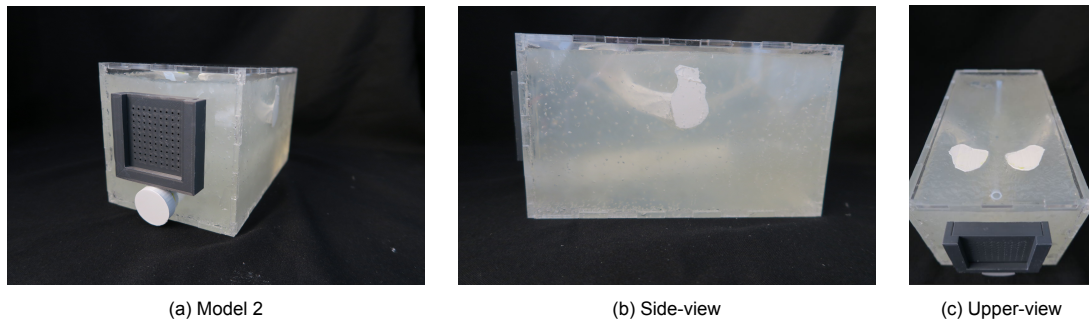


Figure 3.10: Model 2 (a) the side-view (b) and the upper-view (c). The model includes a prostate, urethra, a small pubic bone and adipose tissue. In front, the template for guiding the needles and the front of the rectal insert can be seen.

3.4.3. Model 3

Model 3 consist of a transparent casing including a prostate phantom, an urethra phantom, a large pubic bone and and adipose phantom. The prostate was made of 20% PVA which was solved in a mixture of demiwater and DMSO (10:90) in which a black tracker was inserted at the top of the prostate. Two freeze-thaw cycles were applied on this material. The adipose tissue material consisted of 7% PVA which was solved in a mixture of demiwater and DMSO (10:90). In total, this adipose material underwent one freeze-thaw cycle and consisted of about 2.5 L. The material was more transparent than the material used in model 1 and 2. The material shows to be sufficiently transparent. The pubic bone, rectum insert and the urethra can be seen very well through the material. Also, slight contours of the prostate can be viewed. Figure 3.11 shows model 3 and its transparency. Note that the transparency is not well captured on pictures, in real life the transparency seems improved. The material that was used for the adipose tissue turned out soft but more stiff than the material used in model 1 and 2. The pubic bones are situated in front of the prostate and can be viewed well. The left pubic bone has moved a little backwards during the freezing process. However, the bone remains sufficiently situated in front of the prostate.

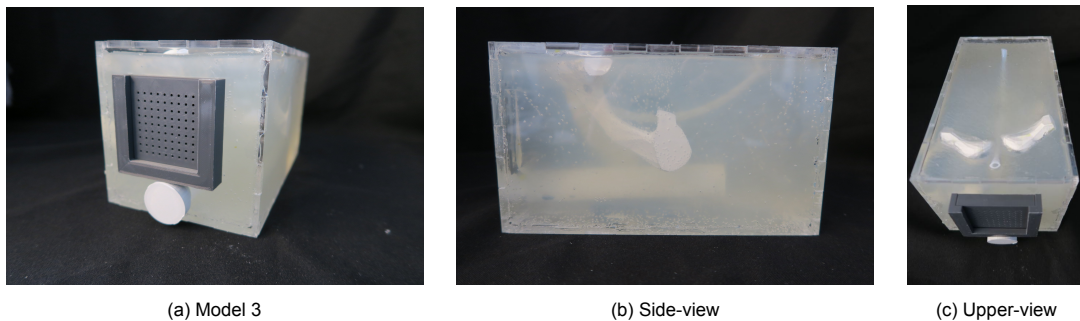


Figure 3.11: Model 3 (a) the side-view (b) and the upper-view (c). The model includes a prostate, urethra, large pubic bone and adipose tissue. In front, the template for guiding the needles and the front of the rectal insert can be seen.

3.5. Discussion

The goal of this part of the study was to design and manufacture a cancerous prostate phantom model. In total, 3 different models were made: model 1 containing a low Young's modulus, model 2 containing a medium Young's modulus and a small pubic bone and model 3 containing a high Young's modulus and a large pubic bone. Based on the results of part I and a literature study on the mechanical characteristics of a cancerous prostate and adipose tissue, materials were chosen for these models.

The geometrical requirements describing the size and location of the prostate in the models were met. A prostate was made of 45 ml (required minimum of 40 ml), positioned 10 mm above the rectum (required range of 0-37 mm) and at 70 mm distance from the front of the casing (required range of 49-72 mm). The urethra had a required diameter of 6 mm and the rectum a minimal diameter of 19 mm, namely 26 mm. A needle insertion opening of 50x50 mm was included at the front of the casing (required minimum of 30x40 mm) The mechanical requirements of the prostate material (62.9 - 221 kPa) and adipose material (0.12 - 50 kPa) was also met for model 1 (prostate: 69.69 kPa, adipose tissue: 10.04 kPa), model 2 (prostate: 103.54 kPa, adipose tissue: 15.71 kPa) and model 3 (prostate: 144.57 kPa, adipose tissue: 24.59 kPa). Furthermore, the demonstrative qualities requirements stated that the casing and prostate material should both be transparent. This was achieved in all the models. However, the adipose tissue material should also be transparent. It was not possible to sufficiently see all the parts included in model 1 and 2. Therefore, the transparency requirement of these models for the adipose tissue material was not met. For model 3, it was possible to view all the different parts and the adipose tissue material in this model was therefore sufficiently transparent. Besides this, the practical requirement of the models were also met. The surrounding casing included dimensions of 120x120x208 mm while the maximal allowed dimensions were set on 300x300x300 mm. Upon writing this thesis, the models were kept for 3 weeks in the fridge and still in perfect shape while a durability of at least one week was required. The manufacturing process took place in the MISIT lab at the 3mE faculty using the present materials and equipment. The total manufacturing time of one model was 5 days in total which is less than the maximal allowed time of one week. It can be concluded that model 3 met all the requirements set for this project.

The results have shown that using a 10:90 mixture of demiwater and DMSO as a solvent of PVA results in a transparent prostate model of 45g. Due to the small size of the prostates, a mass of 45g each, the phantom showed sufficient transparency.

However, the results also show that PVA in combination with demiwater and DMSO (10:90) is a minimal sufficient material for the manufacturing adipose material in a prostate phantom model. The different parts in the phantom can be distinguished, but cloudiness is still present in the material. Therefore, it can be improved. Model 3 shows sufficient transparency to distinguish the different parts in the phantom. For demonstration purposes, it would be an improvement to increase this transparency even further. The transparency results of these models were not in line with the expectation based on the results of part I of this project. The results in part I showed that a small sample of 45 g of 10% PVA solved in demiwater and DMSO (10:90) showed good transparency. However, using a larger volume (2.4 L) resulted in a decrease in transparency due to cloudiness. Fortunately, the transparency in model 3 (7%) was still sufficient enough to distinguish the inner parts. The presence of cloudiness could be explained by the presence of more cloudy-looking parts in a larger volume, which can overlap each other and thereby block the view. During pre-testing in this part of the project, small samples were made from varying concentrations of PVA solved in demiwater and DMSO (10:90) to find differences in transparency and to try to improve it. A lot of pre-testing and trial and error have resulted in the decision to use 3%, 5% and 7% PVA as adipose tissue for these models since these concentrations gave the best transparency results. However, the results show that applying these materials to larger volumes does not result in the transparency seen in the smaller samples.

The transparency was sufficient in one model: model 3. Also in this model, the transparency can be improved since the contours of the prostate are still hard to view. This may be caused by using the same solvent for both prostate and adipose material. A suggestion to improve this would be to use coolant as an additive for the prostate material. Part I showed that adding a large amount of coolant to PVA and demiwater, develops a bright pink prostate with signs of translucency. This translucency was

not as good as in material where DMSO was added. More research is necessary to find the correct additive and the correct amount that should be added to develop a transparent and coloured prostate model which contours can be viewed in a prostate phantom model. Overall more research is needed in finding a transparent heterogeneous material.

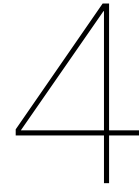
The results show that using a polymethyl methacrylate tube functions as a good model for the urethra in these prostate phantom models. During pre-tests in this part of the project, a polyurethane tube was used to simulate an urethra. Due to the chemical aggressiveness of the material DMSO, which surrounds the tube, the polyurethane was severely damaged. Using a tube made of polymethyl methacrylate, which is more chemical resistant, prevented this damage. The tube was not damaged in any way and model 3 also showed a good visible urethra phantom. For demonstration purposes, it could be an improvement to use a colored urethra and thereby make it even better visible.

The pubic bone phantoms used in this project showed to be a good method to block the prostate phantom. The materials made were light weight, cut off straight and therefore easy to use in the phantom model by using a suspension system. It was shown that it is very well possible to block both smaller and larger parts of the prostate using these models and materials.

Assuming the mechanical results from part I still hold, this project has shown that different models of a prostate phantom can be made in varying its Young's modulus values by using different concentration of PVA in the same solvent material. However, the exact mechanical characteristics of PVA concentrations besides 10% in a mixture of demiwater and DMSO have not yet been determined in this project. The Young's moduli of these materials were estimated based on the results from the material study in part I. These calculations were based on assumptions since changing the PVA concentration does not give a linear change in the resulting Young's modulus. More research is necessary to determine the specific mechanical characteristics of these materials.

The phantom models meet the requirements defined in the introduction of this report. All the required tissues, a prostate, urethra, adipose tissue and a rectum, were present in the models.

It can be concluded that prostate phantom models, varying in Young's modulus, can be made from PVA, demiwater and DMSO. This manufacturing process has shown that using demiwater and DMSO, only in the right ratio (10:90) with the right concentration PVA, can create a sufficient translucent material for both small volumes and larger volumes.



Part III: Phantom Validation

4.1. Methods

This section presents the methods for the experiment used to validate a prostate phantom model. A needle insertion experiment will be performed on the models. Needle insertion experiments have been used in research to validate prostate phantom models, have to shown to distinguish between healthy prostate tissue and tumor prostate tissue and has been assumed to function as a good validation method to test these phantoms [5, 53, 54]. In total, the three different prostate phantom models, made in Part II, will be tested. The goal of this experiment is to collect data on the peak insertion force of the needle upon insertion into the adipose tissue and the prostate phantom of the model. This data will be compared to data found in literature and this comparison will function as a validation of the prostate phantom models.

4.1.1. Materials

Three different prostate phantom models made in part II of this project were used for this experiment: model 1 containing a low Young's modulus, model 2 containing a medium Young's modulus and a small pubic bone and model 3 containing a high Young's modulus and a large pubic bone. The models, which were stored in a refrigerator and the MISIT lab, were placed into room temperature 4 hours prior to testing. A 18Gauge needle (1.27 mm diameter) with beveled tip was used to perform the insertions.

4.1.2. Protocol

The needle was inserted inside the phantom models at a velocity of 5 mm/s. The needle was placed at a specific height with its tip at the front of the opening of the casing of the model but not entering the model yet. The needle was inserted 110 mm into the specimen, inserting deep into the prostate material. The needle insertion experiments were controlled with the program dSPACE ControlDesk 3.7.4. After each run, data was collected on the measured force, position and time of the needle insertion. After each insertion the model was moved to create a new, not yet punctured place, for the needle to insert into. Also, after each run the needle was cleaned with a paper towel.

4.1.3. Experimental Set-up

The needle insertion experiments were performed with a linear stage (Aerotech, PRO-115). The linear stage was used to move the needle into a vertical direction and to retract it. A 22 N force sensor (Futek. iden. LSB200) was mounted onto the linear stage to collect the data on force measurement. A 18Gauge needle was adapted to the force sensor with the tip put downward. The model was placed on its back, with its opening at the front to the top, under the experimental set-up. In this way, the needle can be placed downward through the opening of the model into the adipose tissue material and the phantom prostate. A tissue was placed underneath the model to prevent the moist model from slipping away during the experiment. The experimental set-up can be seen in figure 4.1.

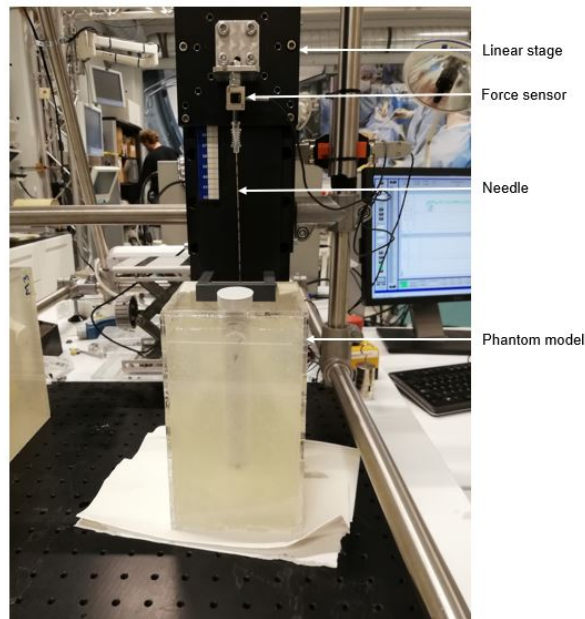


Figure 4.1: Experimental set-up of the needle insertion test consisting of a linear stage, a sensor, a needle and a model. The model is placed on its back with its opening to the top.

4.1.4. Data Analysis

During each insertion, the force, time and position of the insertion was measured and collected. This resulted in raw data including measured force over time. An example of an insertion of the needle inside a model and its prostate can be seen in figure 4.2.

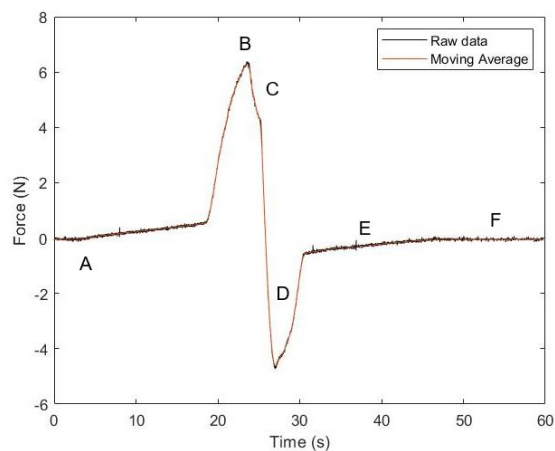


Figure 4.2: An example of the measured force over time over a full needle insertion into a prostate phantom model. First the needle inserts into the adipose tissue material (A). Secondly, the needle is inserted into the prostate phantom which results in the peak force in this graph (B). After the needle has punctured the prostate phantom the force measured is due to the friction between the needle and the prostate phantom material (C). Thereupon, the needle is retracted in the prostate which results in a negative measured force (D). After this, the period is shown when the needle is retracted from the adipose tissue (E). The last part visualized a non moving retracted needle (F).

For every model, an 18Gauge needle was inserted 20 times. As can be seen in figure 4.2, the raw data contained noise. A moving-average fit was used, just as in part I, to eliminate the noise present in the data. The optimal moving-average fit was found at a number of sampling points of 200. Therefore, the force-time graph of each insertion was averaged over 200 sampling points with a moving-average fit. To measure the correct force values in newton, the linear stage was calibrated before the experiment started. The protocol of calibration described in part I of this project was also

used for this calibration. For each insertion, a force-time graph, peak force, standard deviation of the peak force and the median value was determined. The peak-force, which describes the force on the moment of puncturing the phantom prostate wall, was collected. A mean value of all the peak-forces for each model was calculated, as was the median and standard deviation.

4.2. Results

In this section, the results of the needle insertion experiment are presented. A needle was inserted multiple times in three different models made in part II. The force upon the needle during insertion was measured and the peak force upon puncturing the prostate was calculated. The goal is to compare the mean peak force per model with equivalent data on prostate tissue in literature.

4.2.1. Mean Peak Force

A total of 20 insertions were performed on each model. Due to reduced transparency of materials, and therefore reduced visibility of the prostate, and blockage of the pubic bones, not all 20 insertions resulted in the puncture of the prostate tissue. In total, 13, 10 and 20 insertions resulted into the puncture of the prostate for model 1, model 2 and model 3 respectively. An overview of all the force over time figures for every needle insertion can be found in appendix A.1, A.2 and A.3. Table 4.1 and figure 4.3 show the results on the mean and median peak forces and the standard deviation of the mean peak forces measured during the experiment per model. The results show that there is a clear difference in mean peak forces between each model. Model 3 shows the highest median peak force (6.17 N), followed by model 2 (3.55 N) and thereafter model 1 (0.68 N). Model 3 also shows the largest spread and standard deviation in the data (SD=0.95 N) compared to the SD of model 1 (SD=0.20 N) and 2 (SD=0.29 N). A list of all the peak forces resulting from this experiment can be found in A.4. Considering the Young's moduli for each model, a link can be made between the Young's modulus and the mean peak force. A higher Young's modulus would indicate a higher mean peak force value. This was also found in the study by de Jong et al. (2017) [57]. This study conducted a needle insertion experiment on 4% and 7% PVA samples with varying freeze-thaw cycles using a 18Gauge needle. Their results showed that the magnitude of the peak forces exerted on the needle during insertion increased with the number of freeze-thaw cycles. In the first part of this project, it was shown that increased number of freeze-thaw cycles leads to a higher Young's modulus of the material. Based on the literature and the peak force results from this project, a link can be made between the magnitude of the peak forces and the Young's modulus of the material. A higher peak force would indicate a higher Young's modulus.

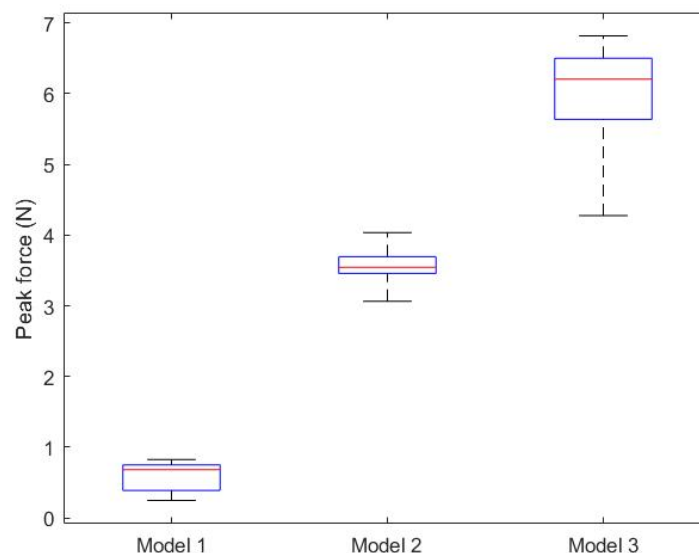


Figure 4.3: A boxplot showing the peak force in Newton per model. The red line represents the median and the bottom and top edges of the box indicate the 25th and 75th percentiles, respectively. The horizontal black lower and upper lines represent the minimal and maximal value, respectively.

Table 4.1: Overview of the mean peak force per model and its median and standard deviation (SD). The sample size (N) per model consists of 13, 10 and 20 for model 1, model 2 and model 3 respectively.

| | PVA prostate (%) | N | Mean Peak Force (N) | Median Peak Force (N) | SD |
|---------|------------------|----|---------------------|-----------------------|------|
| Model 1 | 10% | 13 | 0.57 | 0.68 | 0.20 |
| Model 2 | 15% | 10 | 3.54 | 3.55 | 0.29 |
| Model 3 | 20% | 20 | 5.55 | 6.17 | 0.95 |

4.2.2. Validation

Prostate tissue

A literature study was conducted into the peak forces of a needle into prostate tissue. An overview of the resulting articles and their measured peak forces in newton can be found in table 4.2. The results show a peak force range of 5.2 - 9 N. The goal of this project is to create a prostate phantom which simulates a cancerous prostate as close as possible. Podder et al. (2006) measured the peak forces exerted on different needles during brachytherapy performed on multiple patients with prostate cancer. This study found a mean peak force of 6.28 N during the insertion of a n 18Gauge needle into the prostate during brachytherapy. This result comes close to the median peak force of 6.17 N of model 3 found in this project. The peak forces found in model 1 and 2, resulting from this project, are lower than the mean peak force found by Podder et al. (2006). The stiffness values of model 1 and 2 can lie in a lower region of the adipose tissue values than the stiffness of the adipose tissue in Podder et al. (2006). This results in lower peak force values. The comparison of the results show that the needle-phantom interaction found in model 3 is similar to the needle-prostate interaction during brachytherapy when inserting an 18Gauge needle. The comparison also shows that the needle-phantom interactions found in models 1 and 2 are not similar to the needle-prostate interaction when inserting an 18Gauge needle during brachytherapy.

Li et al. (2015) conducted a needle insertion experiment on a developed prostate phantom. This study used a PVA hydrogel consisting of 3 g PVA, 17 g de-ionized water, 80 g DMSO, 4 g NaCl, 1.5 g NaOH, 3 g epichlorohydrin and 7 freeze-thaw cycles to create a material which was used to simulate a prostate. Scanning electron images of the material showed similar micro-structure to that of human prostate tissue. A needle insertion resulted in a mean mas force of 10.98 N when inserting the needle into the PVA hydrogel. This value lies higher than the highest median peak force found in this project (6.17 N). This shows that the needle-PVA hydrogel interaction, used by Li et al. (2015), is not similar to the needle-phantom interactions found in this project.

Hungr et al. (2012) used a prostate phantom including a perineum, rectum, prostate, surrounding periprostatic tissue and an urethra each made of varying polyvinyl chloride mixtures. The mixtures were said to have an elastic modulus range of 3-200 kPa. The model was validated based on comparing the mechanical characteristics of the phantom to those of in vitro prostate tissue. The peak force of one needle insertion experiment, using an 18Gauge needle, presented in a graph showed a value of about 5.2 N. This value lies close to the mean peak force found in this project for model 3 (5.55±0.95 N). The mean peak forces found in model 1 (0.57±0.20 N) and 2 (3.54±0.29 N) lie lower than this literature value. This comparison shows a similarity between the needle-phantom interaction of model 3 in this project and the needle-phantom interaction of the model manufactured by Hungr et al. (2012).

Considering the results of this project and the results found in literature, a similarity is seen in the median peak force resulting from model 3 and the peak force measured in the study of Podder et al. (2006) performed with a 18Gauge needle. This similarity is also seen between the mean peak force found in this project and the peak force found in the phantom model of Hungr et al. (2012). Keeping in mind that Podder et al. (2006) performed their experiments on patients with prostate cancer, it can be suggested that the mechanical characteristics of the prostate phantom of model 3 would come close the mechanical characteristics of a cancerous prostate. The peak forces found for model 1 and model 2 do not come close to the results found in the literature study and are found to be much lower.

Table 4.2: Overview of the peak insertion forces into prostate tissue/phantom material found in the conducted literature study. Different prostate tissue types and phantom materials were used. The total range of peak forces found consisted of 5.2 - 9 N. The '≈' sign describes results read out of graphs presented in the corresponding study

| Study | Tissue type | Needle | Insertion speed | Peak Force (N) |
|--------------------------|-------------------------------|---------|-----------------|----------------|
| Podder et al. (2006) [4] | Prostate during brachytherapy | 18Gauge | Manually | 6.28±1.64 |
| | Prostate during brachytherapy | 17Gauge | Manually | 8.42±1.52 |
| Li et al. (2015) [54] | Prostate phantom | 17Gauge | 2 mm/s | 10.98±2.3553 |
| Hungr et al. (2012) [5] | Prostate phantom | 18Gauge | 5 mm/s | ≈5.2 |

Adipose tissue

The adipose tissue of the prostate phantom model can also be compared with the results found in Podder et al. (2006). This study presents one graph of the insertion force on a 18Gauge needle during brachytherapy which can be found in figure 4.4. These results represent one needle insertion. The maximal insertion force of 8.46 N is applied when the needle penetrates the perineum after which the insertion force decreases to 5-5.5 N in the interlaying tissue between the perineum and the prostate. Finally, an insertion force of 5.82 N is seen when the needle punctures the prostate wall. Podder et al. (2006) also performed this test with a 17Gauge needle which resulted in an insertion force of about 5 N when moving through the interlaying tissue. The results from this project show a very low needle insertion force when entering the adipose tissue in the phantom prostate model. This force does not exceed 1 N for all the models. These results are much lower than the results found in Podder et al. (2006). This suggests no similarity in needle-phantom interaction and needle-tissue interaction for the interlaying tissue.

Furthermore, the adipose tissue used in this phantom model can also be compared with the results from Hungr et al. (2012). A graph of one needle insertion into the prostate phantom made in this study can be seen in figure 4.5. Region B shows the period in which the needle is inserted into the interlaying tissue between the perineum and the prostate in the phantom model. The force value of this part of the graph lies between 1 and 2 N. This is higher than the value found in this project for the needle insertion in the adipose tissue of the phantom model. In all models, the force exerted upon the needle does not exceed 1 N. This suggests no similarity in needle-phantom interaction found in this project and needle-phantom interaction found in Hungr et al. (2012) for the interlaying tissue.

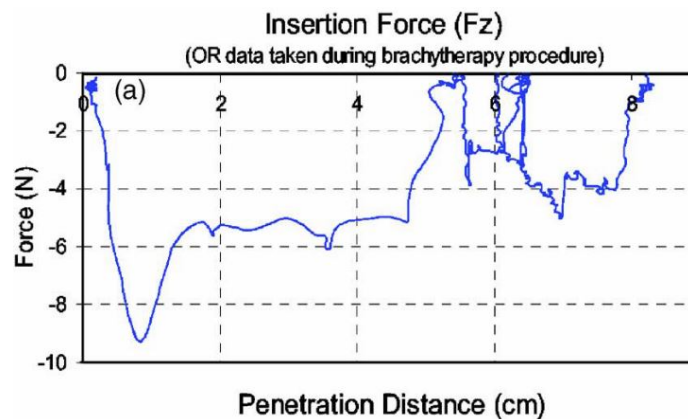


Figure 4.4: Graph derived from Podder et al. (2006) which shows the peak force measured on the insertion of one 18Gauge needle during brachytherapy [4]. A maximal peak force of 8.46 N on the needle is applied when puncturing the perineum. After this insertion the needle drives through the tissue laying between the perineum and the prostate where an insertion force of 5-5.5 N is measured. Finally, an insertion force of 5.82 N is seen when puncturing the prostate.

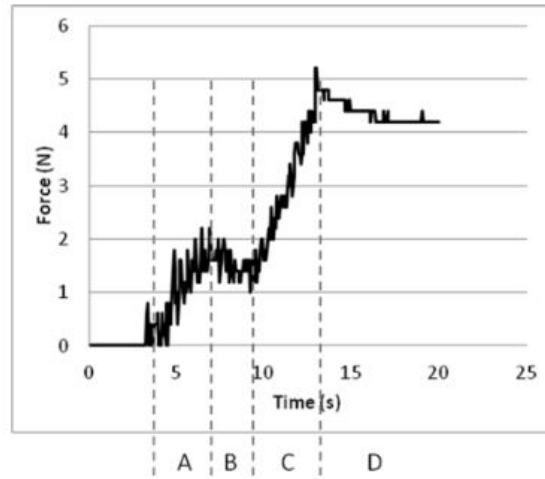


Figure 4.5: Graph derived from Hungr et al. (2012) which shows the peak force measured on the insertion of one 18Gauge needle into the phantom model [5]. The graph shows the insertion of the needle into the perineum (A), the interlaying tissue (B) and the prostate (C). The last part visualized the relaxation of the material (D).

4.3. Discussion

The goal of this project was to design and manufacture a prostate phantom model. A material study was performed to find the optimal biomaterials for the relevant tissue types. Based on these results, materials were selected and a design was made for a cancerous prostate phantom model. After manufacturing three different models, with varying Young's moduli, a needle insertion experiment was performed on each model. The peak forces exerted on the needle during insertion were measured and the mean values were compared with the results of similar experiments found in literature as a validation method. This section discusses the final part in this project: the needle insertion experiment and its results.

This project found higher peak forces when inserting needles into PVA materials with higher concentrations. As found in part I of this project, higher PVA concentration are related to higher Young's moduli. Based on these results, a relationship was found between the Young's modulus of a material and its needle-tissue interaction. Similar results were presented in the study of de Jong et al. (2017) [57] which found higher needle insertion peak forces for materials with a higher number of freeze-thaw cycles, which are also related to higher Young's moduli values. This concludes that higher Young's moduli values cause higher mean peak force values upon an inserting needle.

The median needle insertion peak force found in model 3 is similar to the needle insertion peak force found in a cancerous prostate during brachytherapy in the study from Podder et al. (2006). The mean insertion peak force found in model 3 was also found to be similar to the needle insertion peak force found in a validated prostate phantom model in the study of Hungr et al. (2012). These comparisons suggest that phantom model 3 mimics the needle-tissue interaction of a cancerous prostate. However, the peak forces found in the study by Li et al. (2015) [54] were found to be higher than the peak forces found in this project, including those found in model 3. This is due to a lower Young's modulus value used in this project compared to the stiffness values used in the study by Li et al. (2015). The phantom model of Li et al. (2015) used a PVA hydrogel mixture which was subjected to 7 freeze-thaw cycles. As found in part I of this project, increasing the number of freeze-thaw cycles increases the Young's modulus of the material. The prostate phantom in model 3 of this project was subjected to only 2 freeze-thaw cycles. Consequently, the Young's modulus of the phantom model used in the study of Li et al. (2015) lies in a higher part of the range of possible Young's moduli for a cancerous prostate. This results in higher peak forces during a needle insertion experiment and explains the difference in peak forces found between model 3 in this project and the peak forces found on the phantom of Li et al. (2015).

The peak forces found in phantom model 1 and 2 were lower than the peak forces in the studies found in literature. This suggests that these phantom models do not mimic the needle-tissue interaction of a cancerous prostate. This can be explained by the Young's modulus of these models which are lower than the Young's modulus of model 3. As mentioned in table 1.1, the Young's moduli found in cancerous prostates consist of a very wide range. The Young's moduli of model 1 and 2 lie in the lower part of this range. Possibly, the Young's moduli of the prostates and models used in the experiment of Podder et al. (2006) and Hungr et al. (2012) fall into a higher part of the range. This would explain the difference in peak force found between this project and the studies. Also, the calculations determining the Young's modulus of the material used to mimic the cancerous prostate tissue for this phantom were based on assumptions since changing the PVA concentration does not give a linear change in the resulting Young's modulus. The calculations were based on the maximal increase that was found. The true Young's modulus of this material might lie lower than calculated.

The insertion force of 5 - 5.5 N on the needle while entering the tissue between the perineum and prostate by Podder et al. (2006) was much higher than the results found in this study, which did not exceed 1 N. This is also confirmed by the comparison with the study by Hungr et al. (2012) which showed an insertion force of 1 - 2 N while entering the material between the perineum and prostate of the phantom model. There are multiple reasons which can explain this difference. First, the experiment in this project used a constant needle insertion velocity of 5 mm/s while Podder et al. (2006) performed a needle insertion manually where acceleration is always present and the needle insertion velocity reaches far higher values (max. 800 mm/s) which can result in higher insertion forces on the

needles. Also, the adipose Young's modulus values found in literature were based on adipose tissue originating from tissues as the breast, abdomen, pericardium, omentum and thymus. No values for adipose tissue lying around the prostate was found in this literature study. Furthermore, other types of tissues, such as muscle tissue and arteries, are present around the prostate which can have a higher Young's moduli value than adipose tissue. The true Young's modulus for the tissue lying around the prostate might lie higher than the results of this literature study. Research in mechanical characteristics of the tissue lying around the prostate is necessary.

In total, every model underwent 20 insertions by a 18Gauge needle. However, for model 1 and 2, only 13 and 10, respectively, of these insertions were performed correctly in the sense that the needle inserted the prostate. During the other tries, the needle only inserted the adipose tissue material and missed the prostate. The fact that the 'misses' were so high for model 1 and 2 is due to their poor transparency. It was hard to place the needle correctly while not being able to see the exact location of the prostate. This was not the case in model 3 where the transparency is improved and it was easier to see the pubic bone, urethra and prostate inside the adipose tissue material. The number of insertions were limited due to the small size of the prostate and the fact that the prostate is blocked by pubic bones in two model which also occurs during brachytherapy treatment.

The standard deviations of the peak forces found in this study show the highest spread for model 3 and lowest spread for model 1, with model 2 lying in between these values. This might be due to the fact that model 3 contains the highest PVA concentration in both the adipose tissue material and the prostate material, whereas model 2 has a lower concentration and model 1 the lowest. A higher PVA concentration makes the material more heterogeneous which results in variations in force exerted by the material on the needle. This explains the widest spread in standard deviation found for model 3 which contains the highest PVA concentration.

It can be concluded that the Young's modulus of a material can have an influence on the peak force exerted on a needle when puncturing the material. Besides this, this project also found that needle-PVA material interaction can be influenced easily by adapting the PVA concentration of the material. Also, when combining the results of this project with the results of the literature study it can be concluded that model 3 mimics the needle-prostate interaction found between an 18Gauge needle and a cancerous prostate during brachytherapy. Furthermore, the pubic bones used inside the phantoms have shown to block the prostate successfully. Finally, this experiment shows that more research into the mechanical characteristics of adipose tissue surrounding the prostate is needed to find a material which mimics needle-tissue interaction of adipose tissue in this area. Also, more research is necessary in needle-tissue interaction between a needle and prostate using more of the varying Young's moduli values lying in the wide range found for cancerous prostates. This will give insight in possible varying needle-tissue interactions for the wide range of mechanical characteristics of the cancerous prostate which knowledge is needed when designing phantom models and instruments for brachytherapy.

5

Final Discussion

5.1. Conclusion

This project has shown that PVA can mimic the mechanical characteristics of human tissue. Mechanical characteristics of PVA have been shown to be easily controlled by varying the concentration levels and number of freeze-thaw cycles. The coolant additive reduced swelling in the PVA material and increased the Young's modulus of the material. Also, DMSO resulted in a good solvent for making small volumes transparent and large volumes sufficiently transparent when used in a demiwater:DMSO ratio of 10:90 which was also found to increase the Young's modulus slightly.

By performing a material study on PVA and frequently used additives, this project has created an overview of the effects of these components on the mechanical characteristics of PVA material. This information is very useful for future research on phantom models and projects in the MISIT lab. It can be concluded that PVA can function as a biomaterial for phantom tissue models with adaptable mechanical characteristics.

This project has shown that an easy to manufacture prostate phantom model can be made from the biomaterial PVA. The model has been validated by research performed on prostates during brachytherapy.

When placing this project in context of the ultimate goal to create a prostate phantom model designed for testing new instruments developed for brachytherapy, model 3 resulting from this project seems the best design. This model has shown to exhibit the mechanical characteristics of a prostate and to mimic needle-prostate interaction. To test new instruments developed for brachytherapy, model 3 forms a good test-model. It can therefore be concluded that this project has achieved its goal.

5.2. Future Research

Future research would be useful in multiple areas. First, a larger study on the mechanical characteristics of PVA is necessary to validate the results found in this study and to extend the knowledge of the mechanical characteristics of PVA and possible additives. The material study in this project did not provide the stiffness values of the materials that were used in the phantom models. The Young's moduli of these materials were calculated but since the relationships between different concentrations and additives is not linear, it is hard to make an estimation. Therefore, more research must be done in determining mechanical characteristics of more material combinations of PVA and its additives, or more research is needed in finding a good calculation model for determining Young's moduli for specific materials.

Secondly, the presented transparency in model 3 is sufficient but not optimal. For demonstrative purposes, further increase in transparency is needed. More research is necessary in finding an additive to make PVA more transparent or to find an alternative material for PVA which is also heterogeneous and has a relatively long lasting life. This project used PVA and DMSO as additive to create a transparent material which would mimic human tissue. All the combinations between DMSO and PVA were tested in this project. Therefore, it is not likely to find better transparency when combining PVA with DMSO. It is advised to perform research in finding an alternative material for large transparent tissue mimicking materials.

Finally, more research is needed on needle insertion forces inside a cancerous prostate and its surrounding tissues. This is necessary to improve the prostate model. One research provided data on needle-tissue interaction a needle and a prostate during brachytherapy. Since the anatomical and mechanical characteristics of prostates vary a lot, more research in this field is necessary to obtain a better knowledge of possible interaction between a needle and a prostate.

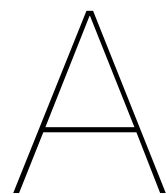
Bibliography

- [1] Prostate Cancer Foundation of Australia. Understanding Brachytherapy for Prostate Cancer, 2020. URL <https://www.prostate.org.au/media/468677/understanding-brachytherapy.pdf>.
- [2] Tae Ho Kim, Dan Bi An, Se Heang Oh, Min Kwan Kang, Hyun Hoon Song, and Jin Ho Lee. Creating stiffness gradient polyvinyl alcohol hydrogel using a simple gradual freezing-thawing method to investigate stem cell differentiation behaviors. *Biomaterials*, 40:51–60, 2015. ISSN 18785905. doi: 10.1016/j.biomaterials.2014.11.017. URL <http://dx.doi.org/10.1016/j.biomaterials.2014.11.017>.
- [3] Rami K Korhonen and Simo Saarakkala. Biomechanics and Modeling of Skeletal Soft Tissues. In *Theoretical Biomechanics*. 2011. doi: 10.5772/19975.
- [4] Tarun Podder, Douglas Clark, Jason Sherman, Dave Fuller, Edward Messing, Deborah Rubens, John Strang, Ralph Brasacchio, Lydia Liao, Wan Sing Ng, and Yan Yu. In vivo motion and force measurement of surgical needle intervention during prostate brachytherapy. *Medical Physics*, 33(8):2915–2922, 2006. ISSN 00942405. doi: 10.1118/1.2218061.
- [5] Nikolai Hungr, Jean Alexandre Long, Vincent Beix, and Jocelyne Troccaz. A realistic deformable prostate phantom for multimodal imaging and needle-insertion procedures. *Medical Physics*, 39(4):2031–2041, 2012. ISSN 00942405. doi: 10.1118/1.3692179.
- [6] World Health Organization. Cancer Key Facts, 2018. URL <https://www.who.int/news-room/fact-sheets/detail/cancer>.
- [7] American Cancer Society. Key Statistics for Prostate Cancer, 2020. URL <https://www.cancer.org/cancer/prostate-cancer/about/key-statistics.html>.
- [8] Nelson N. Stone, Jiten Roy, Suzanne Hong, Yeh Chi Lo, and Richard G. Stock. Prostate gland motion and deformation caused by needle placement during brachytherapy. *Brachytherapy*, 1(3):154–160, 2002. ISSN 15384721. doi: 10.1016/S1538-4721(02)00058-2.
- [9] Subir Nag, David Beyer, Jay Friedland, Peter Grimm, and Ravinder Nath. American brachytherapy society (ABS) recommendations for transperineal permanent brachytherapy of prostate cancer. *I. J. Radiation Oncology*, 44(4):789–799, 1999.
- [10] Peter Grimm and John Sylvester. Advances in brachytherapy. *Cancer treatment and research*, 6(4):191–211, 2004. ISSN 09273042. doi: 10.1007/978-1-4615-5769-2{_}9.
- [11] Peter L. Roberson, Vrinda Narayana, Daniel L. McShan, Raymond J. Winfield, and P. William McLaughlin. Source placement error for permanent implant of the prostate. *Medical Physics*, 24(2):251–257, 1997. ISSN 00942405. doi: 10.1118/1.598058.
- [12] J. E. Dawson, T. Wu, T. Roy, J. Y. Gu, and H. Kim. Dose effects of seeds placement deviations from pre-planned positions in ultrasound guided prostate implants. *Radiotherapy and Oncology*, 32(3):268–270, 1994. ISSN 01678140. doi: 10.1016/0167-8140(94)90027-2.
- [13] Kana Kobayashi, Koji Okihara, Tsuyoshi Iwata, Norihiro Aibe, Naohiro Kodani, Takuji Tsubokura, Kazumi Kamoi, Tsuneharu Miki, and Hideya Yamazaki. Evaluation of dosimetry and excess seeds in permanent brachytherapy using a modified hybrid method: A single-institution experience. *Journal of Radiation Research*, 54(3):479–484, 2013. ISSN 04493060. doi: 10.1093/jrr/rrs126.
- [14] Gang Wan, Zhouping Wei, Lori Gardi, Donal B. Downey, and Aaron Fenster. Brachytherapy needle deflection evaluation and correction. *Medical Physics*, 32(4):902–909, 2005. ISSN 00942405. doi: 10.1118/1.1871372.

- [15] John C Blasko, Peter D Grimm, and Sarada M Reddy. Brachytherapy for Prostate Cancer. 45(3): 165–178, 1995.
- [16] Michael Dattoli and Kent Waller. A simple method to stabilize the prostate during transperineal prostate brachytherapy. *Radiation Oncology*, 38(2):341–342, 1997.
- [17] B. Konh, N. V. Datla, and P. Hutapea. Dynamic estimation of an active surgical needle deflection for brachytherapy procedures. *Proceedings of the IEEE Annual Northeast Bioengineering Conference, NEBEC*, 2014-Decem:1–2, 2014. ISSN 21607001. doi: 10.1109/NEBEC.2014.6972843.
- [18] Bardia Konh and Parsaoran Hutapea. Finite element simulation of an active surgical needle for prostate brachytherapy. *ASME 2013 Conference on Frontiers in Medical Devices: Applications of Computer Modeling and Simulation, FMD 2013*, pages 1–2, 2013. doi: 10.1115/FMD2013-16049.
- [19] Margaret Rox, Maxwell Emerson, Tayfun Efe Ertop, Inbar Fried, Mengyu Fu, Janine Hoelscher, Alan Kuntz, Josephine Granna, Jason E. Mitchell, Michael Lester, Fabien Maldonado, Erin A. Gillaspie, Jason A. Akulian, Ron Alterovitz, and Robert J. Webster. Decoupling Steerability From Diameter: Helical Dovetail Laser Patterning for Steerable Needles. *IEEE Access*, 8:181411–181419, 2020. doi: 10.1109/access.2020.3028374.
- [20] Philip J. Swaney, Jessica Burgner, Hunter B. Gilbert, and Robert J. Webster. A flexure-based steerable needle: High curvature with reduced tissue damage. *IEEE Transactions on Biomedical Engineering*, 60(4):906–909, 2013. ISSN 15582531. doi: 10.1109/TBME.2012.2230001.
- [21] Emily C. Bush, Aliya Gifford, Crystal L. Coolbaugh, Theodore F. Towse, Bruce M. Damon, and E. Brian Welch. Fat-water phantoms for magnetic resonance imaging validation: A flexible and scalable protocol. *Journal of Visualized Experiments*, 2018(139):1–9, 2018. ISSN 1940087X. doi: 10.3791/57704.
- [22] Luis Elvira, Carmen Durán, Ricardo T. Higuti, Marcelo M. Tiago, Alberto Ibáñez, Montserrat Parrilla, Eva Valverde, Javier Jiménez, and Quique Bassat. Development and Characterization of Medical Phantoms for Ultrasound Imaging Based on Customizable and Mouldable Polyvinyl Alcohol Cryogel–Based Materials and 3-D Printing: Application to High-Frequency Cranial Ultrasonography in Infants. *Ultrasound in Medicine and Biology*, 45(8):2226–2241, 2019. ISSN 1879291X. doi: 10.1016/j.ultrasmedbio.2019.04.030.
- [23] Kelly E. Michaelsen, Venkataramanan Krishnaswamy, Adele Shenoy, Emily Jordan, Brian W. Pogue, and Keith D. Paulsen. Anthropomorphic breast phantoms with physiological water, lipid, and hemoglobin content for near-infrared spectral tomography. *Journal of Biomedical Optics*, 19(2):026012, 2014. ISSN 1083-3668. doi: 10.1117/1.jbo.19.2.026012.
- [24] Rui Cao and Zhihong Huang. Tissue mimicking materials for the detection of prostate cancer using shear wave elastography : A validation study. 40(2):1–9, 2013. doi: 10.1118/1.4773315.
- [25] Tsuicheng Chiu, Zhenyu Xiong, David Parsons, Michael R. Folkert, Paul M. Medin, and Brian Hrycushko. Low-cost 3D print–based phantom fabrication to facilitate interstitial prostate brachytherapy training program. *Brachytherapy*, 2020. ISSN 18731449. doi: 10.1016/j.brachy.2020.06.015. URL <https://doi.org/10.1016/j.brachy.2020.06.015>.
- [26] High Intensity Focused Ultrasound Prostate. The prostate, 2020. URL <https://www.hifu-prostate.com/the-prostate2/>.
- [27] Timothy L Hall, D Ph, Christopher R Hempel, Brian J Sabb, and William W Roberts. Acoustic Access to the Prostate. 24(11):1875–1881, 2010.
- [28] Human Anatomy. The Male Urethra, 2020. URL https://theodora.com/anatomy/the_male_urethra.html.
- [29] Genesis. Rectal Ultrasound, 2020. URL https://www.genesishealth.com/care-treatment/endoscopy/tests/rectal_ultrasound/.

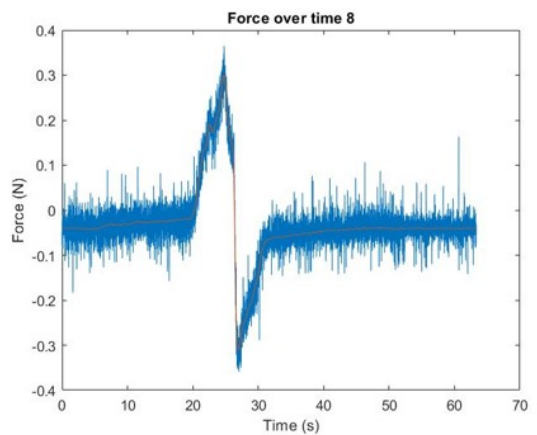
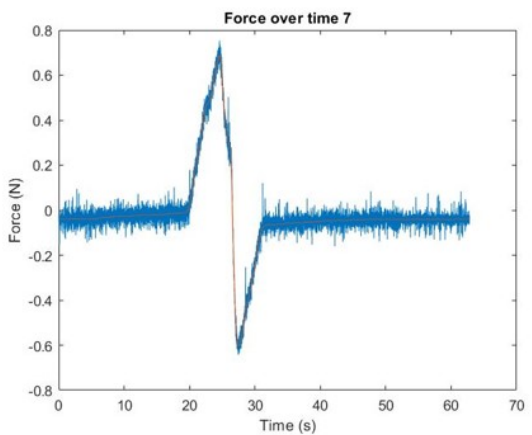
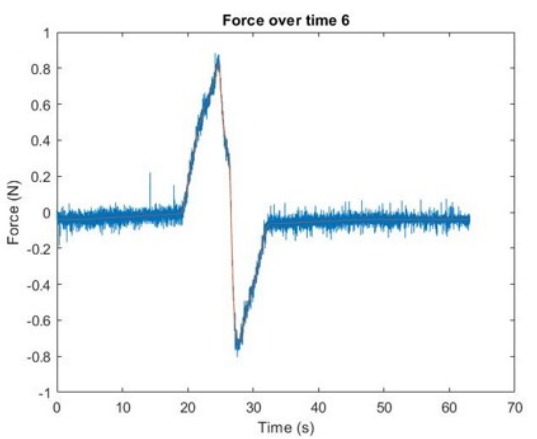
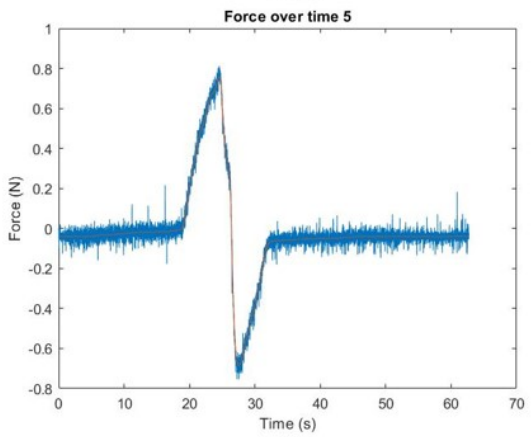
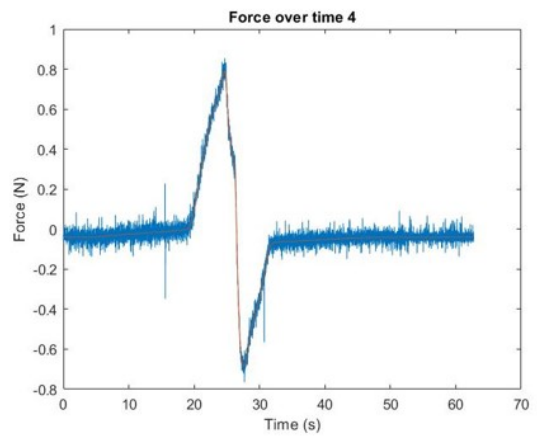
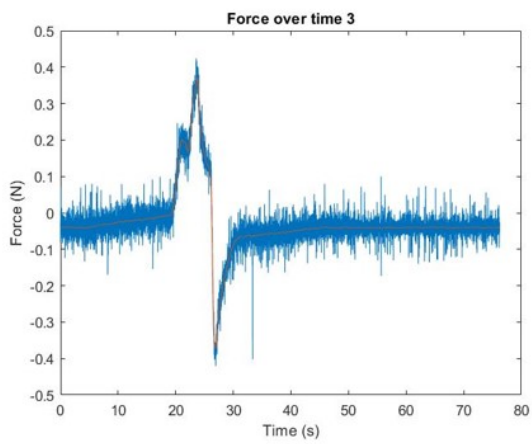
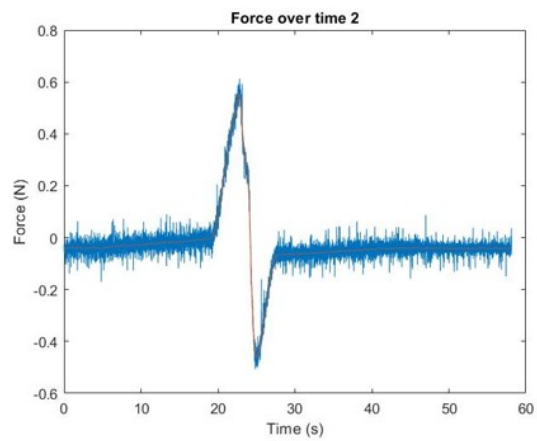
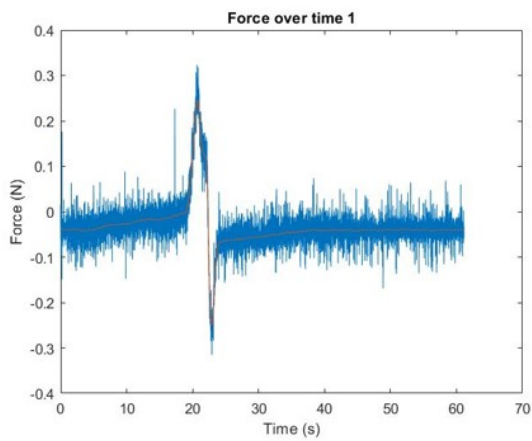
- [30] Jörn Kemper, R. Sinkus, J. Lorenzen, C. Nolte-Ernsting, A. Stork, and G. Adam. MR elastography of the prostate: Initial in-vivo application. *RoFo Fortschritte auf dem Gebiet der Rontgenstrahlen und der Bildgebenden Verfahren*, 176(8):1094–1099, 2004. ISSN 14389029. doi: 10.1055/s-2004-813279.
- [31] Thomas A. Krouskop, Thomas M. Wheeler, Faouzi Kallel, Brian S. Garra, and Timothy Hall. Elastic moduli of breast and prostate tissues under compression. *Ultrasonic Imaging*, 20(4):260–274, 1998. ISSN 01617346. doi: 10.1177/016173469802000403.
- [32] S. Phipps, T. H.J. Yang, F. K. Habib, R. L. Reuben, and S. A. McNeill. Measurement of tissue mechanical characteristics to distinguish between benign and malignant prostatic disease. *Urology*, 66(2):447–450, 2005. ISSN 00904295. doi: 10.1016/j.urology.2005.03.017.
- [33] T. H.J. Yang, S. K.W. Leung, S. Phipps, R. L. Reuben, S. A. McNeill, F. K. Habib, A. Schnieder, and R. Stevens. In-vitro dynamic micro-probing and the mechanical properties of human prostate tissues. *Technology and Health Care*, 14(4-5):281–296, 2006. ISSN 09287329. doi: 10.3233/thc-2006-144-511.
- [34] Man Zhang, Priya Nigwekar, Benjamin Castaneda, Kenneth Hoyt, Jean V. Joseph, Anthony di Sant’Agnese, Edward M. Messing, John G. Strang, Deborah J. Rubens, and Kevin J. Parker. Quantitative Characterization of Viscoelastic Properties of Human Prostate Correlated with Histology. *Ultrasound in Medicine and Biology*, 34(7):1033–1042, 2008. ISSN 03015629. doi: 10.1016/j.ultrasmedbio.2007.11.024.
- [35] Mingbo Zhang, Shuai Fu, Yan Zhang, Jie Tang, and Yun Zhou. Elastic modulus of the prostate: A new non-invasive feature to diagnose bladder outlet obstruction in patients with benign prostatic hyperplasia. *Ultrasound in Medicine and Biology*, 40(7):1408–1413, 2014. ISSN 1879291X. doi: 10.1016/j.ultrasmedbio.2013.10.012.
- [36] M Geerligs. A Literature Review of the Mechanical Behavior of the Stratum Corneum, the Living Epidermis and the Subcutaneous Fat Tissue. *Mechanics of Skin Layers (WBSO 20)*, 06(PR-TN 2006/00450):1–39, 2006.
- [37] Kathryn Nightingale, Stephen McAleavey, and Gregg Trahey. Shear-wave generation using acoustic radiation force: In vivo and ex vivo results. *Ultrasound in Medicine and Biology*, 29(12):1715–1723, 2003. ISSN 03015629. doi: 10.1016/j.ultrasmedbio.2003.08.008.
- [38] Ehsan Omid. Characterization and Assessment of Mechanical Properties of Adipose Derived Breast Tissue Scaffolds as a Means for Breast Reconstructive Purposes. (September):1–81, 2014.
- [39] Abbas Samani, Judit Zubovits, and Donald Plewes. Elastic moduli of normal and pathological human breast tissues: An inversion-technique-based investigation of 169 samples. *Physics in Medicine and Biology*, 52(6):1565–1576, 2007. ISSN 00319155. doi: 10.1088/0031-9155/52/6/002.
- [40] Kenneth C Chu and Brian K Rutt. Polyvinyl alcohol cryogel: An ideal phantom material for MR studies of arterial flow and elasticity. *Magnetic Resonance in Medicine*, 37(2):314–319, 1997. ISSN 07403194. doi: 10.1002/mrm.1910370230.
- [41] Jérémie Fromageau, Elisabeth Brusseau, Didier Vray, Gérard Gimenez, and Philippe Delachartre. Characterization of PVA Cryogel for Intravascular Ultrasound Elasticity Imaging. *IEEE transactions on ultrasonics, ferroelectrics*, 50(10):1318–1324, 2003.
- [42] T. Noguchi, T. Yamamuro, M. Oka, P. Kumar, Y. Kotoura, S. Hyon, and Y. Ikada. Poly(vinyl alcohol) hydrogel as an artificial articular cartilage: evaluation of biocompatibility. *Journal of applied biomaterials : an official journal of the Society for Biomaterials*, 2(2):101–107, 1991. ISSN 10454861. doi: 10.1002/jab.770020205.
- [43] Shauna R. Stauffer and Nikolaos A. Peppast. Poly(vinyl alcohol) hydrogels prepared by freezing-thawing cyclic processing. *Polymer*, 33(18):3932–3936, 1992. ISSN 00323861. doi: 10.1016/0032-3861(92)90385-A.

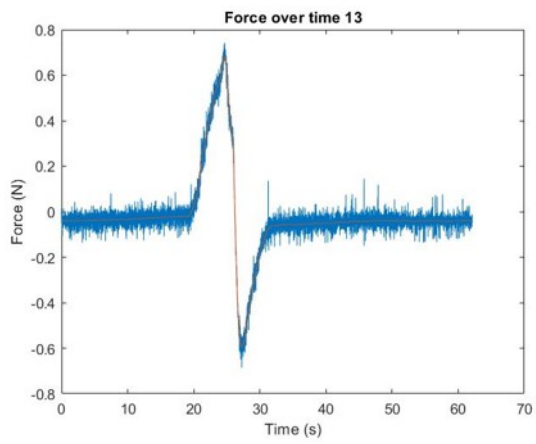
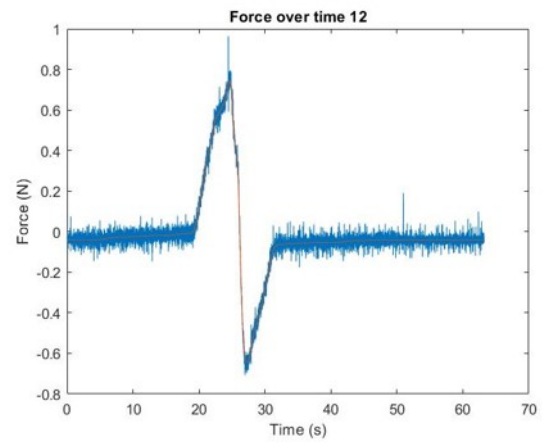
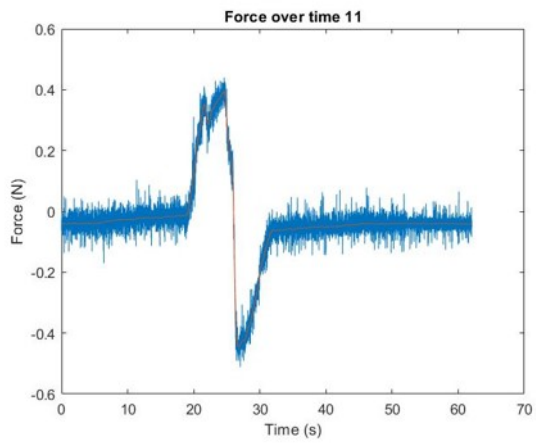
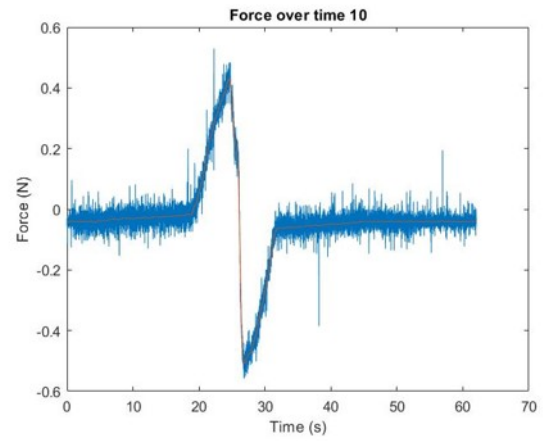
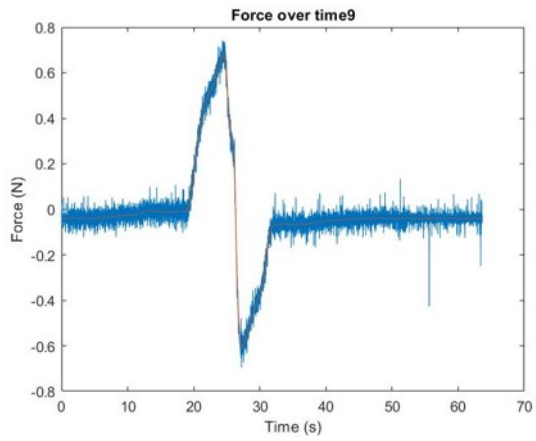
- [44] F. Yokoyama, I. Masada, K. Shimamura, T. Ikawa, and K. Monobe. Morphology and structure of highly elastic poly(vinyl alcohol) hydrogel prepared by repeated freezing-and-melting. *Colloid & Polymer Science*, 264(7):595–601, 1986. ISSN 0303402X. doi: 10.1007/BF01412597.
- [45] W. K. Wan, G. Campbell, Z. F. Zhang, A. J. Hui, and D. R. Boughner. Optimizing the tensile properties of polyvinyl alcohol hydrogel for the construction of a bioprosthetic heart valve stent. *Journal of Biomedical Materials Research*, 63(6):854–861, 2002. ISSN 00219304. doi: 10.1002/jbm.10333.
- [46] C. K. Haweel and S.H. Ammar. Preparation of polyvinyl alcohol from local raw material. *Iraqi Journal of Chemical and Petroleum Engineering*, 9(1):15–21, 2008.
- [47] Fredric L. Buchholz and Nicholas A. Peppas. Super absorbent polymers. *Science and Technology*, 573, 1994.
- [48] W.A. Johnston, F.J. Nicholson, A. Roger, and G.D. Stroud. *Freezing and Refrigerated Storage in Fisheries*. FOOD AND AGRICULTURE ORGANIZATION OF THE UNITED NATIONS, 1994. ISBN ISBN 92-5-103579-2. URL <http://www.fao.org/3/v3630e/V3630E06.htm#:~:text=Productthickness.,increasethefreezingtimefourfold.>
- [49] S. H. Hyon, W. I. Cha, and Y. Ikada. Preparation of transparent poly(vinyl alcohol) hydrogel. *Polymer Bulletin*, 22(2):119–122, 1989. ISSN 01700839. doi: 10.1007/BF00255200.
- [50] Hiroshi Hoshino, Susumu Okada, Hiroshi Urakawa, and Kanji Kajiwara. Gelation of poly(vinyl alcohol) in dimethyl sulfoxide/water solvent. *Polymer Bulletin*, 37(2):237–244, 1996. ISSN 01700839. doi: 10.1007/BF00294127.
- [51] Sohee Kim, Chanhee Kyung, Jong Suk Park, Seung-Pyo Lee, Hye Kyoung Kim, Chul Woo Ahn, Kyung Rae Kim, and Shinae Kang. Normal-weight obesity is associated with increased risk of sub-clinical atherosclerosis. *Cardiovascular diabetology*, 14:58, 5 2015. ISSN 1475-2840 (Electronic). doi: 10.1186/s12933-015-0220-5.
- [52] Abdul Hadi, Abdul Wahab, Amir Putra, Muhammad Noor, Ardiyansyah Syahrom, Muhammad Hanif, Mohd Ayob, Mohammed Rafiq, and Abdul Kadir. Developing functionally graded PVA hydrogel using simple freeze-thaw method for artificial glenoid labrum. *Journal of the Mechanical Behavior of Biomedical Materials*, 91(August 2018):406–415, 2019. ISSN 1751-6161. doi: 10.1016/j.jmbbm.2018.12.033. URL <https://doi.org/10.1016/j.jmbbm.2018.12.033>.
- [53] K. Yan, L. Li, J. Joseph, D. R. Rubens, E. M. Messing, L. Liao, and Y. Yu. A real-time prostate cancer detection technique using needle insertion force and patient-specific criteria during percutaneous intervention. *Medical Physics*, 36(7):3356–3362, 2009. ISSN 00942405. doi: 10.1118/1.3148834.
- [54] Pan Li, Shan Jiang, Yan Yu, Jun Yang, and Zhiyong Yang. Biomaterial characteristics and application of silicone rubber and PVA hydrogels mimicked in organ groups for prostate brachytherapy. *Journal of the Mechanical Behavior of Biomedical Materials*, 49(January 2018):220–234, 2015. ISSN 18780180. doi: 10.1016/j.jmbbm.2015.05.012.
- [55] Charlie Stockley, Lucy Bennett, and Lutz Wymenga. Design and Manufacture of a Prostate Phantom for Pre-Clinical Trials of Novel Steerable Needles. *Technische universiteit Delft*, BM41070, 2020.
- [56] Database Center for Life Science. Body Parts 3D, 2020. URL <https://lifesciencedb.jp/bp3d/>.
- [57] Tonke L. de Jong, Loes H. Pluymen, Dennis J. van Gerwen, Gert Jan Kleinrensink, Jenny Dankelman, and John J. van den Dobbelsteen. PVA matches human liver in needle-tissue interaction. *Journal of the Mechanical Behavior of Biomedical Materials*, 69(November 2016):223–228, 2017. ISSN 18780180. doi: 10.1016/j.jmbbm.2017.01.014. URL <http://dx.doi.org/10.1016/j.jmbbm.2017.01.014>.



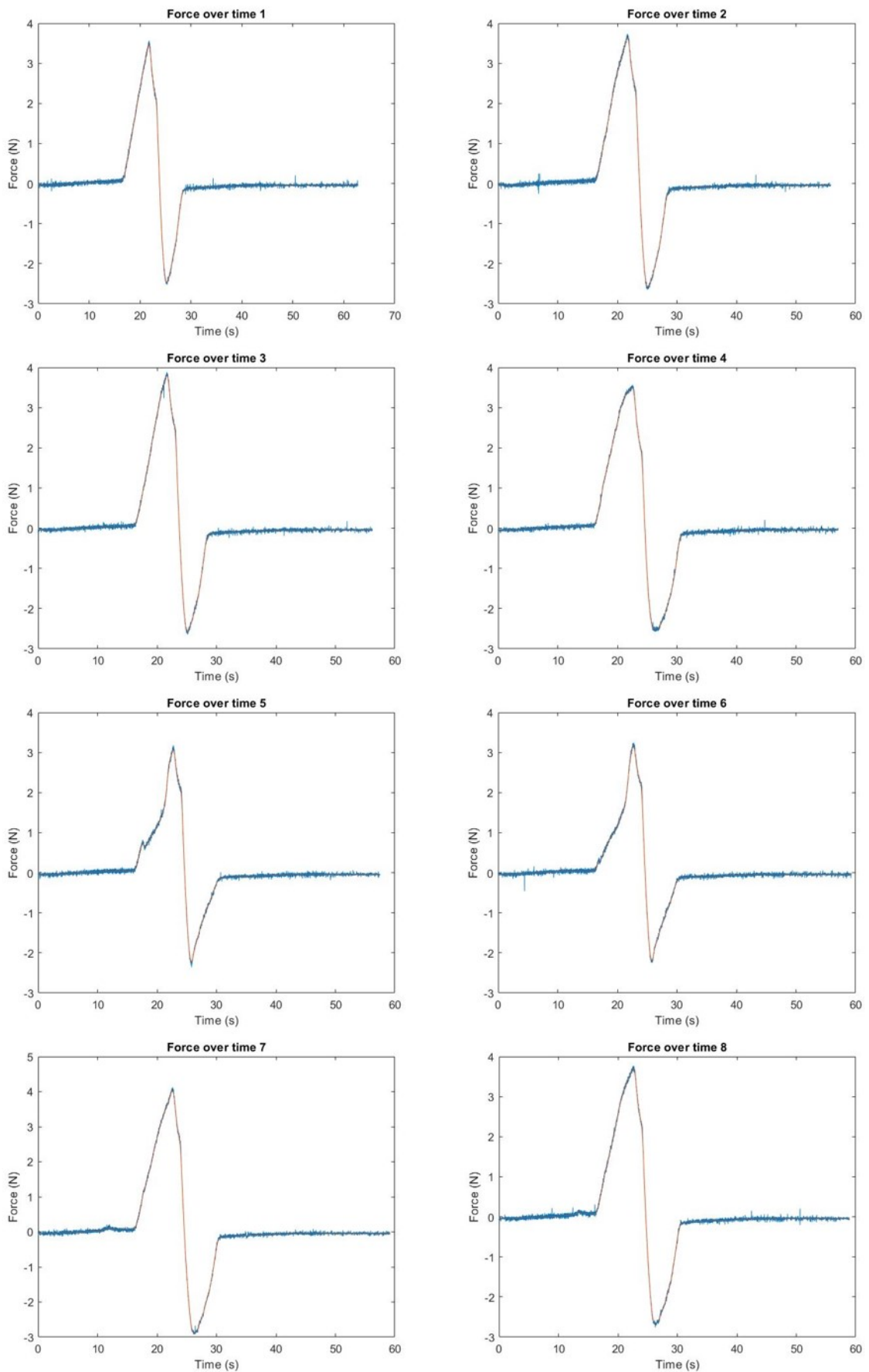
Appendices

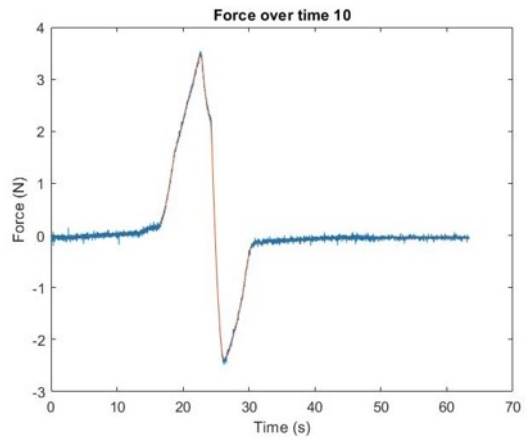
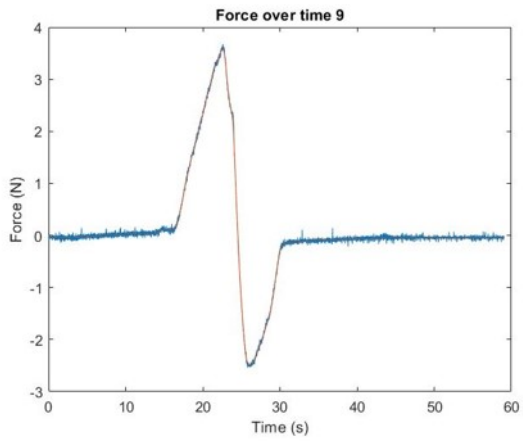
A.1. Needle Insertion Figures Model 1



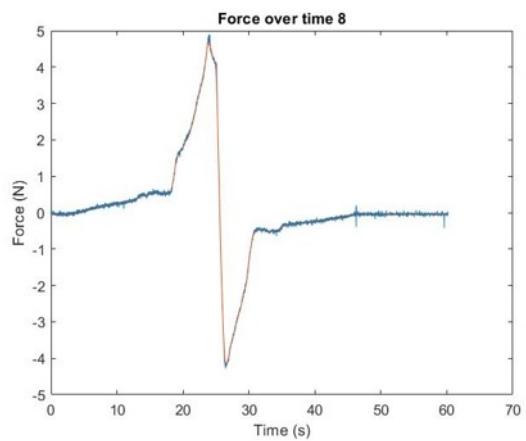
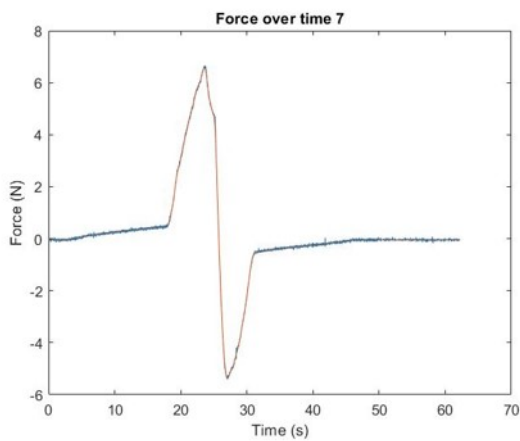
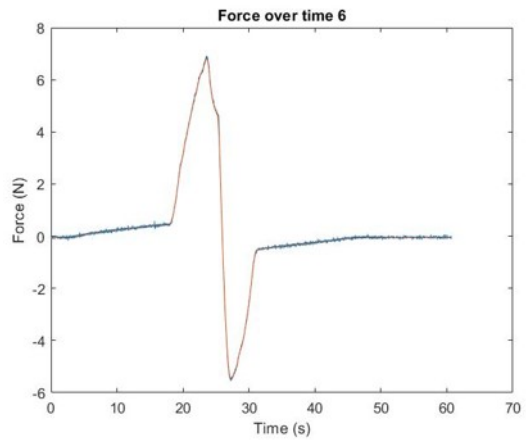
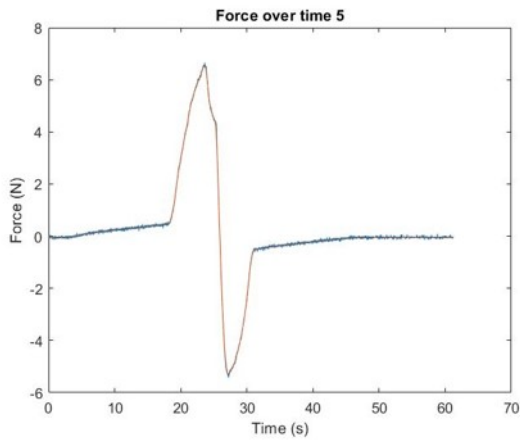
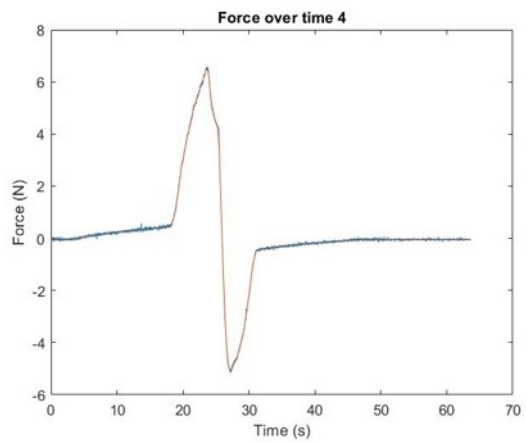
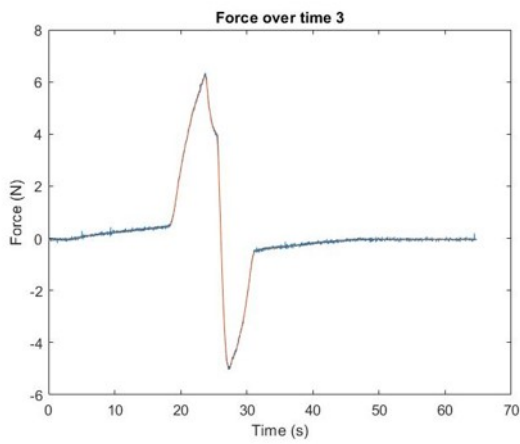
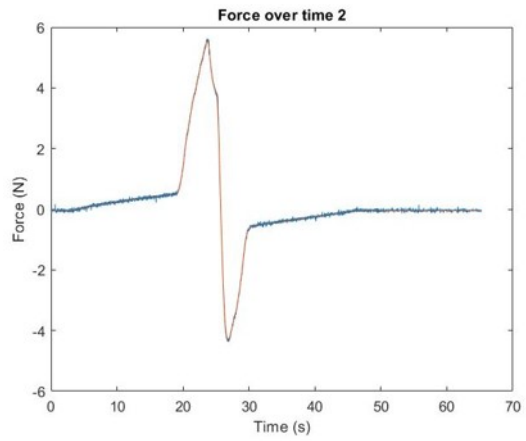
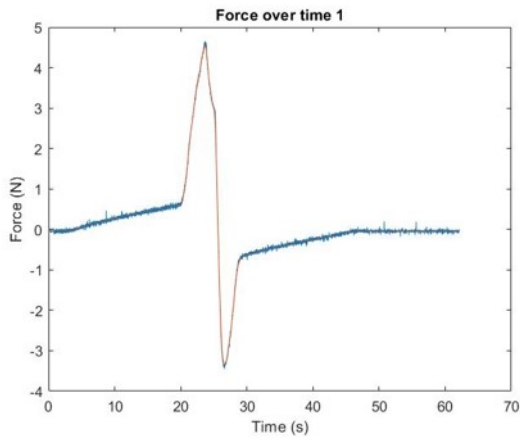


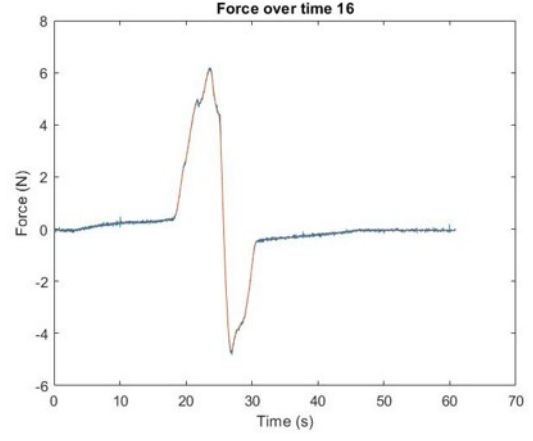
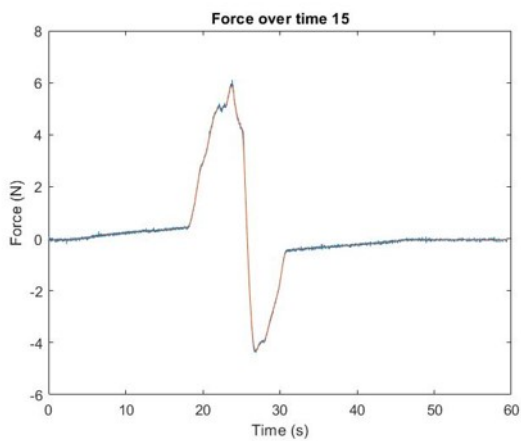
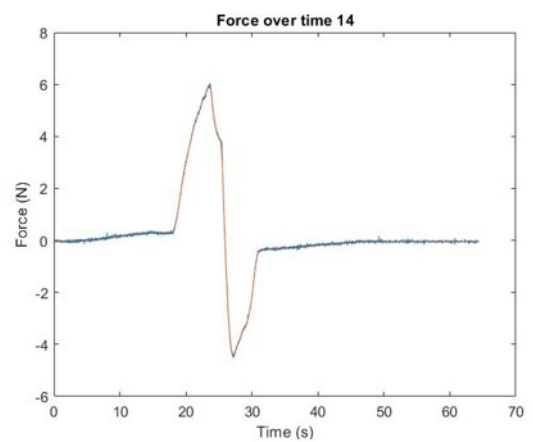
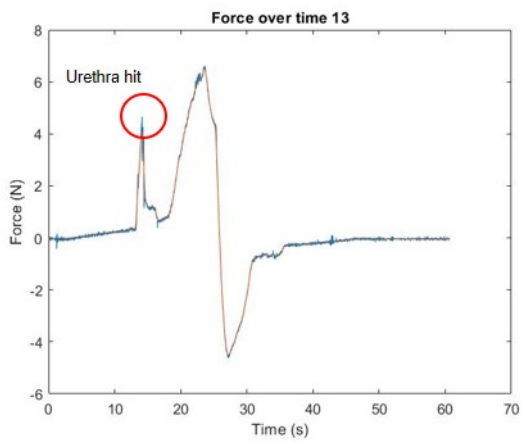
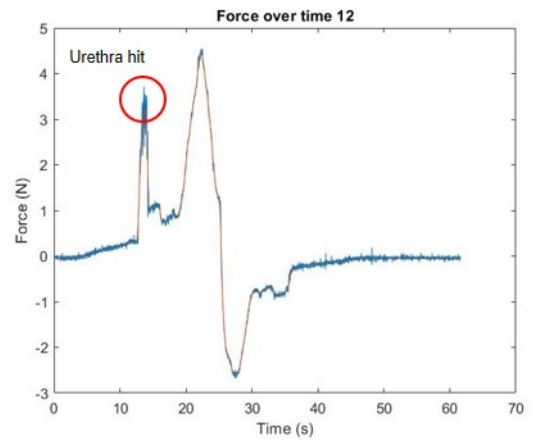
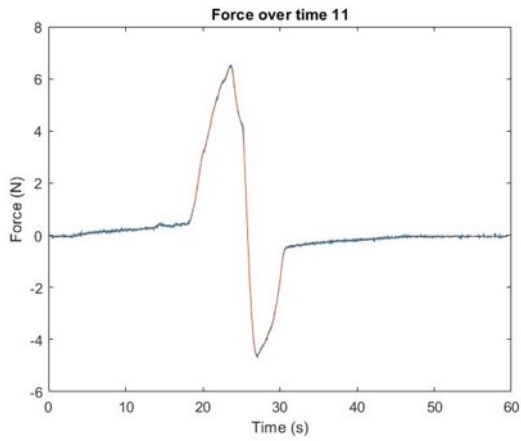
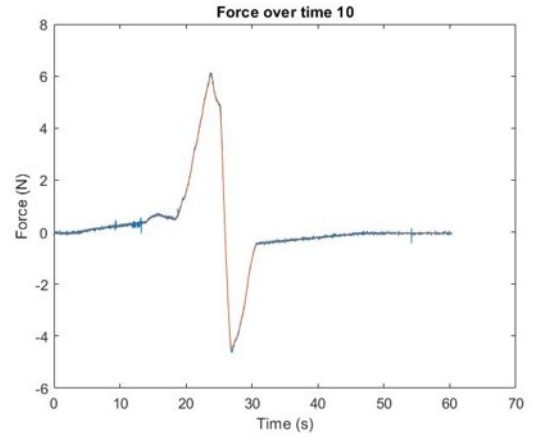
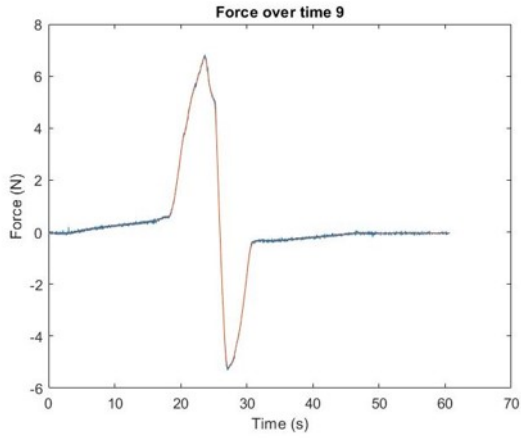
A.2. Needle Insertion Figures Model 2

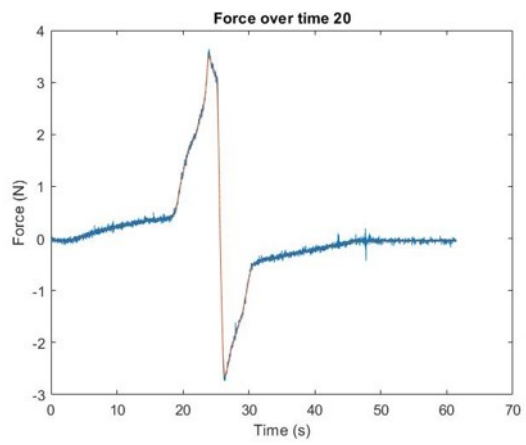
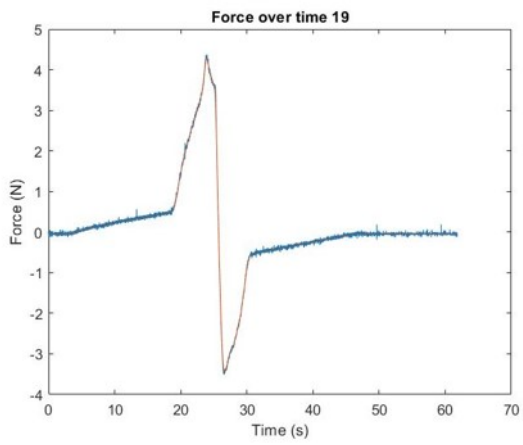
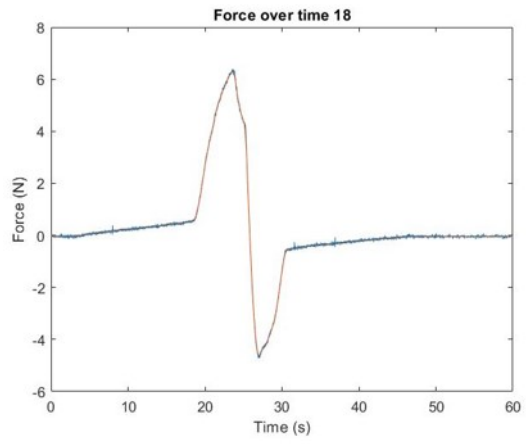
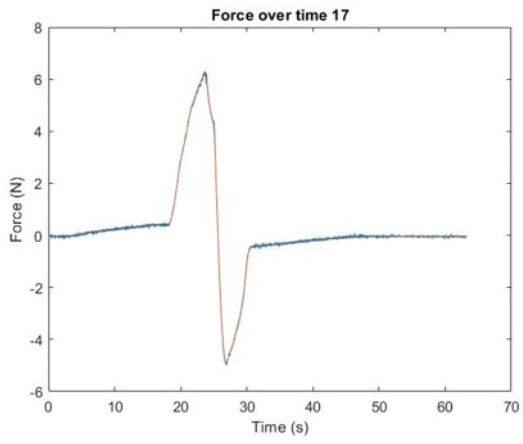




A.3. Needle Insertion Figures Model 3







A.4. Needle Insertion Peak Forces

| | Model 1 | Model 2 | Model 3 |
|------------|----------------|----------------|----------------|
| N1 | 0.25 | 3.46 | 4.57 |
| N2 | 0.55 | 3.64 | 5.55 |
| N3 | 0.37 | 3.80 | 6.22 |
| N4 | 0.79 | 3.50 | 6.49 |
| N5 | 0.76 | 3.06 | 6.53 |
| N6 | 0.83 | 3.15 | 6.82 |
| N7 | 0.69 | 4.04 | 6.58 |
| N8 | 0.30 | 3.70 | 4.72 |
| N9 | 0.68 | 3.59 | 6.71 |
| N10 | 0.43 | 3.46 | 6.04 |
| N11 | 0.39 | | 6.46 |
| N12 | 0.75 | | 4.45 |
| N13 | 0.68 | | 6.51 |
| N14 | | | 5.92 |
| N15 | | | 5.90 |
| N16 | | | 6.12 |
| N17 | | | 6.21 |
| N18 | | | 6.29 |
| N19 | | | 4.28 |
| N20 | | | 3.51 |